frontiers | Frontiers in Earth Science

ORIGINAL RESEARCH
published: 13 September 2022
doi: 10.3389/feart.2022.845544

The Geochemical Evolution of Santa Cruz Island, Galápagos Archipelago

E. L. Wilson[1†], *K. S. Harpp*[2*†], *D. M. Schwartz*[3] *and R. Van Kirk*[2]

[1]Department of Earth and Environment, Franklin and Marshall College, Lancaster, PA, United States, [2]Department of Geology, Colgate University, Hamilton, NY, United States, [3]Department of Geosciences, Boise State University, Boise, ID, United States

Understanding how ocean island volcanoes evolve provides important insight into the behavior of mantle plumes, how plumes interact with mid-ocean ridges, and potential risks posed to inhabitants as the islands age. In this field-based study of the Galápagos Islands, we use radiogenic isotope ratio, major element, and trace element analysis of >70 new lava samples to document the geochemical evolution of Santa Cruz Island over the past ~2 million years, as it has been carried away from the plume. Currently, Santa Cruz is a dormant shield volcano in the central archipelago. Previous work indicates that exposed lavas preserve >1 million years of activity in two eruptive units: *1*) The older Platform Series, exposed primarily in the northeast; and *2*) the Shield Series, which blankets the rest of Santa Cruz and erupted from a WNW trending fissure system. Our new geochemical analyses indicate that the Platform Series lavas are more evolved and isotopically enriched than Shield lavas, but neither as compositionally monotonous nor as isotopically enriched as the younger western Galápagos volcanoes. Santa Cruz formed when the Galápagos Spreading Center (GSC) was closer to the plume than it is today, resulting in enhanced plume-ridge interaction and transport of plume material to the ridge. Consequently, the Platform Series was formed under relatively magma-starved conditions compared to today's western volcanoes. Magma supply was sufficient for partial fractionation and homogenization of melts in shallow reservoirs, but inadequate to support thermochemically buffered networks like those in the present-day western archipelago. The slight depletion of Platform Series lavas relative to Fernandina reflects entrainment of depleted upper mantle and/or diversion of deep, enriched plume melts to the nearby GSC. The younger Shield Series lavas are even more depleted because plate motion has carried the volcano across the compositional boundary of the bilaterally asymmetric plume into its more depleted zone. Shield Series lavas' variable, primitive compositions reflect minimal crustal processing in small, ephemeral, poorly supplied magma reservoirs. Unlike the young western shields, the constructional history of Santa Cruz has been controlled to a significant extent by its proximity to the GSC.

Keywords: mantle plume, Ocean Island Basalt (OIB), volcano evolution, plume-ridge interaction, Galapagos Islands, Galapagos Archipelago, Santa Cruz Island, ocean island evolution

OPEN ACCESS

Edited by:
Michel Pichavant, CNRS Orléans, France

Reviewed by:
Luis E. Lara, Servicio Nacional de Geología y Minería de Chile (SERNAGEOMIN), Chile
Benjamin Bernard, Escuela Politécnice Nacional, Ecuador

***Correspondence:**
K. S. Harpp
kharpp@colgate.edu

†These authors share first authorship

Specialty section:
This article was submitted to Volcanology, a section of the journal Frontiers in Earth Science

Received: *29 December 2021*
Accepted: *29 March 2022*
Published: *13 September 2022*

Citation:
Wilson EL, Harpp KS, Schwartz DM and Van Kirk R (2022) The Geochemical Evolution of Santa Cruz Island, Galápagos Archipelago. Front. Earth Sci. 10:845544. doi: 10.3389/feart.2022.845544

INTRODUCTION

Ocean island volcanoes serve as windows into the composition and behavior of mantle plumes. How the geochemistry of lavas erupted at these volcanoes changes as they are transported downstream provides further insight into temporal and spatial variations of mantle plumes, as well as important constraints on island evolution. The Galápagos Islands are the surface expression of a mantle plume that has been active for at least 14.5 million years (e.g., Werner et al., 1999). Despite both Galápagos and Hawai'i originating as deep mantle plumes (e.g., Morgan, 1972; Wolfe et al., 2009; Weis et al., 2011; French and Romanowicz, 2015), the Galápagos Archipelago is distinct from the Hawaiian mantle plume archetype in multiple ways (Harpp and Weis, 2020). Of most importance for this study, the Galápagos Islands lack a predictable petrologic and geochemical evolutionary sequence like that observed at Hawai'i, in which the islands transition from an alkalic pre-shield to a tholeiitic shield, and eventually to an alkalic post-shield stage, related to changes in magma supply rate as a function of proximity to the Hawaiian plume (e.g., Chen and Frey, 1983; Macdonald et al., 1983; Clague and Dalrymple, 1987, 1988; Geist et al., 2014a).

Furthermore, radiogenic isotopic ratios of Galápagos lavas extend from enriched compositions to signatures indistinguishable from depleted mid-ocean ridge basalt (MORB; e.g., White and Hofmann, 1978; Geist et al., 1988; White et al., 1993; Blichert-Toft and White, 2001; Harpp and White, 2001). In this work, we use "enriched" for material with high time-integrated U/Pb, Th/Pb, and Rb/Sr, as well as low time-integrated Sm/Nd (i.e., high $^{206}Pb/^{204}Pb$, $^{208}Pb/^{204}Pb$, $^{207}Pb/^{204}Pb$, $^{87}Sr/^{86}Sr$, and low $^{143}Nd/^{144}Nd$), and "depleted" for the opposite geochemical systematics. These same adjectives are used as comparative terms for both radiogenic isotope ratios and trace element contents throughout this study. Striking differences distinguish the older, eastern Galápagos Islands from their young western counterparts.

Whereas most of the active western shield volcanoes erupt lavas with a narrow range of major and trace element compositions (e.g., Geist et al., 2014a), the eastern islands exhibit greater compositional variability (e.g., Geist et al., 1986; Harpp and Geist, 2018). Most eastern islands are cut by fissures and faults, many of them trending broadly E-W, instead of the caldera-related structures of the young shields (Chadwick and Dieterich, 1995). The lack of a gravity high corresponding to a residual cumulate body beneath the Santa Cruz and San Cristóbal edifices confirms that these eastern islands do not have buried calderas (Cleary et al., 2020). Consequently, no straightforward evolutionary link between western and eastern Galápagos Islands has been identified to date (Harpp and Geist, 2018), despite detailed geochemical studies on islands and seamounts in the east, including Floreana (Harpp et al., 2014a) and Santiago (Gibson et al., 2012; Schwartz et al., 2020), and in the west (e.g., Geist et al., 1995; Reynolds and Geist, 1995; Allan and Simkin, 2000; Naumann et al., 2002; Geist et al., 2005; Geist et al., 2006; Geist et al., 2014a; Anderson et al., 2018; Schwartz et al., 2020).

Santa Cruz Island is located ~150 km downstream from the presumed plume center between Fernandina and Cerro Azul volcanoes (e.g., Kurz and Geist, 1999; Hooft et al., 2003) and is the second largest island in the archipelago in subaerial extent, covering an area of nearly 1000 km^2 (**Figure 1**). Previous authors have documented the complexity and diversity of Santa Cruz geochemistry (Bow, 1979; White et al., 1993; Kurz and Geist, 1999). For example, $^{87}Sr/^{86}Sr$ ratios in lavas vary from 0.7026 to 0.7031 (White et al., 1993), a significant fraction of the compositional range exhibited by the archipelago (e.g., Harpp and White, 2001). One of the most puzzling aspects of Santa Cruz is that it exhibits such a wide variation in isotopic composition, in striking contrast to the western Galápagos volcanoes, many of which erupt isotopically monotonous lavas and display little elemental variation (e.g., White et al., 1993; Allan and Simkin, 2000; Naumann et al., 2002; Geist et al., 2008; Geist et al., 2014a). An important objective of our study is to explain this dramatic difference in geochemical variation between the older, eastern Galápagos islands such as Santa Cruz and the strongly homogeneous compositions erupted by the young western shield volcanoes, in the context of the Galápagos plume and its compositional structure (e.g., Harpp and Geist, 2018; Harpp and Weis, 2020).

According to the two previous studies of Santa Cruz (Bow, 1979; Schwartz et al., 2022), field evidence indicates that the volcano has experienced two periods of volcanism and two of tectonic activity, spanning at least 1 My (White et al., 1993). Thus, exposed lavas on Santa Cruz provide an opportunity to document the geochemical evolution of Galápagos volcanoes as they have been carried downstream from the plume. In this study, we present new major element, trace element, and radiogenic isotopic data from Santa Cruz Island lavas. Our objectives are to identify the processes responsible for producing some of the most heterogeneous compositions observed at a Galápagos volcano, developing an evolutionary model for the volcanic island, and, at the broadest scale, understanding the compositional structure of the Galápagos plume.

BACKGROUND

Tectonic Setting

The Galápagos Archipelago is located ~1000 km west of South America on the Nazca plate, which is moving eastward at 51 km/Ma (Argus et al., 2011). The east-west trending Galápagos Spreading Center (GSC), where the Nazca and Cocos plates are diverging, is between 150 and 300 km north of the archipelago (**Figure 1A**). The GSC has experienced multiple southward ridge jumps during the last 5 million years, the most recent at ~1 Ma. Consequently, the GSC was closer to the Galápagos plume when the central and eastern islands were forming than it is today (Wilson and Hey, 1995; Mittelstaedt et al., 2012). Santa Cruz is one of several older islands in the central Galápagos, in addition to San Cristóbal, Santiago, Española, Floreana, Rabida,

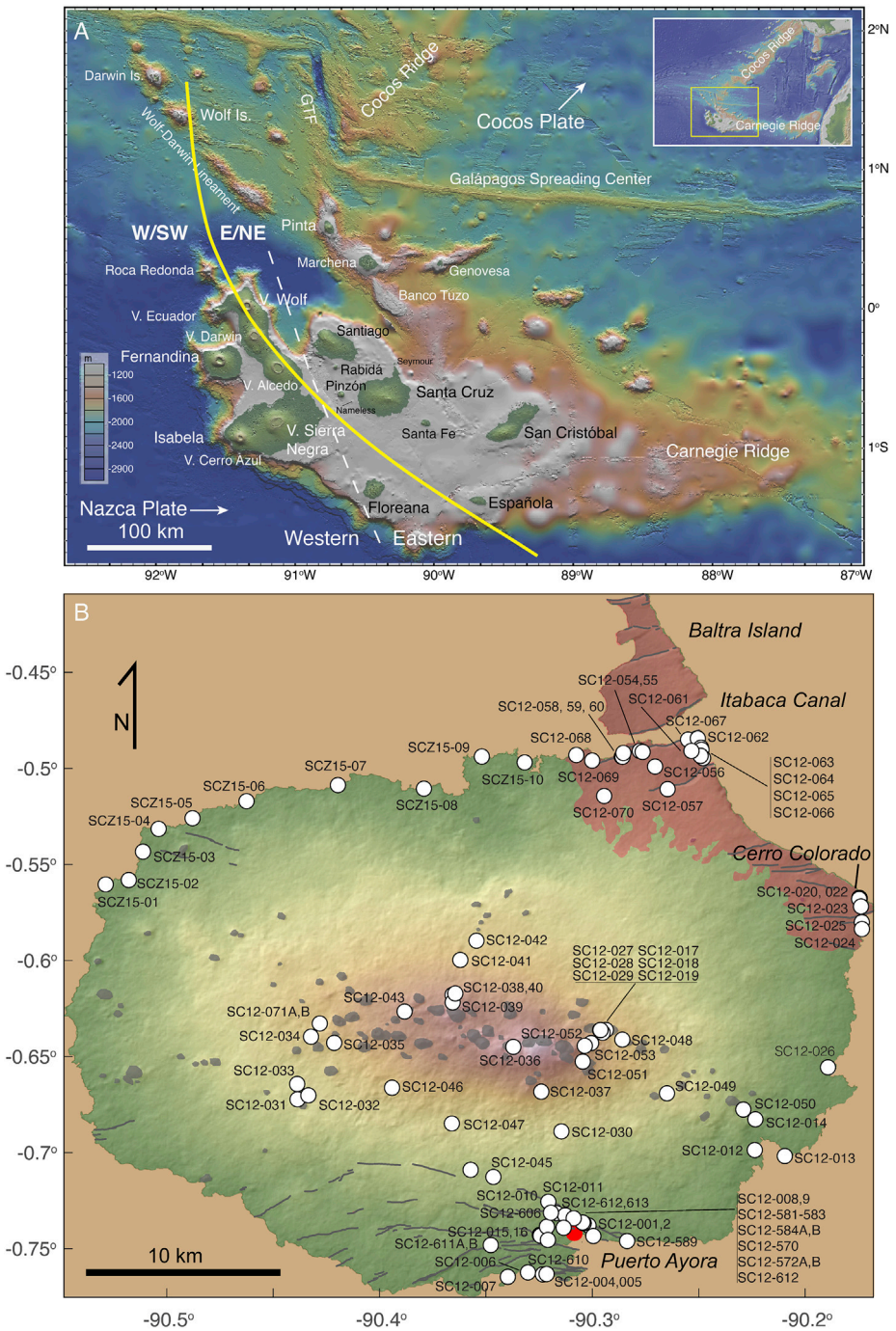

FIGURE 1 | (A) Map of the Galápagos Archipelago. Santa Cruz is located in the central Galápagos. Cocos and Nazca absolute plate motion directions are from Argus et al. (2011). The yellow line denotes the boundary between the enriched, LLSVP-sourced stripe on the W/SW side of the plume and the less enriched, ambient mantle-sourced stripe on the E/NE side of the plume; *see* text for discussion and Harpp and Weis (2020) for further details. The white dashed line indicates the line between the western and eastern volcanic morphologies in the archipelago. **(B)** Digital Elevation Model (DEM) of Santa Cruz with locations for all samples collected during the 2012 and 2015 field excursions to the island. Faults are represented as gray lines. Cinder and tuff cones are colored dark gray. Red circle is the town of Puerto Ayora, and white circles are sampling locations. Light red regions (northeast quadrant and Baltra Island) are Platform Series (Bow, 1979). According to Bow (1979), additional reversely polarized lavas (i.e., >700 ka Ma) are located in the northwest quadrant, but they are not shown here; consequently, it is possible that samples SCZ15-01 through 06 may be Platform Series as well.

Pinzón, and Santa Fe (**Figure 1A**). Santiago, Santa Cruz's neighbor to the northwest, has experienced limited historical activity, having erupted as recently as 1906 (Siebert et al., 2010), and San Cristóbal has ~5 ka lavas along its northern coastline (Geist et al., 1986; Mahr et al., 2016).

Mantle Sources

The geochemistry of Galápagos lavas is complex; lavas ranging from depleted, MORB-like compositions to enriched alkali-olivine basalts have erupted across the archipelago (e.g., White and Hofmann, 1978; Geist et al., 1988; Graham et al., 1993; White et al., 1993; Kurz and Geist, 1999; Blichert-Toft and White, 2001:; Harpp and White, 2001). White and Hofmann (1978) first noted the distinctive, horseshoe-shaped spatial distribution of geochemical signatures in the Galápagos; along the western and southern periphery of the archipelago, volcanoes erupt lavas with geochemically enriched signatures, whereas the central and eastern volcanic centers produce material with depleted, MORB-like signatures (e.g., Geist et al., 1988; White et al., 1993; Harpp and White, 2001).

Initially, the enriched geochemical horseshoe pattern was attributed to plume-asthenosphere mixing (Geist et al., 1988) or thermal entrainment of the asthenosphere into a sheared plume (White et al., 1993; Blichert-Toft and White, 2001; Harpp and White, 2001). Researchers have also invoked a spatially heterogeneous plume, in which multiple mantle reservoirs with different evolutionary histories supply the plume (Hoernle et al., 2000; Gibson et al., 2012; Harpp et al., 2014b; Harpp and Weis, 2020; Gleeson et al., 2021). Harpp and White (2001) established that at least four isotopically distinct mantle endmembers are required to generate the geochemical variation observed across the archipelago: *1*) plume material with primordial helium isotope signatures (PLUME; Graham et al., 1993), supplying the western shields; *2*) ancient recycled material with fluid-mobile element-enriched signatures, concentrated along the southern archipelago near Floreana Island (FLO); *3*) moderately depleted material with elevated $^{207}Pb/^{204}Pb$ and $^{208}Pb/^{204}Pb$ signatures, limited to the northern reaches of the archipelago and whose source remains enigmatic (WD); and *4*) the depleted upper mantle (DUM). Harpp and Weis (2020) proposed that the more enriched signatures originate in the Large Low Shear Velocity Province (LLSVP) at the core-mantle boundary, incorporating ancient, recycled material to provide the enriched signatures, whereas the central and eastern lavas are supplied primarily by less enriched, lower Pacific mantle. They proposed that the compositional boundary between the W/SW enriched and E/NE depleted zones of the bilaterally asymmetric plume runs ~NW-SE, cutting through the archipelago west of Santa Cruz (**Figure 1A**).

Volcanic Evolution

The archetype model for hotspot-generated ocean island evolution is based on Hawai'i (MacDonald and Katsura, 1964; Chen and Frey, 1983; Macdonald et al., 1983; Clague and Dalrymple, 1987; Clague and Dalrymple, 1988). Hawaiian volcanoes experience four lifecycle stages, explained by their proximity to the plume as the edifice is carried northwest by the Pacific plate: *1*) the pre-shield stage, when the volcano is on the upstream periphery of the plume, generating low-degree melts with alkalic compositions; *2*) the shield stage, dominated by high-volume, high-degree melts and tholeiitic lavas; *3*) the post-shield phase, primarily alkalic, low degree melts at the downstream edge of the plume; and *4*) rejuvenated volcanism, which occurs after ~0.25–2.5 Ma of quiescence (e.g., Clague and Dalrymple, 1987, 1988).

Galápagos volcanoes do not conform to the Hawaiian evolutionary sequence (Geist et al., 2014a; Harpp and Geist, 2018; Harpp and Weis, 2020). For example, the central and eastern Galápagos volcanoes do not exhibit clearly defined post-shield or rejuvenation stages (e.g., Geist et al., 1986; Gibson et al., 2012; Harpp et al., 2014a). Furthermore, the eastern Galápagos volcanoes bear little morphological resemblance to the current western shields. The older islands of Santiago, Santa Cruz, San Cristóbal, and Española lack submarine rift zones and calderas characteristic of many western shields (and most Hawaiian volcanoes) and lack buried calderas (Cleary et al., 2020). Like Hawaiian volcanoes, however, the eastern volcanoes also experience extended volcanically active phases, erupting for >2 m.y. beyond when the island was located near the plume center (e.g., Geist et al., 1986; White et al., 1993; Mahr et al., 2016). Finally, petrographic modeling by Geist et al. (1998) indicates that magmatic cooling in the eastern islands, including Santa Cruz, is primarily controlled by clinopyroxene rather than plagioclase. They conclude that the bulk of the fractionation in eastern Galápagos island melts is taking place in the deep crust, at depths within the mantle in the range of 17–23 km. This depth interval is greater than that for the young western shields, whose magmatic plumbing systems are at shallower depths (~10 km; Geist et al., 1998; 2014a) owing to their more robust magma supplies.

As a consequence of the striking differences between the eastern and western Galápagos volcanoes, Harpp and Geist (2018) proposed that the eastern islands are magmatically starved compared to the western shields, preventing development of thermochemically buffered magmatic systems capable of supporting long-lived magma chambers and caldera formation (Geist et al., 2014a). They attribute the lower magma flux to the proximity of the GSC between 1 and 5 Ma (e.g., Wilson and Hey, 1995; Mittelstaedt et al., 2012), which may have diverted plume material toward the ridge, away from the volcanoes developing at the time, which are currently the older, central and eastern Galápagos islands.

Previous Field Studies of Santa Cruz Island

As the largest island in the center of the archipelago, Santa Cruz provides an opportunity to document how ocean islands mature as they are carried downstream from a mantle plume. Three previous field studies of Santa Cruz's development (Bow, 1979; Schwartz, 2014 M.Sc. thesis; Schwartz et al., 2022; the original Masters' thesis of Schwartz is available here: https://drive.google.com/file/d/1iMk9grGWRNORT7K2JxjsoXs4EY6IPKRU/view?usp=sharing), conclude that Santa Cruz has experienced two periods of volcanism and two periods of tectonic activity since

the volcano migrated east from the hotspot center during the last >1 million years, as follows (Ar-Ar ages all from Schwartz et al., 2022):

1. Formation of the Platform Series, emplaced primarily between 1620 ± 15 and 1160 ± 35 ka, with only a trivial volume of activity extending beyond 1160 ka.
2. Normal faulting of the Platform Series, exposed in the NE part of the island and striking sub-parallel to highland vent systems; faulting occurred since 1160 ± 35 ka and likely between 780 and 500 ka (Bow, 1979; Schwartz et al., 2022) and only crosscuts Platform lavas.
3. Formation of the Shield Series between 271 ± 17 and 74 ± 38 ka, erupted from the E-W summit vent system and deposited primarily along the southern flank of the island).
4. Formation of southern flank faults between 274 ± 18 and 38 ± 8 ka, which overlaps with the emplacement of the Shield Series, ending ~20 ka.

The Platform Series consists of lavas exposed primarily along the northeastern coast of Santa Cruz (**Figure 1B**), as well as Baltra and Seymour Islands, which are faulted remains of Santa Cruz (Bow, 1979). Platform Series lavas are both subaerial and submarine, thick (~10 m) pahoehoe flows, and many are interbedded with beach and shallow water deposits (Bow, 1979). Field observations confirm that the Platform Series lies stratigraphically below the Shield Series wherever a contact between the units is exposed. Schwartz et al. (2022) identified Platform Series lavas in several locations (e.g., SC12-572B) along the North Puerto Ayora fault that extends NW from Santa Cruz's largest town, along the south coast of the island. The 416 ± 36 ka (2σ) age of SC12-572B (Schwartz et al., 2022) is anomalously young for a Platform Series lava. Thus, the Platform Series may have been active as recently as ~0.4 Ma (nearly concurrent with some Shield Series flows), and may not have shut down entirely at ~1.1 Ma (White et al., 1993; Schwartz et al., 2022), but the lack of any other Platform Series samples from <1.1 Ma suggests that sample SC12-572B represents only a trivially small-volume tail of activity, and that the bulk of the Platform Series was emplaced between 1.6 and 1.1 Ma.

The Shield Series consists of predominantly pahoehoe flows erupted from the WNW-trending fissure system bisecting the island (**Figure 1B**; Bow, 1979). The fissures are manifested as a quasi-linear arrangement of late-stage cinder cones and pit craters in the highlands and tuff cones near the coast. Gravity studies by Cleary et al. (2020) confirm that they do not define the remnants of an in-filled caldera (Bow, 1979). Shield Series flows exhibit features typical of pahoehoe lava, with inflation lobes and tumuli.

Two Shield Series lavas have been dated using cosmogenic helium techniques, yielding ages between 0.111 ± 0.006 Ma and 0.585 Ma ± 0.013 (Kurz and Geist, 1999). On the basis of Ar-Ar ages and normal paleomagnetic polarity, Schwartz et al. (2022) estimates that the Shield Series became active ~700 ka. Consequently, >1 million years of volcanic and geochemical history are preserved and exposed at Santa Cruz. Unfortunately, dense vegetation severely limits detailed field mapping across most of the island.

Along the northern, eastern, and southern coasts, a series of normal faults strike sub-parallel to the highland cinder cone lineation (Schwartz et al., 2022; **Figure 1B**). Schwartz et al. (2022) proposes that the faults define two distinct periods of tectonic activity. The older faults, limited to the northeast quadrant, only crosscut Platform Series lavas and formed since 1160 ± 35 ka, and likely between 780 and 500 ka (Bow, 1979; Schwartz et al., 2022), as a consequence of regional extension early in the island's construction. The younger faults, along the southern flank, formed contemporaneously with the Shield Series, between 274 ± 18 and 38 ± 8 ka (Schwartz et al., 2022). Schwartz et al. (2022) attributes the younger faults to southward extension of the island caused by E-W-oriented magmatic intrusions that ceased ~20 ka.

MATERIALS AND METHODS

During July and August 2012, we collected >70 samples from Santa Cruz Island (**Figure 1B**), each of which was located by GPS (**Table 1**). An additional 10 samples were collected along the north shore in 2015. Owing to the lack of deeply eroded valleys or a caldera, most samples in this study originate from the uppermost stratigraphic layers of the volcano; only a handful of samples were collected from within pit craters; consequently we have no samples from early in the island's development. The rocks were broken into small chips by a jaw-crusher, and then examined under a binocular microscope to collect ~15 g of fresh material for chemical analysis.

Major and Trace Element Analysis

Samples were analyzed for major elements at Colgate University by X-Ray Fluorescence (XRF) spectroscopy following a method adapted from Norrish and Hutton (1969) on a Philips PW240 instrument. Replicate analyses of USGS Standard Reference Material (SRM) BHVO-2 yielded precision for all major element oxides <0.85% (1σ; **Table 1**). The precision of triplicate analyses of two samples (SC12-001 and SC12-063) yielded <1% relative standard deviation (RSD, 1σ) for all major elements, except P_2O_5 (1.2% RSD, 1σ). A subset of previously collected samples (Bow, 1979) was analyzed by XRF at Washington State University's (WSU) GeoAnalytical Laboratory following procedures described in Johnson et al. (1999). Whole rock major element data were not adjusted for phenocryst content (e.g., crystal accumulation).

Trace element concentrations were determined *via* Inductively Coupled Plasma-Mass Spectrometry (ICP-MS) using a Varian 820MS quadrupole instrument at Colgate University. A 200-ppb internal standard solution of ^{115}In, ^{133}Cs, ^{182}W, and ^{205}Tl was diluted to 1:20 using in-line mixing during analysis. Analyte masses were corrected to the nearest internal standard mass of those listed above to account for instrument drift, according to the method developed by Eggins et al. (1997). External standard curves were created using solutions of USGS SRMs BHVO-2, BIR-1, DNC-1, AGV-2, and W-2. The Pearson correlation coefficients of the standard curves were consistently >0.998. A solution of USGS SRM W-2 was analyzed every five to six samples

TABLE 1 | Santa Cruz sample locations and major element contents.

TABLE 1: Sample location and major element abundances (wt.%)

Sample	Compositional group	Latitude (degrees)	Longitude (degrees)	Altitude (m)	Mg#	SiO_2	TiO_2	Al_2O_3	FeO	CaO	MgO	MnO	K_2O	Na_2O	P_2O_5	Analytical total
SC-194R	Platform	—	—	—	49.74	48.65	2.09	16.84	10.66	11.78	5.92	0.20	0.41	3.14	0.30	96.98
SC-196P	Platform	—	—	—	47.51	47.82	2.76	14.72	13.08	10.89	6.64	0.22	0.36	3.24	0.27	99.19
SC-196R	Platform	—	—	—	47.35	47.78	2.75	14.77	13.12	10.90	6.62	0.22	0.37	3.19	0.27	99.10
SC12-008	Platform exposed in fault	−0.73420	−90.30904	28	63.41	47.07	1.29	16.73	10.44	11.14	10.15	0.18	0.23	2.61	0.17	98.18
SC12-009	Platform exposed in fault	−0.73273	−90.31274	34	52.14	48.46	2.06	17.20	10.13	11.15	6.19	0.17	0.53	3.70	0.40	99.13
SC12-020	Platform	−0.56739	−90.17453	36	45.02	47.57	2.63	14.64	13.28	11.65	6.10	0.23	0.41	3.21	0.29	98.89
SC12-020 re	Platform	−0.56739	−90.17453	36	42.41	46.88	2.59	14.43	14.54	11.48	6.01	0.22	0.40	3.17	0.28	98.89
SC12-022	Platform	−0.56759	−90.17432	28	44.39	46.80	2.67	14.27	14.72	11.07	6.59	0.22	0.37	2.98	0.30	98.16
SC12-025	Platform	−0.58009	−90.17335	27	40.91	49.55	2.26	17.47	10.97	10.75	4.26	0.22	0.56	3.56	0.39	98.77
SC12-054	Platform	−0.49092	−90.27768	50	50.59	46.76	1.96	16.20	12.93	10.80	7.43	0.20	0.35	3.09	0.27	99.24
SC12-055	Platform	−0.49145	−90.27637	40	51.85	46.75	1.87	16.39	12.66	10.81	7.65	0.19	0.33	3.08	0.25	98.94
SC12-056	Platform	−0.49903	−90.27050	48	59.25	47.61	1.77	14.56	12.22	10.22	9.97	0.17	0.35	2.88	0.25	98.83
SC12-057	Platform	−0.51080	−90.26462	88	45.89	46.71	2.36	15.43	13.56	10.82	6.45	0.20	0.45	3.69	0.33	98.73
SC12-058	Platform	−0.49198	−90.28540	14	59.54	46.48	1.64	16.20	11.55	11.44	9.53	0.17	0.25	2.51	0.21	98.70
SC12-059	Platform	−0.49388	−90.28613	28	55.04	47.34	2.09	16.87	11.17	10.91	7.67	0.18	0.33	3.15	0.28	98.57
SC12-059 re	Platform	−0.49388	−90.28613	28	52.41	46.76	2.06	16.66	12.27	10.77	7.58	0.18	0.32	3.11	0.28	98.57
SC12-060	Platform	−0.49394	−90.28582	30	42.17	46.38	2.72	15.18	15.02	10.05	6.14	0.23	0.47	3.44	0.36	98.81
SC12-061	Platform	−0.48504	−90.25501	49	40.95	47.87	3.36	13.08	14.60	11.22	5.68	0.21	0.56	2.97	0.44	98.19
SC12-062	Platform	−0.48445	−90.25042	48	40.68	48.09	3.46	13.12	14.77	10.62	5.68	0.21	0.54	3.07	0.43	98.24
SC12-063	Platform	−0.48924	−90.24891	19	35.02	48.31	3.18	13.49	15.44	9.49	4.67	0.25	0.67	3.85	0.65	98.79
SC12-064	Platform	−0.49030	−90.24870	22	44.26	48.75	3.38	13.49	13.29	10.91	5.92	0.22	0.51	3.06	0.47	99.07
SC12-065	Platform	−0.49461	−90.24798	28	64.02	46.60	1.64	15.57	10.75	11.34	10.73	0.17	0.26	2.68	0.25	98.58
SC12-066	Platform	−0.49347	−90.24911	32	42.13	47.21	2.78	14.39	14.49	10.62	5.92	0.23	0.46	3.53	0.36	99.01
SC12-067	Platform	−0.49090	−90.25342	48	41.18	47.04	2.82	14.58	14.61	10.61	5.74	0.22	0.46	3.54	0.38	99.21
SC12-068	Platform	−0.49303	−90.30752	10	51.39	46.76	2.16	16.54	12.59	10.53	7.47	0.18	0.36	3.11	0.30	98.55
SC12-069	Platform	−0.49594	−90.30007	16	61.38	46.19	1.59	15.26	12.18	10.52	10.86	0.18	0.26	2.71	0.23	99.08
SC12-070	Platform	−0.51437	−90.29446	74	61.61	46.99	1.53	14.55	12.07	10.87	10.87	0.17	0.17	2.58	0.19	98.74
SC12-572B	Platform exposed in fault	−0.73636	−90.30458	38	51.24	48.13	2.09	17.65	9.99	11.34	5.89	0.17	0.54	3.78	0.40	98.97
SC12-572B re	Platform exposed in fault	−0.73636	−90.30458	38	48.62	47.60	2.07	17.46	10.98	11.22	5.83	0.17	0.54	3.74	0.39	98.97
SC-64	Shield Low K/Ti (<0.15)	—	—	—	67.92	46.62	1.06	16.46	10.09	11.06	11.99	0.17	0.09	2.36	0.10	99.27
SC-78	Shield Low K/Ti (<0.15)	—	—	—	67.13	46.46	1.10	15.87	10.71	10.96	12.27	0.17	0.09	2.27	0.09	97.38
SC-163	Shield Low K/Ti (<0.15)	—	—	—	50.38	46.12	2.18	16.61	13.76	9.08	7.84	0.20	0.30	3.63	0.27	99.11
SC-193	Shield Low K/Ti (<0.15)	—	—	—	59.72	46.23	1.59	16.51	11.88	10.23	9.88	0.17	0.23	3.07	0.21	99.00
SC-193 re	Shield Low K/Ti (<0.15)	—	—	—	62.60	47.26	1.60	17.03	10.54	10.05	9.89	0.17	0.22	3.05	0.19	99.66
SC-202	Shield Low K/Ti (<0.15)	—	—	—	66.04	46.88	1.22	16.26	10.65	10.53	11.62	0.17	0.12	2.46	0.10	100.39
SC-206A	Shield Low K/Ti (<0.15)	—	—	—	53.51	46.05	2.70	18.64	11.83	9.67	7.64	0.19	0.14	2.80	0.33	95.94
SC12-001	Shield Low K/Ti (<0.15)	−0.73792	−90.30180	26	60.51	46.11	0.92	17.23	11.32	12.11	9.73	0.17	0.08	2.24	0.08	98.72
SC12-006	Shield Low K/Ti (<0.15)	−0.76233	−90.33024	0	63.79	45.88	1.26	16.07	11.40	11.19	11.27	0.16	0.15	2.46	0.15	98.42
SC12-011	Shield Low K/Ti (<0.15)	−0.73148	−90.31692	47	66.04	45.64	1.14	14.93	11.79	10.79	12.86	0.18	0.15	2.38	0.13	98.83
SC12-013	Shield Low K/Ti (<0.15)	−0.70175	−90.20954	3	61.04	46.06	1.34	15.90	11.79	11.40	10.37	0.17	0.19	2.61	0.17	98.87
SC12-014	Shield Low K/Ti (<0.15)	−0.68263	−90.22337	48	54.85	47.59	1.53	16.15	11.66	11.99	7.95	0.20	0.15	2.56	0.21	99.15
SC12-015	Shield Low K/Ti (<0.15)	−0.74286	−90.32467	41	61.65	46.20	1.29	16.41	11.34	11.52	10.22	0.16	0.16	2.56	0.14	98.80
SC12-015 re	Shield Low K/Ti (<0.15)	−0.74286	−90.32467	41	64.11	46.73	1.30	16.60	10.32	11.65	10.34	0.16	0.16	2.59	0.14	98.80
SC12-016	Shield Low K/Ti (<0.15)	−0.74328	−90.32431	38	58.52	46.63	1.37	16.49	11.73	11.47	9.28	0.17	0.17	2.54	0.15	98.59
SC12-019	Shield Low K/Ti (<0.15)	−0.63662	−90.29538	389	60.03	46.34	1.08	16.91	11.49	11.64	9.68	0.17	0.13	2.42	0.13	99.05
SC12-026	Shield Low K/Ti (<0.15)	−0.65736	−90.18756	18	64.67	46.46	1.28	15.94	10.71	11.88	11.00	0.17	0.09	2.34	0.12	99.30

(Continued on following page)

TABLE 1 | (*Continued*) Santa Cruz sample locations and major element contents.

TABLE 1: Sample location and major element abundances (wt.%)

Sample	Compositional group	Latitude (degrees)	Longitude (degrees)	Altitude (m)	Mg#	SiO_2	TiO_2	Al_2O_3	FeO	CaO	MgO	MnO	K_2O	Na_2O	P_2O_5	Analytical total
SC12-030	Shield Low K/Ti (<0.15)	−0.68891	−90.31452	236	66.24	45.65	1.33	16.24	11.20	10.20	12.33	0.16	0.17	2.50	0.20	98.37
SC12-036	Shield Low K/Ti (<0.15)	−0.64494	−90.33713	794	45.74	46.41	2.61	16.58	13.48	10.11	6.38	0.19	0.33	3.48	0.44	98.64
SC12-042	Shield Low K/Ti (<0.15)	−0.58966	−90.35444	346	64.55	45.46	1.16	15.12	12.23	10.65	12.50	0.17	0.13	2.45	0.12	98.67
SC12-043	Shield Low K/Ti (<0.15)	−0.62654	−90.38822	614	54.76	46.48	1.95	16.06	12.85	9.83	8.73	0.18	0.27	3.34	0.30	98.67
SC12-051	Shield Low K/Ti (<0.15)	−0.65260	−90.30449	540	53.43	46.73	2.25	16.76	12.49	9.44	8.04	0.19	0.31	3.43	0.36	98.83
SC12-071B	Shield Low K/Ti (<0.15)	−0.63275	−90.42808	379	53.50	46.57	2.32	16.56	12.76	9.12	8.24	0.17	0.29	3.64	0.31	98.79
SC12-570	Shield Low K/Ti (<0.15)	−0.73675	−90.30406	—	—	—	—	—	—	—	—	—	—	—	—	—
SC12-581	Shield Low K/Ti (<0.15)	−0.73418	−90.30901	35	60.87	46.09	1.52	15.83	12.17	10.03	10.62	0.17	0.20	3.16	0.21	98.05
SC12-584B	Shield Low K/Ti (<0.15)	−0.73856	−90.32131	31	61.79	46.11	1.29	16.21	11.61	11.27	10.53	0.17	0.16	2.51	0.14	98.23
SCZ15-01	Shield Low K/Ti (<0.15)	−0.56039	−90.52869	0	67.69	46.68	1.05	16.37	10.15	11.21	11.93	0.17	0.09	2.24	0.11	
SCZ15-02	Shield Low K/Ti (<0.15)	−0.55811	−90.51784	0	67.04	46.93	1.03	16.59	9.95	11.39	11.35	0.17	0.11	2.36	0.11	98.78
SCZ15-04	Shield Low K/Ti (<0.15)	−0.53149	−90.50382	0	58.99	47.15	1.50	16.68	11.09	11.61	8.95	0.19	0.15	2.48	0.20	98.33
SCZ15-08	Shield Low K/Ti (<0.15)	−0.51055	−90.37914	0	65.62	46.88	1.28	15.72	11.00	10.41	11.78	0.19	0.15	2.45	0.13	98.22
SCZ15-09	Shield Low K/Ti (<0.15)	−0.49385	−90.35193	0	63.56	47.23	0.97	17.45	10.38	10.98	10.15	0.17	0.10	2.49	0.08	98.61
SCZ15-10	Shield Low K/Ti (<0.15)	−0.49689	−90.33179	0	63.06	47.61	0.99	17.07	10.32	11.31	9.89	0.17	0.10	2.44	0.10	98.42
SC-46	Shield Mid K/Ti (0.15–0.24)	—	—	—	68.44	46.41	1.42	15.92	10.32	10.16	12.56	0.17	0.24	2.61	0.18	100.05
SC-130	Shield Mid K/Ti (0.15–0.24)	—	—	—	55.51	46.86	2.70	15.76	11.84	9.56	8.29	0.20	0.60	3.73	0.45	99.90
SC-135	Shield Mid K/Ti (0.15–0.24)	—	—	—	61.65	47.15	1.94	15.99	10.97	9.43	9.89	0.19	0.44	3.63	0.38	98.58
SC-155	Shield Mid K/Ti (0.15–0.24)	—	—	—	51.87	48.08	2.30	17.53	11.30	9.77	6.83	0.18	0.36	3.27	0.38	98.08
SC12-002	Shield Mid K/Ti (0.15–0.24)	−0.74343	−90.29953	5	58.15	46.37	1.93	15.86	12.33	9.67	9.61	0.17	0.31	3.45	0.29	98.94
SC12-007	Shield Mid K/Ti (0.15–0.24)	−0.76465	−90.33971	0	53.45	46.81	2.08	15.77	12.99	9.15	8.37	0.18	0.41	3.86	0.37	98.81
SC12-010	Shield Mid K/Ti (0.15–0.24)	−0.72552	−90.32068	88	64.76	45.65	1.42	15.77	11.50	10.56	11.85	0.17	0.27	2.54	0.26	98.55
SC12-012	Shield Mid K/Ti (0.15–0.24)	−0.69863	−90.22364	0	57.60	47.27	2.04	16.05	11.44	9.80	8.72	0.19	0.44	3.67	0.38	99.52
SC12-012 re	Shield Mid K/Ti (0.15–0.24)	−0.69863	−90.22364	0	55.02	46.67	2.01	15.85	12.55	9.68	8.61	0.19	0.43	3.63	0.38	99.52
SC12-018	Shield Mid K/Ti (0.15–0.24)	−0.63613	−90.29362	317	58.63	46.09	1.88	15.49	12.40	10.08	9.86	0.19	0.38	3.30	0.31	98.71
SC12-021	Shield Mid K/Ti (0.15–0.24)	−0.56800	−90.17459	33	48.18	47.01	1.98	16.93	12.20	11.53	6.36	0.20	0.32	3.18	0.28	99.02
SC12-023	Shield Mid K/Ti (0.15–0.24)	−0.57188	−90.17373	35	54.39	46.70	2.24	16.31	12.34	9.42	8.26	0.17	0.36	3.81	0.40	98.34
SC12-024	Shield Mid K/Ti (0.15–0.24)	−0.58360	−90.17330	16	53.32	46.67	2.19	16.52	12.48	9.21	8.00	0.17	0.46	3.92	0.39	98.42
SC12-029	Shield Mid K/Ti (0.15–0.24)	−0.63619	−90.29632	455	49.50	46.13	2.30	16.24	13.76	9.16	7.56	0.19	0.43	3.84	0.39	98.50
SC12-031	Shield Mid K/Ti (0.15–0.24)	−0.67224	−90.43854	250	53.11	46.37	2.33	15.84	13.11	8.96	8.33	0.19	0.49	3.92	0.47	98.32
SC12-032	Shield Mid K/Ti (0.15–0.24)	−0.67014	−90.43343	255	55.46	47.14	1.92	17.04	11.50	10.06	8.03	0.16	0.41	3.46	0.28	98.35
SC12-033	Shield Mid K/Ti (0.15–0.24)	−0.66427	−90.43870	227	62.92	46.82	1.38	16.78	10.58	11.12	10.07	0.17	0.22	2.66	0.19	98.76
SC12-034	Shield Mid K/Ti (0.15–0.24)	−0.63963	−90.43221	390	60.10	45.86	1.99	15.74	12.21	10.11	10.32	0.18	0.45	2.80	0.35	98.74
SC12-035	Shield Mid K/Ti (0.15–0.24)	−0.64285	−90.42131	425	54.44	46.23	1.85	16.29	13.17	9.57	8.83	0.18	0.28	3.29	0.29	98.75
SC12-037	Shield Mid K/Ti (0.15–0.24)	−0.66826	−90.32398	480	54.90	45.14	2.48	16.64	13.70	8.76	9.36	0.20	0.48	2.76	0.49	98.32
SC12-038	Shield Mid K/Ti (0.15–0.24)	−0.61789	−90.36569	623	58.42	46.07	2.05	16.98	11.59	10.26	9.13	0.16	0.30	3.21	0.25	98.55
SC12-041	Shield Mid K/Ti (0.15–0.24)	−0.59970	−90.36203	413	53.89	46.33	2.25	16.34	12.70	9.24	8.33	0.18	0.46	3.81	0.37	98.80
SC12-044	Shield Mid K/Ti (0.15–0.24)	−0.70893	−90.35719	145	57.19	46.47	1.84	16.01	12.66	9.03	9.49	0.18	0.34	3.67	0.29	98.62
SC12-046	Shield Mid K/Ti (0.15–0.24)	−0.66620	−90.39413	388	48.23	46.75	2.80	16.29	13.05	8.46	6.82	0.19	0.55	4.56	0.53	99.71
SC12-047	Shield Mid K/Ti (0.15–0.24)	−0.68480	−90.36601	251	54.39	46.94	2.03	16.92	12.06	9.01	8.07	0.16	0.44	4.01	0.36	98.66
SC12-048	Shield Mid K/Ti (0.15–0.24)	−0.64116	−90.28589	434	47.22	46.80	2.77	16.30	13.07	9.03	6.56	0.19	0.62	4.14	0.51	99.05
SC12-050	Shield Mid K/Ti (0.15–0.24)	−0.67753	−90.22904	75	56.83	46.28	2.18	16.43	11.89	10.07	8.78	0.17	0.47	3.40	0.32	98.72
SC12-071A	Shield Mid K/Ti (0.15–0.24)	−0.63275	−90.42808	379	61.37	45.39	1.91	15.69	12.29	10.45	10.95	0.18	0.33	2.50	0.29	98.71
SCZ15-03	Shield Mid K/Ti (0.15–0.24)	−0.54332	−90.51119	0	61.45	47.07	2.03	16.88	10.63	9.68	9.50	0.17	0.36	3.36	0.32	98.39
SCZ15-05	Shield Mid K/Ti (0.15–0.24)	−0.52595	−90.48788	0	57.17	47.47	2.02	17.01	11.27	9.40	8.44	0.18	0.35	3.55	0.33	98.14
SCZ15-06	Shield Mid K/Ti (0.15–0.24)	−0.51707	−90.46250	0	62.57	47.22	1.98	16.78	10.33	9.45	9.69	0.16	0.44	3.60	0.35	98.66

(Continued on following page)

TABLE 1 | (*Continued*) Santa Cruz sample locations and major element contents.

TABLE 1: Sample location and major element abundances (wt.%)

Sample	Compositional group	Latitude (degrees)	Longitude (degrees)	Altitude (m)	Mg#	SiO_2	TiO_2	Al_2O_3	FeO	CaO	MgO	MnO	K_2O	Na_2O	P_2O_5	Analytical total
SCZ15-07	Shield Mid K/Ti (0.15–0.24)	−0.50869	−90.41955	0	56.16	46.81	2.64	16.60	11.74	9.00	8.44	0.17	0.54	3.67	0.39	98.46
SC-151	Shield High K/Ti (>0.24)	—	—	—	45.24	48.24	2.88	17.04	11.58	8.21	5.37	0.20	0.82	4.95	0.71	99.13
SC-164	Shield High K/Ti (>0.24)	—	—	—	47.91	47.56	2.23	16.57	12.55	9.11	6.48	0.20	0.59	4.20	0.51	99.11
SC-172	Shield High K/Ti (>0.24)	—	—	—	50.25	47.71	2.52	16.59	11.68	8.79	6.62	0.20	0.70	4.65	0.53	98.36
SC-203R	Shield High K/Ti (>0.24)	—	—	—	49.69	47.98	2.54	17.11	11.59	8.65	6.42	0.19	0.71	4.28	0.52	98.69
SC-204R	Shield High K/Ti (>0.24)	—	—	—	52.06	47.44	2.59	16.76	11.52	8.81	7.02	0.20	0.78	4.33	0.55	100.62
SC-206B	Shield High K/Ti (>0.24)	—	—	—	46.30	49.04	2.54	17.55	11.22	8.42	5.42	0.20	0.64	4.31	0.65	97.90
SC-48	Shield High K/Ti (>0.24)	—	—	—	49.17	47.76	1.95	17.97	10.57	11.21	5.74	0.17	0.52	3.72	0.38	99.51
SC-48 re	Shield High K/Ti (>0.24)	—	—	—	52.19	48.66	1.99	18.44	9.37	11.09	5.73	0.16	0.51	3.70	0.35	98.87
SC-68	Shield High K/Ti (>0.24)	—	—	—	48.18	48.42	2.68	17.10	11.52	8.18	6.01	0.19	0.77	4.47	0.66	98.20
SC-207	Shield High K/Ti (>0.24)	—	—	—	48.65	48.36	2.43	16.89	11.85	8.16	6.30	0.20	0.63	4.66	0.52	100.31
SC-207 re	Shield High K/Ti (>0.24)	—	—	—	48.53	48.36	2.44	16.85	11.89	8.15	6.29	0.20	0.62	4.67	0.52	99.96
SC12-005	Shield High K/Ti (>0.24)	−0.76335	−90.32322	0	52.34	47.38	1.86	17.56	10.69	11.58	6.58	0.16	0.46	3.39	0.33	98.73
SC12-017	Shield High K/Ti (>0.24)	−0.63613	−90.29362	317	44.35	49.09	2.46	16.26	11.89	8.53	5.31	0.20	0.91	4.79	0.55	101.05
SC12-027	Shield High K/Ti (>0.24)	−0.63759	−90.29519	416	46.22	47.84	2.72	16.64	11.72	8.73	5.65	0.21	0.88	5.01	0.62	98.41
SC12-027 re	Shield High K/Ti (>0.24)	−0.63759	−90.29519	416	43.62	47.22	2.68	16.42	12.85	8.62	5.58	0.20	0.86	4.95	0.61	98.41
SC12-028	Shield High K/Ti (>0.24)	−0.63616	−90.29613	(~450)	53.13	47.60	1.73	16.93	11.52	10.04	7.33	0.18	0.49	3.79	0.39	98.68
SC12-039	Shield High K/Ti (>0.24)	−0.62178	−90.36564	649	49.93	46.99	2.35	16.44	12.71	8.78	7.11	0.19	0.65	4.26	0.51	98.72
SC12-040	Shield High K/Ti (>0.24)	−0.61715	−90.36520	603	49.58	46.70	2.59	16.22	12.68	9.00	7.00	0.20	0.79	4.27	0.56	99.02
SC12-049	Shield High K/Ti (>0.24)	−0.66909	−90.26491	268	49.48	47.58	2.48	15.80	12.87	8.81	7.07	0.19	0.72	3.91	0.55	99.15
SC12-053	Shield High K/Ti (>0.24)	−0.64296	−90.30057	529	45.57	47.64	2.39	16.61	12.69	9.23	5.96	0.20	0.61	4.12	0.54	98.67
SC12-572A	Shield High K/Ti (>0.24)	−0.73636	−90.30458	38	47.58	48.02	2.03	17.65	10.91	11.18	5.55	0.17	0.52	3.56	0.42	98.65
SC12-611B	Shield High K/Ti (>0.24)	−0.74902	−90.34772	31	—	—	—	—	—	—	—	—	—	—	—	—
SC12-004	Shield No K/Ti	−0.76318	−90.32148	6	—	—	—	—	—	—	—	—	—	—	—	—
SC12-045	Shield No K/Ti	−0.71260	−90.34650	137	—	—	—	—	—	—	—	—	—	—	—	—
SC12-052	Shield No K/Ti	−0.64436	−90.30355	554	—	—	—	—	—	—	—	—	—	—	—	—
SC12-582	Shield No K/Ti	−0.73264	−90.31273	—	—	—	—	—	—	—	—	—	—	—	—	—
SC12-583	Shield No K/Ti	−0.73417	−90.30876	41	—	—	—	—	—	—	—	—	—	—	—	—
SC12-584A	Shield No K/Ti	−0.73856	−90.32131	31	—	—	—	—	—	—	—	—	—	—	—	—
SC12-589	Shield No K/Ti	−0.74605	−90.28364	38	—	—	—	—	—	—	—	—	—	—	—	—
SC12-606	Shield No K/Ti	−0.73128	−90.31945	34	—	—	—	—	—	—	—	—	—	—	—	—
SC12-610	Shield No K/Ti	−0.74549	−90.32088	42	—	—	—	—	—	—	—	—	—	—	—	—
SC12-611A	Shield No K/Ti	−0.74902	−90.34772	31	—	—	—	—	—	—	—	—	—	—	—	—
SC12-612	Shield No K/Ti	−0.73911	−90.31348	—	—	—	—	—	—	—	—	—	—	—	—	—
SC12-613	Shield No K/Ti	−0.73911	−90.31348	0	—	—	—	—	—	—	—	—	—	—	—	—

Major element abundances are reported in weight % and normalized to 100%; analytical totals are included for reference. Samples lacking location data were not gathered in the field during our expeditions, but were obtained from existing collections by Bow (1979) and White et al. (1993). Several sample replicates (indicated with "re") for major element analyses are also included. See *text for explanation of compositional groups.*

as an unknown and yielded <4% RSD (1σ) precision for elements with atomic masses greater than 89. Only Sc and Rb registered precisions >8% (1σ) in replicate W-2 solutions run as unknowns; elements with masses less than 89 amu had precisions <8% and usually <5%. Corrections were made for isobaric interferences on Gd.

Radiogenic Isotope Analysis

Strontium, neodymium, and lead radiogenic isotope analyses were performed at the University of Florida's Department of Geological Sciences **Table 3**. Samples were leached aggressively to remove sea salt spray and weathering products according to procedures in Goss et al. (2010). All subsequent chromatographic elemental separations were performed in a class 100 clean laboratory. Samples were diluted with 2% HNO_3 to achieve ~4–6 V total ion current for each solution concentration. To monitor instrument performance, NBS 987 Sr and JNDi Nd standards were analyzed every four samples. External precision for Sr (2σ) is 0.00002 (n = 42) and 0.00002 (n = 91) for Nd. Strontium results were corrected to a $^{88}Sr/^{86}Sr$ value of 0.1194 and neodymium ratios were normalized to a $^{146}Nd/^{144}Nd$ value of 0.7219 using an exponential law for mass bias fractionation. Strontium and neodymium isotope ratios presented here have been corrected to SRM NBS 987 Sr ($^{87}Sr/^{86}Sr$ = 0.710248) and La Jolla ($^{143}Nd/^{144}Nd$ = 0.511858). The Pb standard, NBS 981, achieved a long-term (June 2012–January 2013) average of $^{206}Pb/^{204}Pb$ = 16.938 ± 0.004 (2σ), $^{207}Pb/^{204}Pb$ = 15.488 ± 0.003 (2σ), and $^{208}Pb/^{204}Pb$ = 36.693 ± 0.009 (2σ). The Pb isotopic analyses presented here are corrected to NBS 981 values $^{206}Pb/^{204}Pb$ = 16.9405, $^{207}Pb/^{204}Pb$ = 15.4963, and $^{208}Pb/^{204}Pb$ = 36.7219 (Weis et al., 2006). A subset of Santa Cruz samples were analyzed at the Pacific Centre for Isotopic and Geochemical Research (PCIGR) at the University of British Columbia, according to methods described in Harpp and Weis (2020). All data have been corrected to the same reference values as samples analyzed at the University of Florida.

RESULTS

Petrography

According to thin section observations, lavas in the Platform Series are aphyric to plagioclase-phyric with a subophitic groundmass composed of plagioclase, clinopyroxene, olivine, and opaque oxides. Plagioclase phenocrysts are up to 1 cm long, and constitute 1–3% of Platform Series samples. A plagioclase ultraphyric lava in the Cerro Colorado area contains 25% modal plagioclase, with crystals up to 10 × 5 mm, but its major element composition is not exceptional compared to the others from the same unit. Most lavas have sparse (<2%) olivine phenocrysts ~1 mm in diameter; however, olivine and plagioclase are often present in glomerocrysts up to 1 cm in diameter.

Shield Series lavas include plagioclase- and olivine-phyric rocks. Plagioclase and Ti-rich clinopyroxene are ubiquitous groundmass phases. Olivine is also present in the intergranular to subophitic groundmass. Plagioclase phenocrysts are variable in shape and typically between <1 and 5 mm long. They constitute up to 25% modal abundance in some samples, although the majority have <10% phenocrysts. Olivine phenocrysts are also prevalent in Shield Series lavas, usually <25% modal abundance. Olivine phenocrysts are subhedral to euhedral, ~1–2 mm in diameter, and some contain spinel inclusions. Hawaiites erupted at cinder and tuff cones preserve a pilotaxitic matrix rich in plagioclase microlites, oxidized olivine, and opaque oxides all <1 mm long.

Major Element Compositions

Major element concentrations of Santa Cruz lavas define a wide compositional range that spans values observed across the archipelago (**Figures 2–4**; **Table 1**; e.g., White et al., 1993), despite a relatively small range of SiO_2 contents (45.1–49.6 wt.%); rocks are tholeiitic to weakly alkaline (**Figure 2**). Major element variations do not exhibit any systematic geographic pattern. Santa Cruz lavas have between 4.3 and 12.9 wt.% MgO, extending to both more primitive and evolved compositions than Fernandina and most of the other active volcanoes in the western Galápagos (**Figures 3A–H**; Allan and Simkin, 2000). At a given Mg# value, Santa Cruz has lower TiO_2 and CaO contents than Fernandina, but higher Al_2O_3, FeO_t, Na_2O, and P_2O_5. In general, K_2O values at a given Mg# are higher than those from Fernandina for most of the Shield series, but lower for the Platform Series.

The Platform Series rocks are more fractionated than Shield lavas, but cannot be produced from the more primitive Shield Series samples, owing to their different incompatible element ratios and the distinct trends they define in Harker diagrams. The lack of dominant trends in either the Platform or Shield Series lavas suggests that there is not a single parental melt composition responsible for each geologic unit; instead, there must be an array of primary melt compositions and depths of melt generation within both the Shield and Platform Series. Similarly, the range of FeO_t contents in primitive lavas may signal that the mantle source includes a pyroxenitic component, as has been proposed for other lavas from the central Galápagos (Gleeson et al., 2020).

In CaO-Mg# space (**Figure 3E**), Santa Cruz lavas define two broad trends. The positive trend that includes most of the Shield Series lavas likely reflects control primarily by clinopyroxene fractionation, whereas the shallower trend defined by Platform lavas and a handful of mostly low K_2O/TiO_2 Shield lavas has experienced less clinopyroxene fractionation. The high modal abundance of plagioclase and elevated Al_2O_3 contents of many Shield Series lavas indicates that there has been plagioclase accumulation. In contrast, the Platform Series' lower Al_2O_3 contents suggest greater control by plagioclase fractionation.

The Platform Series defines a horizontal array in Mg#-K_2O/TiO_2 space, varying between ~0.1 and 0.25 in K_2O/TiO_2. The low FeO and MgO values of some Platform Series suggest that a few may have fractionated Fe-Ti oxides, although to a limited extent given that these lavas maintain relatively elevated TiO_2 contents (**Figures 3B,D**). The Shield Series array is negatively sloped in Mg#-K_2O/TiO_2 space; consequently, we have divided the Shield Series into three compositional sub-groups (**Figure 4**). Shield Series lavas with K_2O/TiO_2 <0.15 are classified as the Low K_2O/

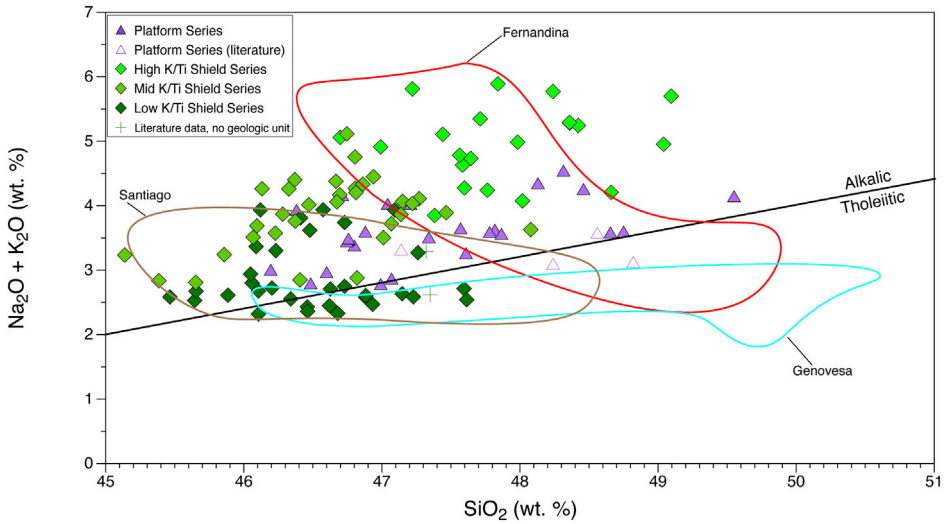

FIGURE 2 | Alkali-silica diagram of Santa Cruz lavas. The alkalic-tholeiitic dividing line is from Macdonald and Katsura, 1964). Fields are literature data. Red: Fernandina, blue: Genovesa, brown: Santiago (White et al., 1993; Harpp et al., 2002; Harpp et al., 2003; Saal et al., 2007; Gibson and Geist, 2010; Gibson et al., 2012; Harpp et al., 2014a). Samples indicated by a cross are literature data from Santa Cruz (White et al., 1993; Kurz and Geist, 1999; Saal et al., 2007); they have not been attributed to either the Platform or Shield Series owing to a lack of GPS coordinates for their origin locations.

TiO_2 suite. These samples have the highest MgO and CaO, and the lowest K_2O, TiO_2, Na_2O, and P_2O_5, of the Shield Series (**Figures 3A,B,E–H**). Samples with K_2O/TiO_2 >0.25 are the High K_2O/TiO_2 suite, and constitute the most evolved lavas within the Shield. Lavas with K_2O/TiO_2 values between 0.15 and 0.25 are designated as the Mid K_2O/TiO_2 suite of the Shield Series (**Figure 4**).

Trace Element Compositions

Broadly, trace element concentrations vary from depleted, near-MORB-like values to more enriched compositions typical of ocean island basalt (**Table 2**; White et al., 1993). The Platform Series exhibits less compositional variability in trace element contents than the Shield Series (**Figures 5–7**).

Rare Earth Elements

Santa Cruz lavas exhibit a wide range of Rare Earth Element (REE) compositions. Chondrite-normalized REE concentrations of Platform Series lavas define nearly linear patterns with slight negative slopes (**Figure 5**). Most Platform Series REE patterns are parallel to each other, with minor variations in slope steepness in the mid-to-heavy REEs. Platform Series lavas mostly have minor negative europium anomalies.

The Shield Series lavas exhibit greater variability than the Platform Series in terms of absolute REE concentrations and their patterns (**Figure 5**). The High K_2O/TiO_2 Shield Series lavas are most similar to the Platform Series, with relatively gentle, negatively sloping patterns and Eu anomalies that range from slightly negative to zero. The Low K_2O/TiO_2 Shield Series has the most depleted REE compositions, with positive light-REE (LREE) slopes for some samples, a common characteristic of MORB (e.g., Workman and Hart, 2005; McLennan and Taylor, 2012); others have gentle negative LREE slopes, more like the High K_2O/TiO_2 suite, but with flatter LREE slopes. The Mid K_2O/TiO_2 Shield lavas resemble the more enriched Low K_2O/TiO_2 group, but several have steeper LREE slopes. A few samples from across the island also exhibit minor negative Ce anomalies.

Incompatible Trace Elements

All three Shield Series K_2O/TiO_2 groups have compositions that overlap significantly but not completely in primitive mantle-normalized trace element contents (**Figure 7**). Generally, the Platform and High K_2O/TiO_2 Shield samples have the highest incompatible trace element (ITE) concentrations, and the Low K_2O/TiO_2 Shield lavas have the lowest. Most Santa Cruz lavas are enriched in the High Field Strength Elements (HFSE; Ti, Nb, Zr, Hf, Ta) compared to less incompatible elements, but the extent of enrichment varies. Within each eruptive unit, ITE concentrations vary by up to a factor of four relative to primitive mantle (**Figure 6**).

The Low K_2O/TiO_2 suite is the least enriched group of the Shield Series, and the High K_2O/TiO_2 lavas are the most enriched (**Figure 6**). Shield Series lavas exhibit positive slopes for the most incompatible trace elements and negative slopes for the less incompatible ones. The Low K_2O/TiO_2 suites have mostly positive Sr anomalies, whereas the High K_2O/TiO_2 and Platform Series lavas' Sr anomalies are negative, and the Mid K_2O/TiO_2 have both types. Many Low and Mid K_2O/TiO_2 suite samples also exhibit small positive Ba anomalies, as is the case for Floreana lavas (e.g., Harpp et al., 2014a). By contrast, the Platform Series has positive Ba but negative Sr anomalies. Taken as a whole, Santa Cruz lavas have ITE contents that span the range between Genovesa's depleted and Fernandina's enriched compositions (**Figure 6**; White et al., 1993; Harpp and White, 2001).

Variations in light (La_n/Sm_n) and heavy REE (HREE) ratios (Sm_n/Yb_n) for Santa Cruz also vary widely (**Figure 7A**). Santa

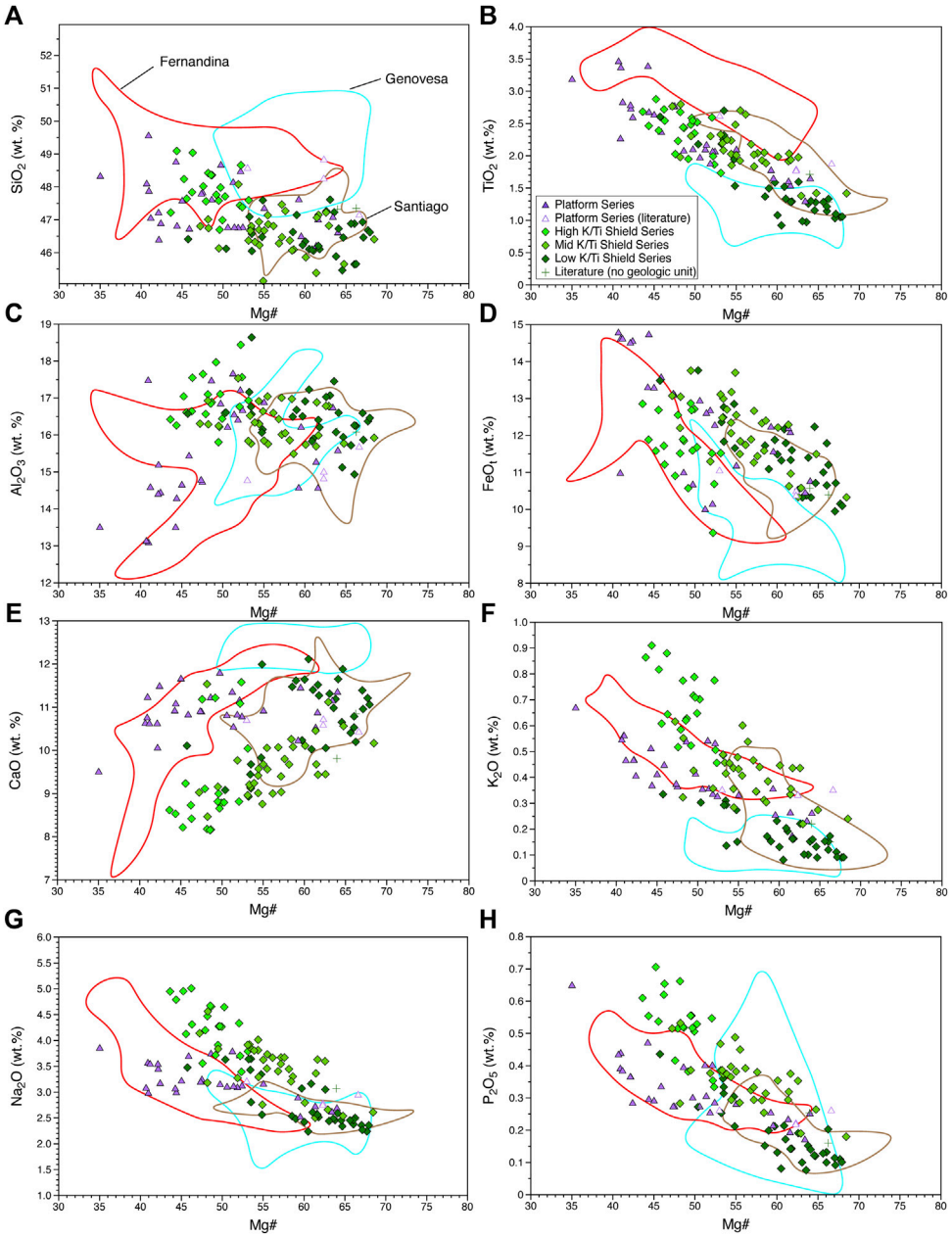

FIGURE 3 | Selected major element variation versus Mg# for Santa Cruz lavas. Fields are literature data. Red: Fernandina, blue: Genovesa, brown: Santiago (White et al., 1993; Harpp et al., 2002; Harpp et al., 2003; Saal et al., 2007; Gibson and Geist, 2010; Gibson et al., 2012; Harpp et al., 2014a). Concentrations are in weight percent (wt.%) and have been normalized to 100%. Mg# = [molar Mg/(Mg + Fe)]. Symbols are larger than 1σ analytical error. Samples indicated by a cross are literature data from Santa Cruz (White et al., 1993; Kurz and Geist, 1999; Saal et al., 2007); they have not been attributed to either the Platform or Shield Series owing to a lack of GPS coordinates for their origin locations. **(A)** SiO_2-Mg#; **(B)** TiO_2-Mg#; **(C)** Al_2O_3-Mg#; **(D)** FeOtotal-Mg#; **(E)** CaO-Mg#; **(F)** K_2O-Mg#; **(G)** Na_2O-Mg#; **(H)** P_2O_5-Mg#

Cruz lavas define a broad range in La_n/Sm_n at $Sm_n/Yb_n < 2.6$. The Shield Series' Low K_2O/TiO_2 lavas have the greatest variability in LREE and HREE ratios, and the Mid K_2O/TiO_2 lavas overlap the Low K_2O/TiO_2 group in all but the lowest values; the Shield's High K_2O/TiO_2 suite exhibits less variation as well as the island's highest La_n/Sm_n values. The Platform Series overlaps the Shield's Mid K_2O/TiO_2 lavas, but also has some of the highest Sm_n/Yb_n observed on the island. Compared to the rest of the Galápagos Archipelago, LREE and HREE ratios of Santa Cruz lavas extend between the fields of Fernandina and Genovesa, with little overlap into the shallow-melting, low Sm_n/Yb_n field of Floreana (White et al., 1993; Harpp et al., 2014a).

Ratios of comparably incompatible trace elements are relatively consistent across Santa Cruz, whereas the Platform

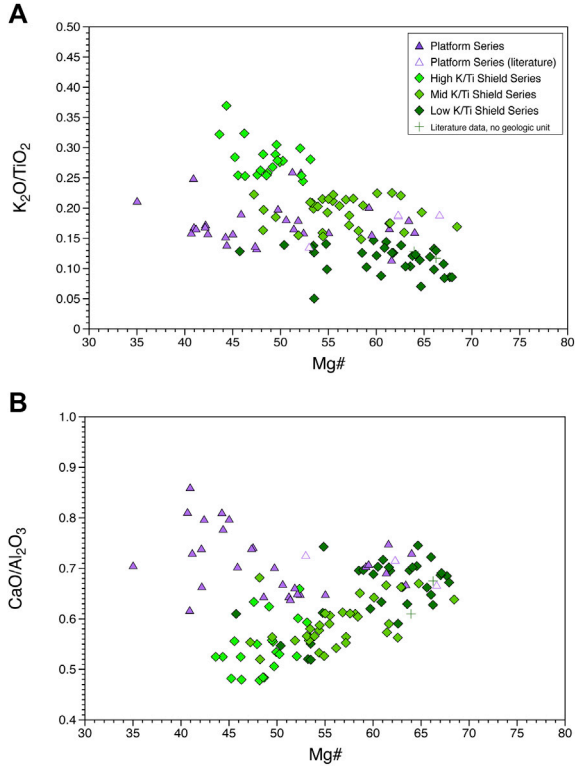

FIGURE 4 | Major element ratio variation with Mg# for Santa Cruz lavas. **(A)** K_2O/TiO_2, to illustrate how Shield Series sub-groups were defined. **(B)** CaO/Al_2O_3. Concentrations are in weight percent (wt.%) and have been normalized to 100%. Symbols are larger than 1σ analytical error. Samples indicated by a cross are literature data from Santa Cruz (White et al., 1993; Kurz and Geist, 1999; Saal et al., 2007); they have not been attributed to either the Platform or Shield Series owing to a lack of GPS coordinates for their origin locations.

Series is slightly more enriched in the more incompatible elements and in fluid-mobile elements. For instance, the Nb/Zr ratio of the Platform Series is 0.064 (± 0.009 1σ; n = 32), and the Shield value is 0.049 ± 0.011 (1σ; n = 93); the Platform Series Ba/La is 7.97 (± 3.89 1σ; n = 32) compared to the Shield Series' 5.34 (± 1.24 1σ; n = 94). Santa Cruz ITE ratios define distinct fields from those of most other Galápagos volcanoes, and usually fall between the Fernandina and Genovesa fields. Across the archipelago, Santa Cruz ITE ratios are most similar to Santiago's less enriched lavas (**Figure 7**; Gibson et al., 2012) and rocks from Volcán Wolf (Geist et al., 2005).

The variation across Santa Cruz in La_n/Sm_n (Platform: 1.17–1.97; Shield: 0.51–2.15) and Sm_n/Yb_n (Platform: 1.67–2.56; Shield: 0.98–2.55) indicates that the island's lavas were generated across a range of extents and depths of melting, similar to those at Santiago Island (Gibson et al., 2012). Comparison of Sm_n/Yb_n values as an indication of depth of melting reveals that the Platform and Shield Series' averages are similar, but the Shield Series varies more than the Platform (Platform average Sm_n/Yb_n = 1.90 ± 0.23 (1σ), n = 31; Shield average Sm_n/Yb_n = 1.91 ± 0.34 (1σ), n = 90). The Shield and Platform Series lavas have nearly identical Sm_n/Yb_n maxima (~2.55), but the Shield minimum indicates shallower melting (0.98) than Platform lavas (1.67). The Shield's Low K_2O/TiO_2 lavas exhibit the shallowest melting, with an average Sm_n/Yb_n of 1.63 (± 0.34 (1σ), n = 32). The Shield Mid and High K_2O/TiO_2 rocks have higher averages, indicative of deeper melting (Shield Mid Sm_n/Yb_n = 2.10 ± 0.20 (1σ), n = 33; Shield High Sm_n/Yb_n = 2.14 ± 0.19 (1σ), n = 16).

Isotopic Ratios

Basalts from Santa Cruz define a wider range of isotopic ratios than those erupted at most other Galápagos Islands (**Figures 8A–D**; **Table 3**, e.g., White et al., 1993). The $^{87}Sr/^{86}Sr$ ratios vary from 0.702633 to 0.702959, and ε_{Nd} values extend from 7.77 to 9.43. Lead isotopic ratio ranges are 18.531–18.947 for $^{206}Pb/^{204}Pb$, 15.519–15.560 for $^{207}Pb/^{204}Pb$, and 38.071–38.515 for $^{208}Pb/^{204}Pb$. Platform Series lavas are generally more enriched than the Shield Series. Even though there is overlap between the two groups, taking into account analytical uncertainty, the averages of the Platform and Shield Series lavas in all isotopic ratios are significantly different from each other at >95% certainty. The enrichment in Platform over Shield Series lavas supports previous observations based on fewer samples (White et al., 1993).

The most depleted signatures of the Shield Series (e.g., $^{87}Sr/^{86}Sr < 0.7027$; $\varepsilon_{Nd} > 9$) resemble material erupted at Genovesa Island in the Northern Galápagos Volcanic Province (NGVP; e.g., Harpp et al., 2003; Harpp et al., 2014c). The most enriched Santa Cruz lavas are comparable to the enriched material erupted at other eastern Galápagos volcanoes, including Santiago and San Cristóbal, which also display comparable ranges in isotopic ratios (e.g., Geist et al., 1986; Gibson et al., 2012). Santa Cruz lavas are not as enriched as those produced at volcanic centers closer to the leading edge of the plume, such as Fernandina, Volcán Sierra Negra, and Volcán Cerro Azul (e.g., White et al., 1993; Allan and Simkin, 2000; Naumann et al., 2002).

Relationship between Incompatible Trace Element Ratios and Isotopic Ratios

Santa Cruz geochemical variations are consistent with the archipelago-wide observation first noted by Kurz and Geist (1999) that ε_{Nd} has a strong negative correlation with Nb/La (**Figure 9**), and therefore that Nb/La can be a proxy for plume material (highest Nb/La = greatest plume contribution). Santa Cruz compositions extend from the depleted Genovesa field and overlap with the depleted end of the Santiago field. Santiago, in turn, extends toward Fernandina's enriched compositions, resulting in a relatively coherent array in Nb/La-ε_{Nd} space. The average Nb/La of the older Platform Series (1.00 ± 0.08 1σ; n = 31) is significantly higher than that of the Shield Series (0.88 ± 0.12 1σ; n = 89), consistent with radiogenic isotope ratio systematics that indicate a decrease in the contribution of enriched plume material to Santa Cruz lavas over time (**Figures 8E,F**; White et al., 1993). Variations in isotopic ratios with ITE ratios such as La_n/Sm_n whose elements differ more in their incompatibility than Nb/La display a different pattern. Most Galápagos lavas define a broadly binary array in ε_{Nd}-La_n/Sm_n

TABLE 2 | Trace element abundances of Santa Cruz lavas, reported in parts per million (ppm). One replicate analysis (indicated by "re") is included.

Sample	Comp. Group	Sc	V	Cr	Co	Ni	Cu	Zn	Rb	Sr	Y	Zr	Nb	Ba	La	Ce	Pr	Nd	Sm	Eu	Gd	Tb	Dy	Ho	Er	Tm	Yb	Lu	Hf	Ta	Pb	Th	U
SC-194	Platform	37.7	305	156	55.7	58.0	76.6	94.5	6.45	322	41.3	199	13.2	67.3	12.5	30.4	4.53	20.6	5.67	1.75	6.13	1.05	6.69	1.38	3.78	0.55	3.41	0.50	4.45	0.80	1.29	1.07	0.33
SC-194R	Platform	35.4	285	134		51.9	74.0	91.2	6.35	315	38.8	194	11.5	64.5	12.4	30.1	4.41	20.7	5.95	2.04	6.85	1.16	7.37	1.52	4.08	0.58	3.59	0.52	4.71	0.77	0.99	1.08	0.33
SC-196	Platform	40.4	393	124	77.2	63.0	99.8	109	5.00	272	40.3	181	11.7	68.6	12.3	28.9	4.45	21.3	6.00	1.98	6.53	1.10	6.95	1.44	4.00	0.58	3.53	0.52	4.13	0.73	1.23	0.82	0.25
SC-196P	Platform	40.3	388	114		60.7	97.4	108	4.93	270	37.5	174	10.5	63.9	11.0	27.9	4.18	19.9	5.86	2.15	6.89	1.18	7.44	1.52	3.99	0.57	3.40	0.48	4.27	1.28	1.00	0.78	0.24
SC-196R	Platform	39.9	389	113		61.4	97.6	108	4.94	270	37.8	176	10.1	63.8	11.0	28.0	4.17	20.0	5.85	2.21	6.85	1.17	7.43	1.52	4.05	0.56	3.37	0.49	4.29	0.72	0.92	0.78	0.25
SC12-008	Platform exp. fault	36.7	248	146	36.9	66.2	51.6	75.2	7.50	308	34.3	222	15.6	88.3	15.3	36.2	4.78	20.2	5.03	1.65	5.42	0.91	5.62	1.18	3.24	0.47	2.95	0.43	4.36	1.00	1.39	1.35	0.47
SC12-009	Platform exp. fault	29.0	240	265	56.8	233	65.7	72.5	2.88	247	23.4	134	6.90	45.7	7.29	18.6	2.69	12.1	3.30	1.13	3.65	0.62	3.98	0.84	2.31	0.34	2.09	0.31	2.72	0.45	0.82	0.53	0.16
SC12-020	Platform	39.5	377	134	47.1	69.6	51.5	101	3.25	279	35.2	158	10.1	67.3	9.70	24.6	3.68	17.7	5.05	1.71	5.55	0.94	5.98	1.24	3.37	0.49	3.01	0.44	3.69	0.64	0.81	0.68	0.11
SC12-022	Platform	41.0	433	123	48.5	64.0	98.8	111	3.73	275	39.5	181	11.5	70.6	10.7	27.4	4.07	19.4	5.60	1.93	6.20	1.06	6.65	1.39	3.83	0.55	3.35	0.49	4.13	0.73	1.23	0.78	0.24
SC12-025	Platform	33.4	302	75.7	35.3	33.7	74.6	108	5.53	279	52.6	269	18.5	101	20.2	48.1	6.70	30.1	8.10	2.37	8.42	1.43	8.86	1.82	5.01	0.73	4.41	0.64	6.16	1.16	1.63	1.68	0.20
SC12-054	Platform	35.0	273	69.0	49.1	102	80.5	94.9	4.18	305	35.5	206	9.69	74.6	9.93	25.2	3.69	17.5	4.91	1.69	5.40	0.93	5.80	1.23	3.40	0.49	3.05	0.46	4.40	0.62	1.13	0.72	0.22
SC12-055	Platform	36.1	280	73.0	52.8	116	91.5	93.3	3.77	315	35.1	166	9.29	59.0	10.5	24.6	3.72	17.7	4.79	1.58	5.19	0.87	5.47	1.14	3.14	0.46	2.88	0.42	3.53	0.58	1.06	0.67	0.21
SC12-056	Platform	28.3	216	414	54.4	278	74.6	89.6	4.52	278	27.4	140	10.3	74.2	9.42	22.7	3.23	14.9	4.03	1.34	4.46	0.74	4.75	0.98	2.63	0.38	2.32	0.34	3.12	0.64	1.09	0.74	0.21
SC12-057	Platform	38.4	307	124	45.6	62.0	77.0	95.8	5.57	366	36.8	210	11.7	80.0	11.9	30.8	4.53	20.8	5.55	1.87	6.01	1.01	6.14	1.28	3.51	0.50	3.11	0.45	4.40	0.74	1.41	0.76	0.24
SC12-058	Platform	33.6	246	299	47.5	150	92.3	74.9	2.54	386	26.8	130	7.27	57.0	7.40	19.1	2.81	13.3	3.80	1.32	4.25	0.71	4.54	0.93	2.58	0.37	2.28	0.33	2.82	0.46	0.96	0.50	0.09
SC12-059	Platform	31.5	256	101	46.1	110	69.1	87.1	4.07	346	34.2	181	10.3	73.4	10.8	26.9	3.92	18.3	4.97	1.70	5.53	0.91	5.68	1.16	3.23	0.46	2.84	0.42	3.80	0.66	1.17	0.71	0.22
SC12-060	Platform	37.2	348	43.0	46.7	62.0	80.7	124	4.30	299	57.1	242	13.5	90.7	15.1	36.7	5.57	26.1	7.30	2.42	8.13	1.38	8.62	1.85	5.20	0.74	4.55	0.67	5.26	0.88	1.44	0.95	0.28
SC12-061	Platform	41.2	422	91.0	48.3	55.0	138	133	8.50	324	53.7	283	22.7	127	20.7	51.1	7.32	33.7	8.86	2.70	8.91	1.48	8.61	1.72	4.53	0.63	3.80	0.55	6.27	1.37	1.48	1.51	0.49
SC12-062	Platform	36.8	413	81.0	44.5	50.0	131	129	8.80	316	47.0	284	22.5	108	18.7	46.3	6.74	31.5	8.60	2.71	8.96	1.44	8.33	1.65	4.44	0.61	3.65	0.52	6.62	1.48	1.54	1.49	0.51
SC12-063	Platform	35.1	303	61.0	37.7	29.0	56.2	148	5.90	296	71.2	334	22.6	464	22.2	53.1	7.80	36.6	10.1	3.36	11.2	1.89	11.6	2.43	6.76	0.96	5.85	0.84	7.26	1.44	1.78	1.65	0.17
SC12-064	Platform	35.1	375	96.7	41.4	49.3	98.9	125	7.43	327	48.6	281	22.2	271	19.1	47.9	7.03	32.0	8.74	2.81	9.13	1.47	8.66	1.74	4.52	0.63	3.74	0.54	6.58	1.46	1.46	1.50	0.47
SC12-065	Platform	30.3	237	418	53.7	228	86.8	77.7	2.67	290	24.9	130	7.53	64.7	7.57	19.1	2.77	13.0	3.63	1.27	4.08	0.68	4.24	0.87	2.40	0.35	2.12	0.32	2.79	0.48	0.95	0.57	0.15
SC12-066	Platform	37.9	427	81.0	42.1	49.0	77.2	111	4.26	276	48.4	242	13.6	112	13.6	34.6	5.09	23.8	6.64	2.21	7.38	1.27	7.87	1.67	4.65	0.67	4.12	0.61	5.32	0.89	1.38	0.97	0.32
SC12-067	Platform	40.4	442	87.0	45.3	52.0	73.8	115	5.06	274	47.6	239	13.5	88.4	13.2	33.6	4.96	23.2	6.51	2.16	7.21	1.24	7.74	1.64	4.57	0.66	4.07	0.60	5.21	0.87	1.37	0.95	0.26
SC12-068	Platform	29.8	250	99.0	47.7	117	70.4	91.1	3.71	339	35.2	186	10.9	74.4	11.4	28.0	4.07	19.1	5.16	1.76	5.57	0.93	5.80	1.19	3.24	0.47	2.91	0.43	3.94	0.71	1.16	0.75	0.20
SC12-069	Platform	32.5	249	402	50.7	201	75.2	82.7	3.59	273	31.0	145	10.7	148	9.47	23.0	3.34	15.5	4.22	1.45	4.79	0.79	5.17	1.08	2.96	0.44	2.71	0.40	3.20	0.69	1.07	0.63	0.18
SC12-070	Platform	31.6	229	493	62.3	325	83.4	89.0	1.93	262	28.8	112	7.09	136	7.40	17.3	2.63	12.1	3.41	1.19	3.89	0.67	4.35	0.92	2.52	0.37	2.22	0.32	2.43	0.43	0.85	0.44	0.13
SC12-572B	Platform exp. fault	38.3	295	172	40.4	69.1	52.2	88.1	9.32	340	40.6	254	18.3	112	18.3	41.6	5.56	24.3	6.06	1.96	6.45	1.08	6.73	1.40	3.87	0.57	3.53	0.52	5.17	1.18	1.80	1.45	0.43
SC-64	Shield Low K/Ti	40.4	393	124	77.2	63.0	99.8	109	5.00	272	40.3	181	11.7	68.6	12.3	28.9	4.47	21.0	6.00	1.98	6.59	1.10	6.95	1.44	3.96	0.58	3.53	0.52	4.13	0.73	1.23	0.82	0.25
SC-78	Shield Low K/Ti	30.0	215	515	76.3	308	80.5	70.7		248	20.1	81.3	4.17	29.4	3.35	10.6	1.74	8.76	2.65	0.93	3.07	0.53	3.43	0.73	2.02	0.30	1.80	0.26	1.86	0.87	0.69	0.22	0.05
SC-163	Shield Low K/Ti	26.4	182	179		140	61.5	85.1	1.78	382	38.0	220	9.19	58.7	13.2	33.4	4.94	23.5	6.10	2.21	6.95	1.16	7.19	1.50	3.99	0.56	3.46	0.52	4.67	0.75	1.07	0.69	0.22

(Continued on following page)

TABLE 2 | (*Continued*) Trace element abundances of Santa Cruz lavas, reported in parts per million (ppm). One replicate analysis (indicated by "re") is included.

Sample	Comp. Group	Sc	V	Cr	Co	Ni	Cu	Zn	Rb	Sr	Y	Zr	Nb	Ba	La	Ce	Pr	Nd	Sm	Eu	Gd	Tb	Dy	Ho	Er	Tm	Yb	Lu	Hf	Ta	Pb	Th	U
SC-202	Shield Low K/Ti	30.0	215	515	76.3	308	80.5	70.7		248	20.1	81.3	4.17	29.4	3.48	11.0	1.81	8.85	2.65	0.93	3.07	0.53	3.43	0.73	2.02	0.30	1.80	0.27	1.86	0.87	0.69	0.22	0.05
SC-206A	Shield Low K/Ti	37.9	260	229	58.9	122	76.6	90.8		403	37.9	240	10.4	59.0	12.1	32.9	4.99	23.1	6.05	2.00	6.27	1.02	6.12	1.26	3.38	0.49	3.05	0.45	4.72	0.77	1.35	0.60	0.19
SC12-001	Shield Low K/Ti	35.6	213	212	54.4	165	92.4	64.7	0.28	172	20.6	47.3	1.62	11.1	1.95	5.51	1.00	5.31	1.85	0.71	2.55	0.46	3.25	0.74	2.15	0.32	2.06	0.30	1.25	0.12	0.27	0.04	
SC12-006	Shield Low K/Ti	32.7	209	399	58.0	237	69.2	70.7	0.65	313	21.2	92.8	3.97	22.6	4.76	12.9	2.02	9.88	2.89	1.04	3.35	0.57	3.60	0.76	2.14	0.30	1.88	0.27	2.12	0.26	0.52	0.21	0.07
SC12-011	Shield Low K/Ti	36.0	229	548	60.4	308	39.2	68.8	1.48	170	22.2	79.1	3.85	20.0	4.02	10.7	1.64	7.91	2.35	0.82	2.93	0.53	3.59	0.79	2.30	0.35	2.21	0.33	1.78	0.26	0.46	0.21	0.05
SC12-013	Shield Low K/Ti	29.8	210	279	51.2	188	83.5	66.8	1.57	285	19.9	95.0	4.57	26.2	4.96	13.4	2.06	9.89	2.85	1.02	3.32	0.55	3.50	0.73	2.00	0.29	1.77	0.25	2.14	0.30	0.58	0.24	0.08
SC12-014	Shield Low K/Ti	44.2	291	234	49.5	111	97.3	78.1	0.62	195	30.5	101	5.43	31.6	5.20	14.1	2.22	10.9	3.34	1.20	4.14	0.73	4.84	1.03	2.96	0.44	2.77	0.41	2.35	0.35	0.43	0.19	0.06
SC12-015	Shield Low K/Ti	34.2	212	309	53.7	184	55.6	62.3	0.97	302	19.1	84.7	3.54	22.6	4.16	11.5	1.82	9.04	2.68	0.98	3.10	0.53	3.32	0.70	1.92	0.28	1.73	0.25	2.00	0.23	0.45	0.18	0.04
SC12-016	Shield Low K/Ti	33.9	248	602	56.5	173	80.6	74.7	1.32	309	22.0	99.2	4.18	22.8	4.75	13.4	2.11	10.3	3.02	1.07	3.54	0.59	3.74	0.79	2.19	0.32	1.94	0.28	2.21	0.27	0.61	0.20	0.08
SC12-019	Shield Low K/Ti	27.5	215	204	49.7	149	76.3	56.8	0.47	232	15.2	58.1	2.53	14.3	2.78	8.15	1.25	6.18	1.92	0.73	2.34	0.40	2.62	0.56	1.57	0.23	1.40	0.21	1.39	0.17	0.32	0.07	
SC12-026	Shield Low K/Ti	36.1	257	380	59.0	219	119	73.1		260	21.8	71.1	2.34	23.3	2.10	8.67	1.55	8.09	2.58	0.94	2.91	0.54	3.50	0.74	2.07	0.30	1.84	0.27	1.79	0.16	0.60	0.10	0.05
SC12-030	Shield Low K/Ti	28.2	170	455	65.0	406	56.5	63.9	0.92	310	22.1	135	5.21	27.1	6.70	18.0	2.74	12.9	3.44	1.18	3.82	0.63	3.91	0.80	2.21	0.32	2.01	0.30	2.71	0.34	0.72	0.33	0.10
SC12-036	Shield Low K/Ti	34.8	242	157	40.8	55.0	51.0	84.4	0.88	389	36.2	242	13.0	73.3	14.4	36.8	5.41	24.8	6.16	2.00	6.49	1.03	6.30	1.28	3.49	0.50	3.08	0.45	4.77	0.79	1.28	0.86	0.27
SC12-042	Shield Low K/Ti	30.7	214	698	69.6	393	85.2	72.2	1.38	230	18.5	74.7	3.36	35.0	3.73	10.4	1.63	7.92	2.39	0.85	2.73	0.48	3.06	0.65	1.80	0.26	1.60	0.24	1.79	0.22	0.65	0.24	0.07
SC12-043	Shield Low K/Ti	28.9	210	263	56.4	177	69.8	88.7	3.09	348	32.6	203	6.45	33.7	8.85	25.0	3.87	18.5	4.96	1.66	5.40	0.87	5.33	1.11	3.12	0.45	2.76	0.41	3.96	0.41	1.09	0.40	0.13
SC12-051	Shield Low K/Ti	27.1	187	179	50.7	138	67.7	82.5	1.61	397	42.0	244	11.4	59.3	15.4	38.9	5.68	25.7	6.44	2.03	6.59	1.10	6.92	1.45	3.99	0.58	3.59	0.53	4.87	0.71	1.54	0.76	0.25
SC12-071B	Shield Low K/Ti	25.8	180	212	49.8	153	58.4	78.5	3.70	545	33.1	245	9.16	63.3	11.7	31.6	4.79	22.1	5.62	1.92	5.82	0.94	5.67	1.14	3.16	0.45	2.76	0.41	4.62	0.60	1.54	0.60	0.19
SC12-570	Shield Low K/Ti	29.6	181	163	51.8	162	65.8	58.4						8.50	1.86	4.85	0.93	4.81	1.67	0.66	2.28	0.42	2.92	0.65	1.92	0.29	1.83	0.28					
SC12-581	Shield Low K/Ti	27.2	197	364	63.0	306	72.2	75.1	1.91	326	23.6	147	4.79	25.5	6.28	18.2	2.84	13.1	3.55	1.23	3.92	0.66	4.08	0.84	2.35	0.34	2.07	0.31	2.88	0.31	0.73	0.26	0.07
SC12-584B	Shield Low K/Ti	37.9	248	499	54.8	181	72.5	72.5	1.50	286	23.9	102	4.27	23.0	4.94	13.8	2.17	10.8	3.23	1.13	3.69	0.64	4.10	0.87	2.43	0.35	2.17	0.32	2.37	0.28	0.54	0.22	0.08
SCZ15-01	Shield Low K/Ti	34.4	215	454	67.1	435	90.2	63.3	1.36	218	18.3	73.3	2.17	22.4	3.05	8.84	1.42	7.05	2.22	0.84	2.75	0.48	3.08	0.65	1.82	0.27	1.66	0.25	1.66	0.15	1.36	0.17	0.05
SCZ15-02	Shield Low K/Ti	28.2	166	471	89.3	866	77.9	60.7	1.40	182	12.7	56.2	1.60	19.3	2.22	6.52	1.03	5.26	1.69	0.63	2.08	0.37	2.35	0.50	1.34	0.20	1.25	0.19	1.23	0.11	1.08	0.13	0.04
SCZ15-04	Shield Low K/Ti	44.6	316	263	59.0	189	93.0	92.8	1.46	204	32.9	149	9.57	38.7	8.60	21.4	3.02	14.0	3.88	1.34	4.46	0.75	4.91	1.03	2.94	0.43	2.70	0.39	3.10	0.57	1.08	0.41	0.17
SCZ15-08	Shield Low K/Ti	41.2	253	382	69.2	364	101	82.3	1.87	226	27.4	88.9	4.42	34.2	4.83	13.0	1.96	9.42	2.78	1.03	3.37	0.59	3.98	0.87	2.48	0.38	2.46	0.37	1.91	0.29	0.84	0.24	0.08
SCZ15-09	Shield Low K/Ti	39.6	264	306	59.6	170	94.7	74.9	1.18	223	23.0	66.3	2.14	18.7	2.86	7.94	1.28	6.47	2.15	0.83	2.84	0.51	3.48	0.76	2.22	0.34	2.18	0.33	1.51	0.15	0.84	0.15	0.12
SCZ15-10	Shield Low K/Ti	39.5	254	347	62.9	200	110	78.0	1.35	232	21.8	61.5	2.08	19.1	2.56	7.33	1.17	5.88	1.95	0.77	2.62	0.47	3.23	0.72	2.08	0.32	2.05	0.31	1.41	0.14	0.71	0.14	0.07
SC-46	Shield Mid K/Ti	29.7	212	584		306	79.4	72.2	2.56	349	20.9	119	5.08	32.5	6.47	17.4	2.62	12.3	3.39	1.34	3.89	0.66	4.14	0.84	2.26	0.33	1.97	0.29	2.72	0.65	0.74	0.39	0.12
SC-130	Shield Mid K/Ti	25.5	194	141	61.5	121	68.7	91.9	9.29	490	49.6	371	22.3	123	29.5	64.4	9.18	38.1	8.57	2.62	8.60	1.38	8.35	1.67	4.63	0.67	4.17	0.61	6.87	1.36	2.62	1.66	0.51
SC-135	Shield Mid K/Ti	29.4	204	485		234	80.9	85.4	5.52	330	34.2	241	10.4	58.9	13.6	33.8	4.86	22.5	5.85	2.02	6.37	1.06	6.56	1.36	3.65	0.53	3.25	0.50	4.87	0.82	1.37	0.83	0.29
SC-155	Shield Mid K/Ti	31.3	213	148	54.1	95.0	75.8	83.5	2.28	434	33.2	234	13.1	78.9	13.4	34.5	4.97	22.7	5.64	1.86	5.75	0.92	5.55	1.14	3.12	0.45	2.76	0.41	4.43	1.15	1.48	0.82	0.25
SC12-002	Shield Mid K/Ti	28.7	188	284	52.0	202	57.2	75.1	3.20	456	30.0	195	6.86	38.5	9.97	25.7	3.81	17.7	4.76	1.61	5.13	0.82	5.00	1.03	2.87	0.41	2.55	0.37	3.93	0.45	1.01	0.47	0.14

(Continued on following page)

TABLE 2 | (*Continued*) Trace element abundances of Santa Cruz lavas, reported in parts per million (ppm). One replicate analysis (indicated by "re") is included.

Sample	Comp. Group	Sc	V	Cr	Co	Ni	Cu	Zn	Rb	Sr	Y	Zr	Nb	Ba	La	Ce	Pr	Nd	Sm	Eu	Gd	Tb	Dy	Ho	Er	Tm	Yb	Lu	Hf	Ta	Pb	Th	U
SC12-007	Shield Mid K/Ti	21.8	154	306	49.8	197	63.8	70.4	4.11	322	29.5	215	9.56	53.5	10.9	27.7	4.05	18.8	4.73	1.57	5.08	0.81	4.94	1.01	2.81	0.40	2.51	0.36	4.09	0.61	1.30	0.62	0.20
SC12-010	Shield Mid K/Ti	30.5	221	722	62.0	285	48.9	74.5	2.78	384	23.5	140	6.50	36.1	7.77	19.1	2.91	13.6	3.63	1.25	3.90	0.64	3.92	0.81	2.22	0.32	2.00	0.29	2.87	0.42	0.80	0.42	0.14
SC12-012	Shield Mid K/Ti	24.8	201	221	48.1	194	61.4	79.5	4.76	281	35.2	238	11.7	67.8	12.0	31.4	4.60	20.2	5.10	1.66	5.58	0.92	5.78	1.21	3.30	0.48	2.99	0.43	4.39	0.75	1.35	0.77	0.26
SC12-018	Shield Mid K/Ti	32.5	235	368	52.6	216	55.2	78.0	5.00	356	32.3	204	10.6	57.9	12.8	30.7	4.64	21.0	5.24	1.67	5.37	0.88	5.64	1.15	3.17	0.46	2.86	0.42	4.08	0.67	1.37	0.75	0.22
SC12-021	Shield Mid K/Ti	42.4	332	216	46.9	69.0	72.5	88.6	2.87	338	37.8	177	9.41	79.2	10.7	26.1	3.96	18.4	5.02	1.65	5.53	0.92	5.91	1.22	3.37	0.50	3.02	0.44	3.76	0.59	1.15	0.58	0.17
SC12-023	Shield Mid K/Ti	26.7	187	205	48.2	147	59.9	82.0	4.08	516	36.0	252	9.76	55.9	12.6	33.7	5.15	24.0	6.09	1.93	6.07	1.00	6.20	1.26	3.45	0.49	3.09	0.46	4.99	0.62	1.45	0.63	0.21
SC12-024	Shield Mid K/Ti	26.0	177	179	50.8	143	63.2	84.2	6.39	516	35.0	249	12.7	73.0	15.0	37.5	5.37	24.3	5.88	1.90	5.84	0.95	5.66	1.16	3.24	0.47	2.92	0.43	4.82	0.79	1.57	0.85	0.27
SC12-029	Shield Mid K/Ti	29.4	192	169	51.5	129	58.1	90.4	5.81	402	40.2	253	11.7	59.6	12.9	33.9	5.07	23.9	6.09	1.93	6.37	1.06	6.50	1.34	3.72	0.54	3.37	0.50	4.90	0.70	1.61	0.73	0.25
SC12-031	Shield Mid K/Ti	26.8	197	250	49.4	169	67.6	92.2	6.88	397	41.8	363	13.7	70.3	17.8	43.8	6.16	27.7	6.80	2.14	6.95	1.14	6.88	1.39	3.81	0.55	3.43	0.51	5.95	0.86	1.73	0.99	0.33
SC12-032	Shield Mid K/Ti	29.3	205	205	44.7	103	75.7	72.8	6.24	458	30.2	189	11.5	73.6	12.6	29.7	4.38	20.0	5.04	1.68	5.26	0.85	5.31	1.08	2.92	0.42	2.58	0.38	3.82	0.71	1.40	0.80	0.21
SC12-033	Shield Mid K/Ti	31.4	215	274	59.6	263	72.0	69.7	1.89	307	23.7	122	4.99	36.6	6.04	16.3	2.51	12.1	3.30	1.13	3.67	0.62	3.96	0.84	2.32	0.34	2.14	0.32	2.54	0.32	0.81	0.37	0.12
SC12-034	Shield Mid K/Ti	32.1	230	389	55.0	209	50.5	84.7	6.23	428	32.2	234	11.9	70.0	13.6	34.1	5.02	22.6	5.55	1.75	5.77	0.93	5.64	1.14	3.14	0.46	2.80	0.40	4.64	0.75	1.36	0.86	0.26
SC12-035	Shield Mid K/Ti	26.8	176	278	52.8	220	77.3	76.4	2.06	357	30.0	185	8.14	41.8	9.73	25.8	3.80	17.6	4.58	1.54	4.99	0.82	5.09	1.04	2.87	0.42	2.61	0.38	3.70	0.53	1.01	0.57	0.14
SC12-037	Shield Mid K/Ti	34.7	259	309	52.9	179	73.0	97.1	2.92	497	44.9	333	16.5	87.5	19.3	47.7	6.85	31.1	7.43	2.27	7.36	1.20	7.28	1.48	4.00	0.57	3.46	0.51	6.16	1.00	1.88	1.15	0.31
SC12-038	Shield Mid K/Ti	29.5	223	248	49.1	140	50.9	71.6	2.92	555	27.2	163	8.31	55.5	9.88	24.0	3.74	17.3	4.50	1.53	4.57	0.73	4.43	0.89	2.41	0.35	2.12	0.30	3.38	0.54	1.12	0.44	0.14
SC12-041	Shield Mid K/Ti	29.1	194	226	53.8	161	61.2	82.9	4.74	495	34.7	247	11.8	66.7	13.0	34.3	5.02	23.0	5.70	1.83	5.84	0.94	5.60	1.16	3.22	0.46	2.89	0.43	4.77	0.72	1.59	0.78	0.25
SC12-044	Shield Mid K/Ti	26.2	166	394	57.7	247	72.4	75.2	3.71	389	29.4	205	9.37	56.5	10.5	28.0	4.07	18.4	4.57	1.50	4.78	0.78	4.80	0.98	2.68	0.40	2.46	0.36	3.78	0.56	1.36	0.60	0.20
SC12-046	Shield Mid K/Ti	24.5	182	132	43.3	109	46.3	88.3	6.93	525	42.9	349	16.0	85.6	21.3	53.0	7.52	33.3	7.89	2.45	7.80	1.25	7.58	1.53	4.17	0.60	3.68	0.54	6.55	1.01	2.20	1.22	0.37
SC12-047	Shield Mid K/Ti	21.3	144	145	38.8	98.0	60.4	67.6	5.61	521	29.7	234	11.7	80.3	13.4	33.9	4.78	21.4	5.34	1.83	5.38	0.86	5.20	1.06	2.90	0.41	2.55	0.38	4.45	0.76	1.69	0.85	0.23
SC12-048	Shield Mid K/Ti	26.4	200	158	44.6	115	55.5	96.5	9.95	465	42.5	324	19.0	92.4	19.9	49.0	6.94	30.6	7.36	2.27	7.48	1.22	7.37	1.48	4.09	0.59	3.63	0.53	6.25	1.20	2.07	1.44	0.45
SC12-050	Shield Mid K/Ti	29.9	233	245	48.0	145	66.4	83.0	6.85	489	31.4	229	14.3	90.9	13.6	34.2	4.82	21.9	5.53	1.84	5.71	0.91	5.35	1.09	2.92	0.41	2.55	0.38	4.62	0.90	1.90	0.99	0.27
SC12-071A	Shield Mid K/Ti	35.9	262	442	57.6	231	51.9	78.3	1.18	446	30.8	209	11.0	72.6	12.9	30.6	4.58	20.9	5.13	1.65	5.28	0.85	5.15	1.04	2.91	0.42	2.53	0.36	4.18	0.69	1.36	0.75	0.15
SCZ15-03	Shield Mid K/Ti	29.9	195	268	53.9	204	61.7	53.0	5.31	493	29.0	237	10.3	74.2	11.7	29.8	4.40	20.3	5.22	1.71	5.49	0.89	5.38	1.10	2.83	0.42	2.46	0.37	4.60	0.68	2.57	0.73	0.25
SCZ15-05	Shield Mid K/Ti	30.6	192	205	54.6	160	75.6	82.9	4.65	444	35.3	227	9.64	55.6	11.0	29.5	4.43	20.0	5.21	1.75	5.47	0.90	5.41	1.14	3.10	0.46	2.81	0.41	4.35	0.60	1.91	0.59	0.19
SCZ15-06	Shield Mid K/Ti	29.7	196	278	56.8	227	64.5	73.5	5.51	526	30.3	223	11.8	65.7	11.6	29.6	4.35	19.6	4.83	1.66	4.99	0.79	4.73	0.96	2.61	0.38	2.26	0.34	4.19	0.72	1.78	0.73	0.26
SCZ15-07	Shield Mid K/Ti	23.9	212	199	53.9	183	59.0	92.2	7.23	550	34.6	233	19.7	95.0	16.4	40.4	5.65	24.7	6.01	2.01	5.97	0.91	5.58	1.08	2.96	0.41	2.56	0.36	4.56	1.19	1.73	1.14	0.37
SC-48	Shield High K/Ti	32.9	254	143		64.3	56.8	74.4	8.42	339	31.7	209	13.8	87.1	15.5	35.7	4.76	20.6	5.31	1.86	5.84	0.97	6.14	1.28	3.40	0.48	3.01	0.45	4.51	1.13	1.26	1.28	0.41
SC-48 re	Shield High K/Ti	37.7	305	156	55.7	58.0	76.6	94.5	6.45	322	41.3	199	13.2	67.3	12.5	30.4	4.53	20.6	5.67	1.75	5.95	1.05	6.56	1.38	3.78	0.56	3.41	0.50	4.45	0.80	1.29	1.07	0.33
SC-68	Shield High K/Ti	24.0	185	94.1		82.5	47.9	92.5	10.7	476	42.2	378	21.5	129	24.3	59.6	8.14	35.2	8.28	2.83	8.38	1.39	8.42	1.69	4.43	0.63	3.94	0.60	7.51	1.54	2.37	1.76	0.56
SC-203R	Shield High K/Ti	25.5	194	141	61.5	121	68.7	91.9	9.29	190	49.6	371	22.3	123	29.5	64.4	9.18	38.1	8.57	2.62	8.60	1.35	8.11	1.64	4.72	0.67	4.09	0.62	6.87	1.36	2.62	1.66	0.51
SC-204R	Shield High K/Ti	24.7	204	182		131	58.0	87.3	11.2	463	39.2	309	20.2	122	22.1	53.7	7.43	32.1	7.66	2.64	7.80	1.29	7.81	1.56	4.10	0.58	3.58	0.54	6.38	1.36	1.58	1.54	0.41

(Continued on following page)

TABLE 2 | (*Continued*) Trace element abundances of Santa Cruz lavas, reported in parts per million (ppm). One replicate analysis (indicated by "re") is included.

Sample	Comp. Group	Sc	V	Cr	Co	Ni	Cu	Zn	Rb	Sr	Y	Zr	Nb	Ba	La	Ce	Pr	Nd	Sm	Eu	Gd	Tb	Dy	Ho	Er	Tm	Yb	Lu	Hf	Ta	Pb	Th	U
SC-206B	Shield High K/Ti	22.2	173	91.3		62.7	46.5	91.4	8.28	489	46.9	446	24.8	149	27.9	66.8	9.23	39.0	9.02	2.97	8.96	1.47	9.10	1.84	4.87	0.70	4.34	0.66	8.43	1.93	2.85	1.97	0.47
SC-207	Shield High K/Ti	22.7	164	138		107	62.8	93.8	7.29	409	42.6	371	15.9	86.2	20.2	51.1	7.15	32.0	7.72	2.63	8.00	1.34	8.37	1.70	4.55	0.66	4.09	0.63	7.22	1.44	2.32	1.39	0.43
SC12-005	Shield High K/Ti	37.1	263	162	41.5	88.0	63.6	80.1	8.19	312	34.4	217	15.4	86.7	15.5	36.1	4.85	20.6	5.18	1.69	5.55	0.91	5.63	1.17	3.35	0.48	2.96	0.44	4.39	0.99	1.43	1.33	0.45
SC12-017	Shield High K/Ti	25.5	204	79.0	34.7	61.0	45.9	91.7	11.2	465	45.3	393	21.1	118	24.1	59.1	8.15	34.2	7.91	2.38	7.79	1.24	7.29	1.50	4.21	0.62	3.83	0.57	7.24	1.32	2.58	1.75	0.52
SC12-027	Shield High K/Ti	24.9	188	84.0	37.2	66.9	34.2	91.4	11.1	461	42.1	389	26.1	131	26.7	65.0	8.69	36.1	8.17	2.44	7.96	1.28	7.61	1.52	4.01	0.58	3.55	0.52	7.09	1.57	2.30	1.65	0.56
SC12-028	Shield High K/Ti	30.0	203	224	43.1	138	57.1	82.4	7.06	343	39.3	291	13.2	72.2	18.1	42.3	5.82	25.1	5.91	1.82	6.06	1.00	6.22	1.29	3.71	0.54	3.38	0.51	5.30	0.82	1.81	1.04	0.34
SC12-039	Shield High K/Ti	27.1	201	180	45.3	152	63.1	92.6	8.92	435	43.4	318	18.1	92.8	21.5	52.3	7.18	30.9	7.20	2.22	7.16	1.15	6.84	1.41	4.04	0.58	3.56	0.53	5.89	1.10	2.04	1.18	0.37
SC12-040	Shield High K/Ti	28.7	228	154	43.1	116	61.8	96.5	11.1	491	44.5	346	24.7	126	24.2	58.1	7.92	34.0	7.78	2.38	7.74	1.24	7.17	1.48	4.09	0.59	3.63	0.54	6.43	1.47	2.21	1.66	0.52
SC12-049	Shield High K/Ti	27.4	253	128	38.7	90.0	75.8	102	10.1	402	43.2	322	23.7	128	21.2	51.7	7.13	30.8	7.38	2.34	7.65	1.22	7.20	1.49	4.17	0.60	3.71	0.56	6.10	1.44	2.64	1.40	0.46
SC12-053	Shield High K/Ti	26.5	183	105	38.1	64.0	57.7	89.2	8.85	392	47.5	380	16.5	87.0	18.7	47.5	6.96	32.0	7.97	2.46	8.21	1.33	8.06	1.65	4.67	0.67	4.23	0.64	7.32	1.08	2.25	1.24	0.42
SC12-572A	Shield High K/Ti	34.0	268	192	38.3	70.0	48.0	84.1	7.37	369	40.6	238	17.2	220	18.7	41.6	5.76	24.3	5.95	1.99	6.47	1.05	6.50	1.35	3.72	0.54	3.35	0.50	4.80	1.11	1.77	1.38	0.42
SC12-611B	Shield High K/Ti	28.4	201	363	47.5	181	53.8	81.2	6.45	353	38.8	270	14.3	82.1	16.1	39.6	5.55	24.6	5.99	1.91	6.13	1.02	6.20	1.27	3.52	0.51	3.17	0.48	4.98	0.91	1.46	1.02	0.34
SC12-004	Shield No K/Ti	36.1	275	170	41.0	79.0	47.1	77.0	7.37	335	34.0	208	14.5	89.4	16.7	34.1	4.97	21.0	5.16	1.66	5.40	0.90	5.53	1.15	3.26	0.47	2.89	0.43	4.15	0.91	1.57	1.17	0.38
SC12-582	Shield No K/Ti	25.6	188	232	48.1	171	59.1	66.4	1.81	312	23.5	150	5.04	26.7	6.34	19.0	2.88	13.4	3.63	1.25	3.83	0.66	4.09	0.85	2.40	0.34	2.12	0.32	3.02	0.33	0.81	0.29	0.09
SC12-583	Shield No K/Ti	27.0	200	326	56.3	239	60.2	70.5	1.81	332	23.4	143	4.67	27.6	6.07	17.9	2.75	12.7	3.47	1.22	3.67	0.63	3.87	0.81	2.28	0.33	2.01	0.30	2.83	0.30	0.75	0.27	0.08
SC12-584A	Shield No K/Ti	34.2	238	459	62.6	246	74.7	71.5	0.88	288	19.9	19.4	3.79	21.1	4.30	12.3	1.96	9.39	2.78	1.00	3.05	0.55	3.42	0.71	1.99	0.29	1.75	0.26	2.07	0.25	0.46	0.19	0.12
SC12-589	Shield No K/Ti	34.3	253	260	53.9	164	93.7	73.6	3.28	324	22.2	131	7.46	40.0	7.96	20.4	2.89	12.7	3.37	1.17	3.62	0.62	3.77	0.78	2.18	0.31	1.90	0.28	2.67	0.46	0.80	0.48	0.13
SC12-606	Shield No K/Ti	31.8	203	612	62.1	311	74.4	65.9	1.70	307	19.3	103	4.60	25.4	5.18	14.3	2.23	10.4	2.90	1.03	3.13	0.55	3.36	0.70	1.95	0.28	1.70	0.25	2.27	0.30	0.60	0.26	0.08
SC12-610	Shield No K/Ti	30.9	196	396	63.1	314	70.4	68.2	1.12	277	19.8	85.0	3.63	20.1	4.15	11.5	1.88	9.06	2.69	0.96	2.96	0.53	3.40	0.72	2.00	0.29	1.78	0.26	1.97	0.24	0.47	0.18	0.05
SC12-611A	Shield No K/Ti	30.8	232	728	63.1	317	71.6	77.3	2.05	278	22.3	112	6.47	33.2	6.59	17.1	2.56	11.6	3.22	1.11	3.51	0.62	3.81	0.79	2.23	0.32	1.96	0.30	2.39	0.40	0.62	0.33	0.10
SC12-612	Shield No K/Ti	30.2	217	283	49.2	140	54.9	67.9	1.32	275	20.7	93.7	4.20	24.4	4.63	13.3	2.10	10.1	2.95	1.06	3.25	0.58	3.64	0.76	2.13	0.31	1.84	0.27	2.17	0.27	0.56	0.21	0.06

space (**Figure 9**). Unlike Santiago (Gibson et al., 2012), isotopic and ITE ratios do not correlate at Santa Cruz.

Mantle Components at Santa Cruz

Isotopic ratios from Santa Cruz define nearly linear arrays, suggesting that mixing between two primary endmembers, PLUME and DUM, controls most of the island's geochemical variation (**Figures 8A–D**; Harpp and White, 2001). We applied a simple two-component mixing calculation (Langmuir et al., 1978) to estimate contributions of DUM and PLUME, using the isotopic ratios and absolute concentrations of Sr, Nd, and Pb from Harpp and Weis (2020).

According to our estimates, Platform Series lavas have higher contributions of PLUME (20–40%) than the Shield Series (5–35%). In this first-order examination of mantle endmembers, we did not model in detail the role of either WD or FLO, given how much of the variation at Santa Cruz can be explained with mixtures of PLUME and DUM. Owing to the fact that the WD endmember is distinctive primarily in its Pb isotope ratios, it is challenging to distinguish unequivocally whether Santa Cruz signatures are the result of mixing among DUM-PLUME and WD or DUM-PLUME and FLO. Mixing curves calculated for $^{207}Pb^*/^{206}Pb^*$-$^{208}Pb^*/^{206}Pb^*$, however, suggest that WD is the likely reservoir augmenting the dominant combination of DUM and PLUME (**Figure 8D**). Santa Cruz exhibits little evidence that FLO, the component thought to consist of ancient recycled material, is contributing significantly to its source (e.g., Harpp and White, 2001; Harpp and Weis, 2020); this conclusion is supported by Santa Cruz's lack of other compositional features characteristic of Floreana, such as concave-up REE patterns or more extreme Sr and Pb isotopic ratios (Harpp et al., 2014a).

The depleted component responsible for Santa Cruz lavas could be the upper mantle (e.g., Geist et al., 1988; White et al., 1993; Harpp and White, 2001; Blichert-Toft and White, 2001), or it could be intrinsic to the plume, with deep mantle origins (e.g., Hoernle et al., 2000). According to studies of the Icelandic plume by Fitton et al. (1997, 2003), lavas generated at mid-ocean ridges from the upper mantle have distinct signatures in Nb/Y-Zr/Y space compared to basalts sourced by mantle plumes. Fitton et al. (1997) define a reference line (ΔNb) in Nb/Y-Zr/Y space that delimits the lower boundary of the Icelandic array. Lavas with ΔNb >0 are thought to be generated from lower mantle sources (i.e., plume), whereas those with ΔNb <0 are derived from the depleted upper mantle. Santa Cruz lavas land primarily in the quadrant defined by Nb/Zr < 0.06 and ΔNb <0, which corresponds to the depleted MORB source (**Figure 7**). Other Galápagos lavas with similar signatures include those from Genovesa (Harpp et al., 2003), many from Santiago (Gibson et al., 2012), a few from San Cristóbal (Geist et al., 1986; White et al., 1993), and numerous from the NGVP (e.g., Harpp and Geist, 2002; Harpp et al., 2014c; Sinton et al., 2014). A handful of Platform and High K_2O/TiO_2 Shield Series lavas have Nb/Zr > 0.06 (but less than 0.09), which qualify as enriched MORB (Fitton et al., 1997). No Santa Cruz samples have ΔNb >0. Thus, consistent with findings based primarily on isotopic data by Harpp and Weis (2020) for the archipelago as a whole, the depleted material contributing to Santa Cruz lavas' geochemical signatures is likely supplied primarily by the depleted upper mantle, rather than a depleted source intrinsic to the plume.

Trace Element Modeling: Depth and Extent of Melting

To constrain melt generation conditions at Santa Cruz, we apply a simple model to a representative subset of samples that assumes equilibrium melting of the dominant PLUME and DUM mantle components (*see* Supplementary Material for details; **Supplementary Table S1**; Harpp and White, 2001). The compositions of most Platform Series samples can be reproduced by melting 1–10% of a mixed DUM-PLUME mantle source, with 10–30% generated in the garnet stability field. All the modeled Platform lavas require small degree melts of their more enriched source (0.1–1%). The Shield Series lavas, on average, need greater contributions from the depleted mantle source and also exhibit more variation in the degree of melting than the Platform Series. Low K_2O/TiO_2 group lavas are generated by the highest melt fractions (1–20%), High K_2O/TiO_2 requires the least melting (0.5–5%), and Mid K_2O/TiO_2 is generated by an intermediate amount of melting (1–7%) of their mixed mantle sources. The Shield Series melts are generated at shallower depths than the Platform Series, with only minor melting (0-<20%) in the garnet stability field. The Low and Mid K_2O/TiO_2 groups are produced at slightly shallower depths than the High K_2O/TiO_2 lavas, but there is considerable variability within each Shield sub-group in all melt parameters (especially the Low and Mid K_2O/TiO_2 sub-units).

Compositional Variation of Santa Cruz Lavas

Across Santa Cruz

To document the variation of Santa Cruz lava compositions and to compare them to other volcanoes in the Galápagos, probability density function and interquartile ranges (Wessa, 2021) were generated for Mg#, La_n/Sm_n, Sm_n/Yb_n, and Nb/La (**Figure 10**). We chose Mg# as an indicator of shallow fractionation, $La_{(n)}/Sm_{(n)}$ as a proxy for extent of melting, $Sm_{(n)}/Yb_{(n)}$ to track depth of melting, and Nb/La as a measure of Galápagos plume contribution, which is rich in the refractory TITAN elements (Jackson et al., 2008; Kurz et al., 2014).

As stated above, the older Platform Series is more evolved and less variable than the Shield Series; Platform Series lavas have a lower Mg# Maximum Density (MD) than the Shield Series, and a slightly lower interquartile range (IR) (**Figure 10**; Platform MD: 44.4, IR: 10.7; Shield MD: 53.9, IR: 11.5). The sub-groups within the Shield Series increase in Mg# MD and IR from the High to Low K_2O/TiO_2 groups (**Figure 10**).

The Platform Series has La_n/Sm_n and Sm_n/Yb_n values that overlap the Shield Series, but the Shield lavas exhibit ~4 times the variability of Platform lavas (Platform La_n/Sm_n MD: 1.36, IR: 0.12; Shield La_n/Sm_n MD: 1.43, IR: 0.50; Platform Sm_n/Yb_n MD: 1.87, IR: 0.10; Shield Sm_n/Yb_n MD: 1.92, IR: 0.44). Within the Shield Series, the High K_2O/TiO_2 group was generated by the smallest extents of melting at the greatest average depths (La_n/Sm_n MD: 1.86, IR: 0.15; Sm_n/Yb_n MD: 2.25, IR: 0.27). Through

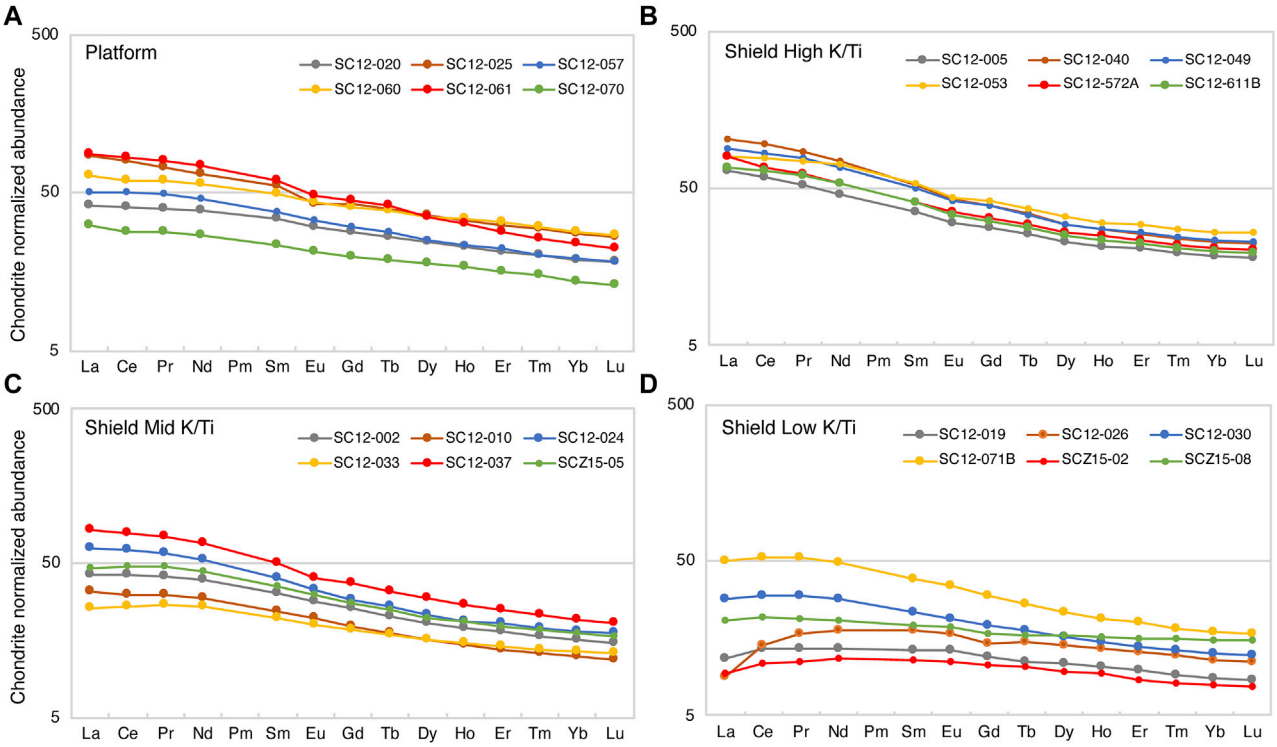

FIGURE 5 | Representative chondrite-normalized rare earth element (REE) values. Normalizing values are from McDonough and Sun (1995). All symbols are larger than 1σ analytical error. **(A)** Platform Series. **(B)** High K_2O/TiO_2 Shield Series. **(C)** Mid K_2O/TiO_2 Shield Series. **(D)** Low K_2O/TiO_2 Shield Series.

the Mid and Low K_2O/TiO_2 groups, extent of melting increases and extends to progressively shallower depths (Mid Shield La_n/Sm_n MD: 1.51, IR: 0.23; Sm_n/Yb_n MD: 2.20, IR: 0.27; Low Shield La_n/Sm_n MD: 0.97, IR: 0.41; Sm_n/Yb_n MD: 1.65, IR: 0.41). The most primitive lavas (Low K_2O/TiO_2 Shield lavas) from Santa Cruz were generated at the shallowest depths and by the greatest extents of melting, on average.

Our proxy for the contribution from the Galápagos plume source, Nb/La, is higher in the Platform than the Shield Series (Platform Nb/La MD: 0.97, IR: 0.08; Shield Nb/La MD: 0.88, IR: 0.13). Platform lavas exhibit less variation in Nb/La than the Shield Series, and the Low K_2O/TiO_2 group has the greatest variability (Nb/La MD: 0.85, IR: 0.16), consistent with radiogenic isotope signatures.

Taken together, the La_n/Sm_n, Sm_n/Yb_n, and Nb/La variations across Santa Cruz suggest that Platform Series lavas were generated by slightly higher extents of melting (on average) at comparable depths to the Shield Series, but with a greater contribution from the enriched PLUME source. Furthermore, Platform Series melts experienced more fractionation than the Shield Series. Platform Series lavas, however, exhibit considerably narrower ranges in incompatible trace element ratios, indicating that they were homogenized significantly more than Shield Series lavas. Within the Shield Series, many of the melts were generated by variable but small degrees of melting of a more depleted source than the Platform Series, likely across a wide range of melt column lengths (Gibson and Geist, 2010), and with little homogenization compared to the Platform Series lavas.

Comparison With Galápagos Archipelago

Probability density functions for the four geochemical metrics Mg#, La_n/Sm_n, Sm_n/Yb_n, and Nb/La from Fernandina, two Isabela volcanoes (Volcán Alcedo and Volcán Sierra Negra), and Santiago are compared to Santa Cruz (**Figure 10**; White et al., 1993; Geist et al., 1995; Reynolds and Geist, 1995; Kurz and Geist, 1999; Allan and Simkin, 2000; Gibson et al., 2012; Geist et al., 2014a). Consistent with previous findings (White et al., 1993; Harpp and Geist, 2018), the older islands in the Galápagos (Santa Cruz and Santiago) produce lava compositions that vary more in all four metrics (Mg#, La_n/Sm_n, Sm_n/Yb_n, and Nb/La) than Fernandina and Volcán Sierra Negra, two of the archipelago's youngest volcanoes.

Santa Cruz Platform lavas have similar Mg# MD values to Fernandina, Volcán Sierra Negra, and Volcán Alcedo, but greater variability than Fernandina and Volcán Sierra Negra (**Figure 10**); the wider interquartile range of Volcán Alcedo reflects its bimodal compositional distribution, which includes rhyolites from an explosive event ~100 ka (Geist et al., 1995). The distribution of Mg# in Shield Series lavas most closely resembles Santiago's geochemical profile (White et al., 1993; Gibson et al., 2012), also with greater variation in Mg# than Fernandina or Volcán Sierra Negra.

Platform Series lavas have an MD for La_n/Sm_n close to that of Fernandina, a Sm_n/Yb_n MD lower than Fernandina's, and more depleted isotopic and Nb/La ratios (**Figures 8**, **10**). Like Fernandina and Volcán Sierra Negra, the Platform Series has a narrow range of

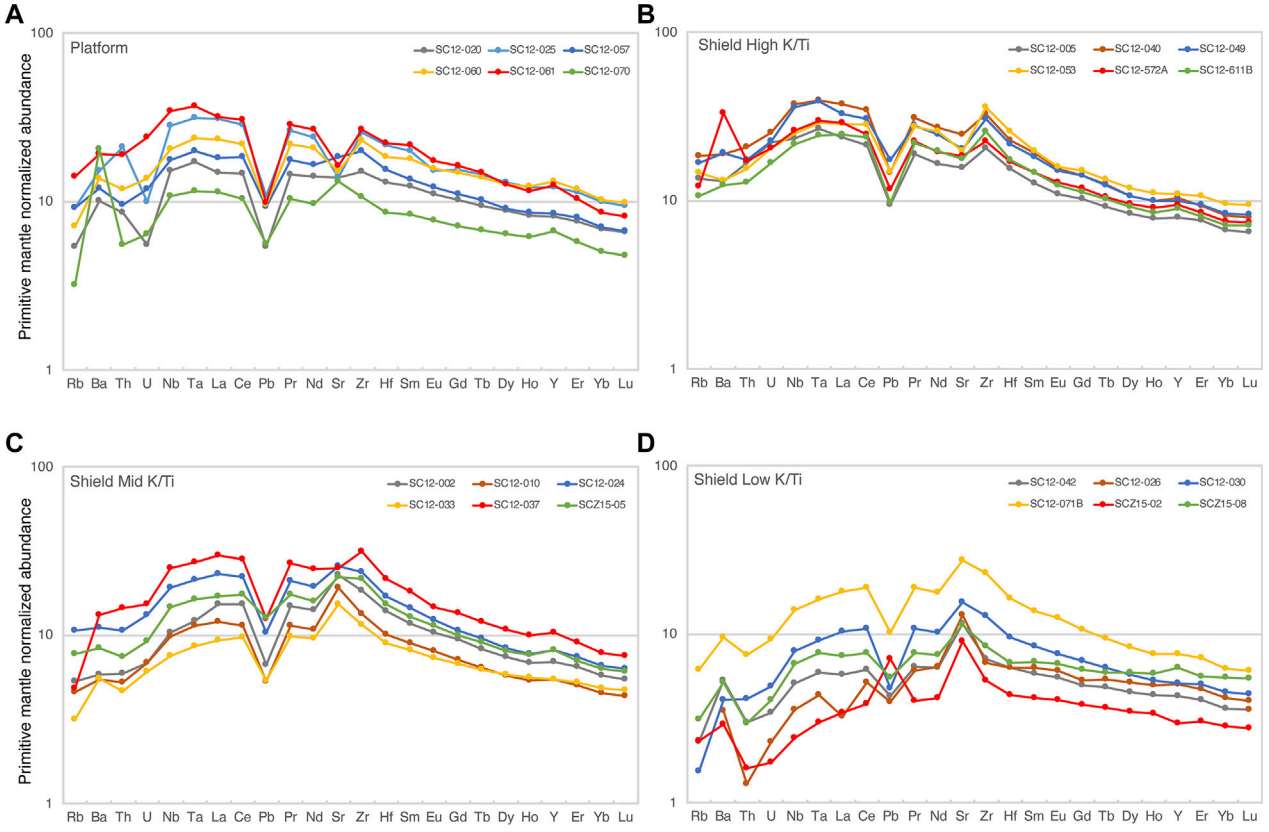

FIGURE 6 | Representative trace element contents of Santa Cruz lavas normalized to primitive mantle (McDonough and Sun, 1995). All symbols are larger than 1σ analytical error. **(A)** Platform Series. **(B)** High K_2O/TiO_2 Shield Series. **(C)** Mid K_2O/TiO_2 Shield Series. **(D)** Low K_2O/TiO_2 Shield Series.

La_n/Sm_n and Sm_n/Yb_n. Thus, compared to Fernandina and Volcán Sierra Negra, Platform melts were generated by broadly similar extents of melting at shallower depths of a more depleted mantle source, which reflect longer melt columns owing to the volcano's proximity to the GSC and therefore its thinner lithosphere (Gibson and Geist, 2010). By contrast, Shield Series samples exhibit greater variation in degree and depth of melting than the Platform Series or the western shields, resembling the more primitive, variable Santiago lavas (**Figure 10**; Gibson et al., 2012).

In terms of Nb/La, the ITE plume proxy, all Santa Cruz lavas exhibit values close to the MD of Santiago and lower than those of the western shields (**Figure 10**). Thus, even though Platform Series lavas are enriched compared to the Shield Series, none of the Santa Cruz lavas are as enriched as those from the western archipelago.

DISCUSSION

Petrogenetic Development of Santa Cruz Island

Melt Generation Processes at Santa Cruz

Geochemical variations in the Platform and Shield Series indicate that melts of the two units were generated under distinct sets of conditions. The key differences between the two units include:

1) The Platform Series requires more melting in the garnet stability field (10–30%) than the Shield Series (0–20%), according to REE systematics (e.g., Gibson and Geist, 2010).
2) Shield Series lavas exhibit more variation than the Platform Series in all melting parameters, including source composition, depth of melting, and extent of melting (**Figure 10**), specifically: a. whereas average depths of melting for both the Shield and Platform Series are comparable, some Shield Series melts were generated at significantly shallower depths, as reflected by the samples with lower Sm_n/Yb_n ratios than the Platform Series; and b. most lavas from the Platform Series result from 1 to 10% melting of a mixed PLUME-DUM source, whereas the Shield Series was produced by a greater range in extents of melting (1–20%) of a more depleted mixed PLUME-DUM source.

In general, depth and extent of melting at hotspot-generated ocean islands are controlled by mantle composition (e.g., Ito and Mahoney, 2005), thickness of the lithosphere (e.g., McKenzie and O'Nions, 1991; Gibson and Geist, 2010), and proximity to the plume (potential temperature; e.g., Herzberg and Gazel, 2009).

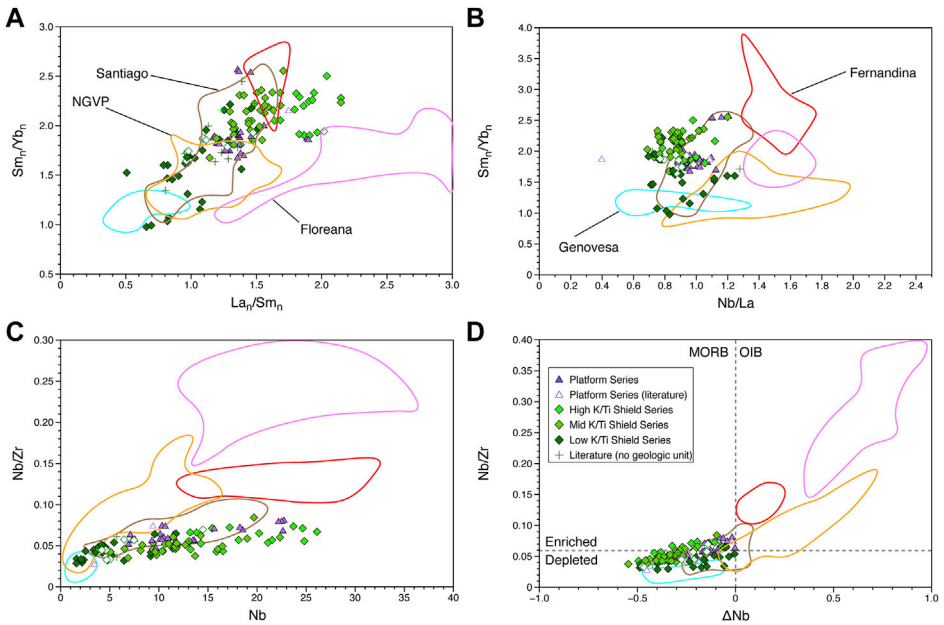

FIGURE 7 | Santa Cruz incompatible trace element ratio variations relative to selected Galápagos Islands. Fields are literature data. Red: Fernandina, blue: Genovesa, brown: Santiago, pink: Floreana, yellow: Northern Galápagos Volcanic Province (Bow and Geist, 1992; White et al., 1993; Harpp et al., 2002; Harpp et al., 2003; Saal et al., 2007; Gibson and Geist, 2010; Gibson et al., 2012; Harpp et al., 2014a; Harpp et al., 2014c). **(A)** Chondrite-normalized La_n/Sm_n and Sm_n/Yb_n ratios (McDonough and Sun, 1995). **(B)** Nb/La versus chondrite-normalized Sm_n/Yb_n ratios. **(C)** Nb versus Nb/Zr. **(D)** ΔNb versus Nb/Zr discrimination diagram to identify origin of depleted signatures. ΔNb (Fitton et al., 1997) = 1.74 + log(Nb/Y) − 1.92 log(Zr/Y). ΔNb >0 is attributed to lower mantle origin (OIB field); ΔNb <0 indicates depleted mantle origin (MORB field). Lavas with Nb/Zr > 0.06 are considered enriched, and those with Nb/Zr < 0.06 are depleted according to Fitton et al. (2003). Several Floreana literature data extend to Nb/Zr = 0.655 and ΔNb = 0.939, but are not shown. Samples indicated by a cross are literature data from Santa Cruz (White et al., 1993; Kurz and Geist, 1999; Saal et al., 2007); they have not been attributed to either the Platform or Shield Series owing to a lack of GPS coordinates for their origin locations.

Variation in mantle composition only explains a small part of the observed melt systematics across Santa Cruz. Enriched mantle sources initiate melting at greater depths than depleted material because they are more fertile and capable of melting at lower temperatures owing to different source lithologies and/or volatile content (e.g., Hirschmann, 2000; Gleeson and Gibson, 2021). Consequently, variable extents of melting of a mixed source result in a direct correlation between incompatible trace element ratios and radiogenic isotope ratios (e.g., at Santiago; Gibson et al., 2012). At Santa Cruz, ITE ratios do not correlate strongly with radiogenic isotope ratios (**Figure 9**), suggesting that a model in which a plum-pudding mantle made of mixed depleted and enriched components becomes progressively depleted with increasing extents of melting is not the dominant process controlling chemical heterogeneity of the island's lavas (e.g., Ito and Mahoney, 2005). We cannot rule out, however, the possibility that chemical and lithologic heterogeneities in the mantle contribute in part to the observed chemical and isotopic variations.

Lithospheric thickness affects the average depth of melting if upwelling and melting continues to the base of the lithosphere (e.g., Klein and Langmuir, 1987; Ellam, 1992; Ito and Mahoney, 2005; Gibson and Geist, 2010). According to Gibson and Geist (2010), typical geochemical estimates for lithospheric thickness are ~57 km in the western Galápagos and ~53 km in the east. Gibson et al. (2012) document a strong correlation between ITE and radiogenic isotope ratios at Santiago, which they attribute to differential melting of a compositionally heterogeneous mantle across an abrupt lithospheric gradient, coupled with a slight shift in bulk source composition across the lithospheric discontinuity. According to their model, enriched and depleted components are intermixed at a short spatial scale beneath Santiago, on the order of kilometers. Beneath the western half of the island, thicker lithosphere limits the top of melt columns so that melts are dominated by the enriched component of the heterogeneous mantle; farther east, where the lithosphere is thinner and melt columns are longer, more of the refractory depleted material melts, diluting the enriched signal. The lack of a correlative relationship between ITE and isotopic ratios on Santa Cruz (**Figure 9**), however, also eliminates lithospheric thickness as a primary control on the geochemical variations on Santa Cruz.

The remaining factor influencing depth and extent of melting at Santa Cruz is distance from the plume center and intensity of magma supply. The potential temperature of the Galápagos plume is ~1350–1400°C (e.g., Ito et al., 1997; Hooft et al., 2003), and thermal anomalies are typically 200–300°C greater than the ambient mantle (Herzberg et al., 2007). Hotter upwelling plumes cause the mantle to intersect the solidus at greater depths than the ambient mantle, supplying overlying volcanoes with higher magmatic fluxes. The oldest recently dated Platform Series

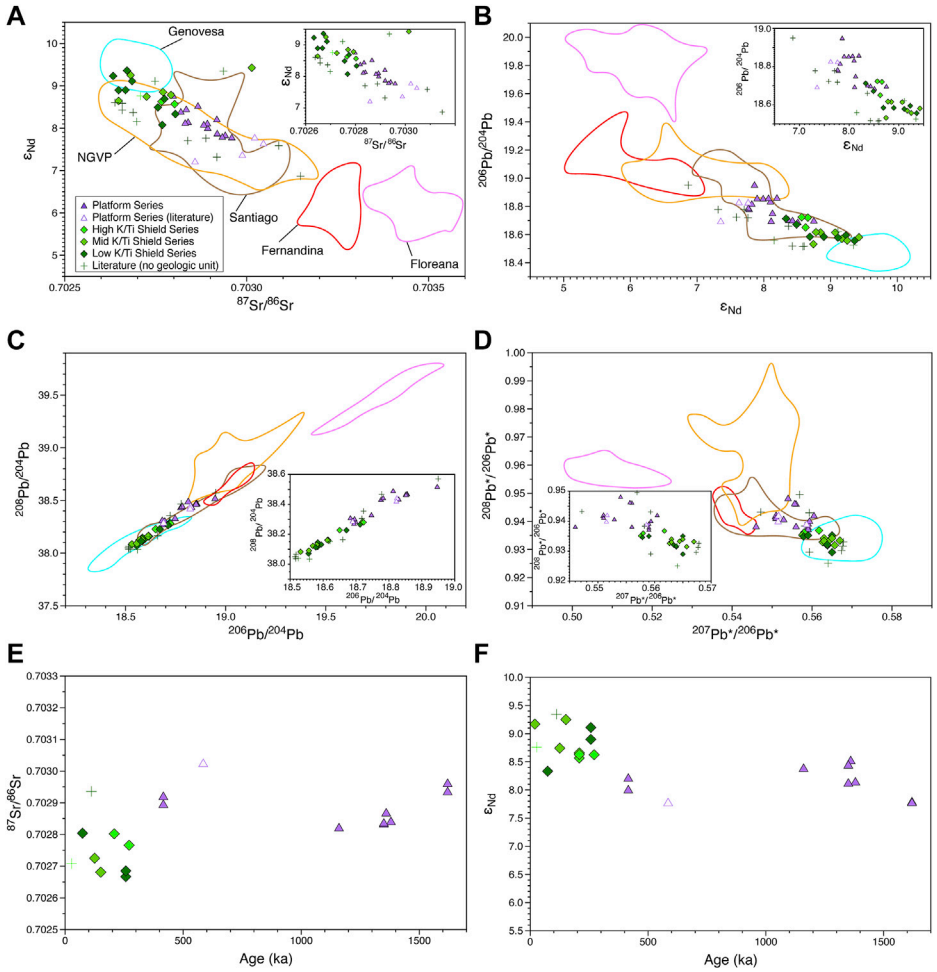

FIGURE 8 | Variations in radiogenic isotope ratios for Santa Cruz lavas. Fields are literature data. Red: Fernandina, blue: Genovesa, brown: Santiago, pink: Floreana, yellow: Northern Galápagos Volcanic Province (Bow and Geist, 1992; White et al., 1993; Harpp et al., 2002; Harpp et al., 2003; Saal et al., 2007; Gibson and Geist, 2010; Gibson et al., 2012; Harpp et al., 2014a; Harpp et al., 2014c). Symbols are larger than 1σ analytical error. **(A)** $^{87}Sr/^{86}Sr$ versus ε_{Nd}; note that two Shield Series samples offset from the main array to higher $^{87}Sr/^{86}Sr$ values are likely contaminated by seawater and their compositions are not considered in further discussion; **(B)** ε_{Nd} versus $^{206}Pb/^{204}Pb$; **(C)** $^{206}Pb/^{204}Pb$ versus $^{208}Pb/^{204}Pb$; **(D)** $^{207}Pb^*/^{206}Pb^*$ versus $^{208}Pb^*/^{206}Pb^*$. Radiogenic lead calculation: $^{208}Pb^*/^{206}Pb^* = [(^{208}Pb/^{204}Pb)_{sample}-(^{208}Pb/^{204}Pb)_{Earth\ Initial}]/[(^{206}Pb/^{204}Pb)_{sample}-(^{206}Pb/^{204}Pb)_{Earth\ Initial}]$, with $(^{208}Pb/^{204}Pb)_{Earth\ Initial} = 29.475$ and $(^{206}Pb/^{204}Pb)_{Earth\ Initial} = 9.307$ based on Canyon Diablo Troilite (Galer and O'Nions, 1985). $^{207}Pb^*/^{206}Pb^* = [(^{207}Pb/^{204}Pb)_{sample}-(^{207}Pb/^{204}Pb)_{Earth\ Initial}]/[(^{206}Pb/^{204}Pb)_{sample}-(^{206}Pb/^{204}Pb)_{Earth\ Initial}]$, with $(^{207}Pb/^{204}Pb)_{Earth\ Initial} = 10.294$ and $(^{206}Pb/^{204}Pb)_{Earth\ Initial} = 9.307$ based on Canyon Diablo Troilite (Galer and O'Nions, 1985). **(E)** $^{87}Sr/^{86}Sr$ variations in Santa Cruz lavas over time (in ka), for all available dates of study samples; **(F)** ε_{Nd} variations in Santa Cruz lavas over time (in ka), for all available dates of study samples. Samples indicated by a cross are literature data from Santa Cruz (White et al., 1993; Kurz and Geist, 1999; Saal et al., 2007); they have not been attributed to either the Platform or Shield Series owing to a lack of GPS coordinates for their origin locations.

lava of Santa Cruz (SC12-020; 1620 ka ± 15 (1σ); Schwartz et al., 2022), was formed when the island was in the current location of Volcán Alcedo, on Isabela Island ~80 km to the west, and most dated Platform Series have ages >1 Ma. We suggest that the Platform Series' greater depth of melt generation, more enriched compositions, and lesser geochemical variation are consistent with its location closer to the hotter plume center.

The low extent of mantle melting suggested by our modeling to generate the Platform Series (1–10%) may be explained by the fact that seismic tomography places the hottest part of the Galápagos plume center to the south and west of Fernandina Island (Hooft et al., 2003; Villagomez et al., 2007; Villagomez et al., 2014). By the time the oldest Platform Series lavas were emplaced, the volcano had moved to the eastern edge of the plume's core and was experiencing a waning magma flux (e.g., Geist et al., 2014a). This is a similar condition to the active Volcán Wolf today, which also taps a depleted source at the northern periphery of the Galapagos plume (Geist et al., 2005).

The younger Shield Series lavas erupted when Santa Cruz was closer to the island's current location, after an apparent hiatus of ~500 ka. Thus, they erupted >150 km from the tomographically identified core of the plume (e.g., Villagómez et al., 2014).

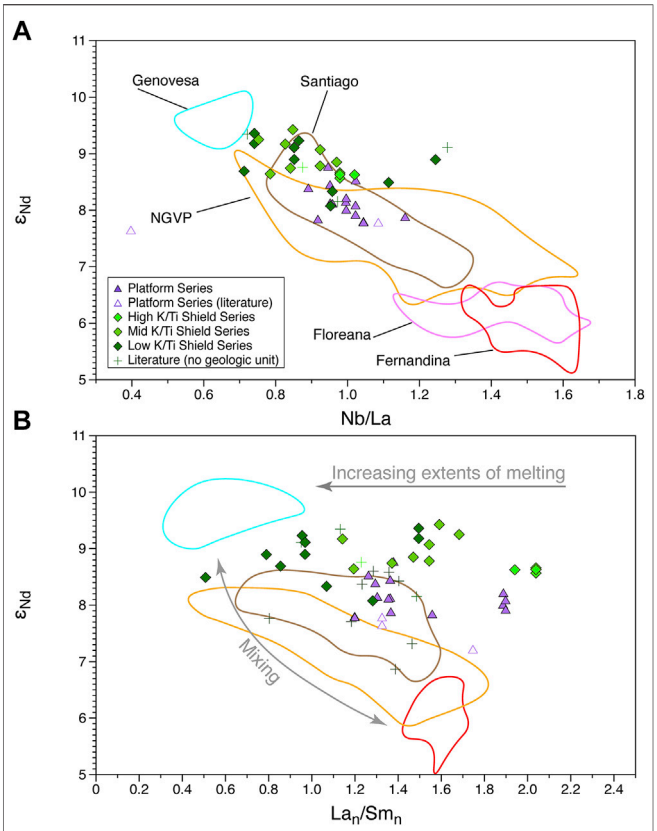

FIGURE 9 | Variations in radiogenic isotope ratios and incompatible trace element ratios for Santa Cruz lavas. Fields are literature data. Red: Fernandina, blue: Genovesa, brown: Santiago, pink: Floreana, yellow: Northern Galápagos Volcanic Province (Bow and Geist, 1992; White et al., 1993; Harpp et al., 2002; Harpp et al., 2003; Saal et al., 2007; Gibson and Geist, 2010; Gibson et al., 2012; Harpp et al., 2014a; Harpp et al., 2014c). Symbols are larger than 1σ analytical error. **(A)** Nb/La versus ε_{Nd}. **(B)** La_n/Sm_n (normalized to primitive mantle; McDonough and Sun, 1995) versus ε_{Nd}. Samples indicated by a cross are literature data from Santa Cruz (White et al., 1993; Kurz and Geist, 1999; Saal et al., 2007); they have not been attributed to either the Platform or Shield Series owing to a lack of GPS coordinates for their origin locations.

Magmatic Processing Prior to Eruption at Santa Cruz

The Platform Series is more evolved and less compositionally variable in its trace element and isotopic variations than the Shield Series (**Figures 2**, **3**, **10**). Furthermore, Platform Series lavas fractionated at shallower depths than the Shield Series, in a regime controlled primarily by plagioclase crystallization, and have, on average, lower phenocryst contents than Shield lavas. The Shield Series lavas experienced deeper fractionation, reflected by stronger clinopyroxene control (**Figure 4**; Geist et al., 1998) and higher average Sm_n/Yb_n values. Taken together, our data indicate that Platform Series magmas were stored in shallower, more mature magmatic bodies that were sufficiently developed to cause partial homogenization of trace element concentrations and isotopic ratios. The Platform Series' greater variability in Mg# relative to western volcanoes such as Fernandina, however, indicates that the Platform Series plumbing system was not able to develop a fully thermochemically buffered system (Geist et al., 2014a; Harpp and Geist, 2018). By contrast, the magmatic reservoirs in which Shield Series melts resided were poorly developed, neither thermochemically buffered nor networked, and likely located at a variety of depths.

Compared to the present-day western shields such as Fernandina, the characteristics of the Platform and Shield Series are those of relatively magma-starved systems, with the Shield Series being supplied by an even lower magma flux than the Platform Series. Similar geochemical systematics related to magma supply are observed at mid-ocean ridges. For example, in high-magma supply areas along the GSC, Colman et al. (2012) observe lower MgO content, lower phenocryst contents, and shallower depths of crystallization, all characteristics of both the Platform and Shield Series, but especially the latter. Colman et al. (2012) argue that low-magma supply ridges have deeper chambers because the magma tends to equilibrate thermally with the mid-to-lower crust, yielding more primitive magmas and higher phenocryst contents. We conclude that magmatic processing conditions at Santa Cruz shifted between the eruption of the Platform Series ~1 Ma and the younger Shield Series. Platform Series lavas were generated by melting a moderately enriched mantle, though more depleted than the current source for Fernandina, to broadly similar extents at, on average, shallower depths than Fernandina (**Figure 10**). Furthermore, western Galápagos shields such as Fernandina and Volcán Sierra Negra exhibit narrow ranges of major and trace element contents, reflecting a thermally buffered magmatic system that efficiently homogenizes melts en route to the surface (Geist et al., 2014a). By contrast, Platform Series lavas have more heterogeneous major element compositions but comparably narrow ranges in trace element ratios, suggesting that the Platform's magmatic plumbing system was sufficiently robust to homogenize melts prior to eruption but inadequate to achieve thermal buffering (Geist et al., 2014a). The younger Shield Series lavas at Santa Cruz were produced from a more depleted mantle source *via* a wide variety of extents and depths of melting similar to those at Santiago (Gibson et al., 2012). Magma supply to the Shield Series, in turn, was considerably lower than that of the Platform Series; Shield Series melts experienced limited crustal processing in small, poorly networked, likely ephemeral magma reservoirs, resulting in more variable and more primitive erupted compositions (e.g., Geist et al., 2014a; Harpp and Geist, 2018).

Magma Supply and Influence of the GSC Across the Archipelago

Construction of Santa Cruz in a Magma-Starved Regime

Geist et al. (2014a) propose a three-stage model for the evolution of the present-day western Galápagos shield volcanoes. The *Juvenile Phase* (e.g., Volcán Cerro Azul, on Isabela; **Figures 1**, **10**) occurs when a volcano is at the leading edge of the hotspot

TABLE 3 | Radiogenic isotope ratios for Santa Cruz lavas.

Sample	Compositional Group	$^{206}Pb/^{204}Pb$	$^{206}Pb/^{204}Pb$ 2s	$^{207}Pb/^{204}Pb$	$^{207}Pb/^{204}Pb$ 2s	$^{208}Pb/^{204}Pb$	$^{208}Pb/^{204}Pb$ 2s	$^{87}Sr/^{86}Sr$	$^{87}Sr/^{86}Sr$ 2s
SC12-008	Platform exposed in fault	18.8542	0.0007	15.5517	0.0007	38.4651	0.002	0.702882	0.000006
SC12-008 re	Platform exposed in fault	18.8522	0.001	15.5492	0.0008	38.4597	0.002		
SC12-009	Platform exposed in fault	18.6941	0.002	15.5406	0.001	38.2675	0.003	0.702798	0.000009
SC12-020	Platform	18.7765	0.0008	15.5542	0.0007	38.4290	0.002	0.702933	0.00001
SC12-020	Platform	18.783	0.001	15.558	0.001	38.440	0.002	0.702959	0.00001
SC12-025	Platform	18.8133	0.0008	15.5604	0.0007	38.4872	0.002	0.702941	0.000008
SC12-059	Platform	18.6910	0.001	15.5409	0.0009	38.2904	0.002	0.702831	0.00001
SC12-059	Platform	18.696	0.0008	15.545	0.0008	38.300	0.002	0.702834	0.00001
SC12-060	Platform	18.699	0.0008	15.543	0.0008	38.282	0.002	0.702819	0.00001
SC12-064	Platform	18.9473	0.0008	15.5590	0.0008	38.5151	0.002	0.702919	0.000007
SC12-065	Platform	18.7469	0.0008	15.5418	0.0007	38.3258	0.002	0.702839	0.00001
SC12-067	Platform	18.683	0.0007	15.548	0.0006	38.306	0.002	0.702866	0.000009
SC12-070	Platform	18.830	0.0009	15.558	0.0007	38.431	0.002	0.702892	0.00001
SC12-572B	Platform exposed in fault	18.8515	0.0008	15.5514	0.0009	38.4635	0.002	0.702893	0.000007
SC12-572B	Platform exposed in fault	18.856	0.0005	15.553	0.0005	38.466	0.001	0.702918	0.00002
SC12-011	Shield Low K/Ti (<0.15)	18.712	0.0009	15.540	0.001	38.265	0.002	0.702804	0.00001
SC12-015	Shield Low K/Ti (<0.15)	18.584	0.001	15.524	0.001	38.116	0.002	0.702667	0.00002
SC12-015	Shield Low K/Ti (<0.15)	18.5780	0.002	15.5201	0.002	38.1127	0.004	0.702685	0.000007
SC12-026	Shield Low K/Ti (<0.15)	18.6711	0.001	15.5303	0.001	38.2267	0.003	0.702756	0.000006
SC12-051	Shield Low K/Ti (<0.15)	18.5559	0.0008	15.5190	0.0008	38.0712	0.002	0.702671	0.00001
SC12-584B	Shield Low K/Ti (<0.15)	18.594	0.001	15.525	0.0009	38.131	0.002	0.702633	0.00001
SCZ15-01	Shield Low K/Ti (<0.15)	18.5839	0.0008	15.5346	0.0007	38.1446	0.002	0.702774	0.000008
SC12-012	Shield Mid K/Ti (0.15-0.24)	18.6148	0.012	15.5322	0.0007	38.1630	0.002	0.702770	0.000008
SC12-012	Shield Mid K/Ti (0.15-0.24)	18.617	0.0009	15.531	0.0007	38.157	0.002	0.702792	0.00001
SC12-012 re	Shield Mid K/Ti (0.15-0.24)	18.6142	0.012	15.5322	0.0008	38.1635	0.002		
SC12-012 re2	Shield Mid K/Ti (0.15-0.24)	18.6129	0.0008	15.5307	0.0008	38.1597	0.002		
SC12-024	Shield Mid K/Ti (0.15-0.24)	18.581	0.0006	15.527	0.0006	38.130	0.002	0.703014	0.00001
SC12-033	Shield Mid K/Ti (0.15-0.24)	18.5690	0.0008	15.5284	0.0007	38.1223	0.002		
SC12-038	Shield Mid K/Ti (0.15-0.24)	18.531	0.0007	15.523	0.0006	38.083	0.002	0.702725	0.00001
SC12-046	Shield Mid K/Ti (0.15-0.24)	18.557	0.0008	15.525	0.0006	38.091	0.002	0.702681	0.00001
SC12-027	Shield High K/Ti (>0.24)	18.7201	0.0008	15.5432	0.0007	38.2853	0.002		
SC12-027	Shield High K/Ti (>0.24)	18.723	0.006	15.543	0.0006	38.280	0.001	0.702802	0.00001
SC12-040	Shield High K/Ti (>0.24)	18.650	0.0007	15.542	0.0006	38.227	0.002	0.702766	0.00001

Sample	Compositional Group	$^{143}Nd/^{144}Nd$	$^{143}Nd/^{144}Nd$ 2s	C_{Nd}	$^{176}Hf/^{177}Hf$	$^{176}Hf/^{177}Hf$ 2s	C_{Hf}
SC12-008	Platform exposed in fault	0.513052	0.000008	8.07	0.283124	0.000005	11.98
SC12-008 re	Platform exposed in fault	0.513043	0.000009	7.90			
SC12-009	Platform exposed in fault	0.513087	0.000006	8.75	0.283133	0.000005	12.32
SC12-020	Platform	0.513037	0.000006	7.78	0.283103	0.000006	11.25
SC12-020	Platform	0.513036	0.000006	7.77			
SC12-025	Platform	0.513039	0.000006	7.82	0.283091	0.000006	10.82
SC12-059	Platform	0.513054	0.000006	8.11	0.283124	0.000006	11.98
SC12-059	Platform	0.513070	0.000005	8.43			
SC12-060	Platform	0.513067	0.000005	8.37			
SC12-064	Platform	0.513041	0.000004	7.86	0.283088	0.000004	10.73
SC12-065	Platform	0.513055	0.000007	8.13	0.283112	0.000007	11.58
SC12-067	Platform	0.513074	0.000005	8.51			
SC12-070	Platform	0.513053	0.000006	8.10			
SC12-572B	Platform exposed in fault	0.513048	0.000008	7.99	0.283112	0.000006	11.56
SC12-572B	Platform exposed in fault	0.513058	0.000006	8.20			
SC12-011	Shield Low K/Ti (<0.15)	0.513065	0.000006	8.33			
SC12-015	Shield Low K/Ti (<0.15)	0.513094	0.000007	8.90			
SC12-015	Shield Low K/Ti (<0.15)	0.513105	0.000006	9.11	0.283142	0.000004	12.63
SC12-026	Shield Low K/Ti (<0.15)	0.513073	0.000006	8.49	0.283127	0.000003	12.10
SC12-051	Shield Low K/Ti (<0.15)	0.513118	0.000006	9.36	0.283146	0.000005	12.76
SC12-051 re	Shield Low K/Ti (<0.15)	0.513109	0.000006	9.18			
SC12-584B	Shield Low K/Ti (<0.15)	0.513111	0.000006	9.23			
SCZ15-01	Shield Low K/Ti (<0.15)	0.513083	0.000006	8.69	0.283134	0.000005	12.34

(Continued on following page)

(Continued on following page)

TABLE 3 | (*Continued*) Radiogenic isotope ratios for Santa Cruz lavas.

Sample	Compositional Group	$^{143}Nd/^{144}Nd$	$^{143}Nd/^{144}Nd$ 2s	C_{Nd}	$^{176}Hf/^{177}Hf$	$^{176}Hf/^{177}Hf$ 2s	C_{Hf}
SC12-012	Shield Mid K/Ti (0.15-0.24)	0.513091	0.000007	8.85	0.283140	0.000003	12.57
SC12-012	Shield Mid K/Ti (0.15-0.24)	0.513088	0.000007	8.78			
SC12-012 re	Shield Mid K/Ti (0.15-0.24)	0.513103	0.000006	9.07			
SC12-024	Shield Mid K/Ti (0.15-0.24)	0.513121	0.000007	9.43			
SC12-033	Shield Mid K/Ti (0.15-0.24)	0.513108	0.000005	9.17	0.283146	0.000005	12.77
SC12-038	Shield Mid K/Ti (0.15-0.24)	0.513086	0.000005	8.74			
SC12-046	Shield Mid K/Ti (0.15-0.24)	0.513112	0.000003	9.25			
SC12-027	Shield High K/Ti (>0.24)	0.513082	0.000005	8.66	0.283131	0.000003	12.22
SC12-027	Shield High K/Ti (>0.24)	0.513077	0.000006	8.57			
SC12-027 re	Shield High K/Ti (>0.24)	0.513081	0.000005	8.63	0.283134	0.000004	12.33
SC12-040	Shield High K/Ti (>0.24)	0.513080	0.000005	8.63			

Analytical details and uncertainties are reported in the Methods section of the text. Italicized samples were analyzed at the Pacific Centre for Isotopic and Geochemical Research at the University of British Columbia; methodological details are available in Harpp and Weis (2020). Several replicate analyses (indicated by "re") are also included.

and the magmatic system is functioning in an unsteady thermal state. When the ~5 km-deep magmatic system is immature and poorly networked, individual batches of magma experience distinct crystallization histories, resulting in moderately heterogeneous geochemical signatures.

Next, the volcano moves into the *Mature Steady-State Phase*. Located directly above the plume stem, magma supply is sufficiently robust to achieve a steady thermal state, as exemplified by Fernandina, Volcán Wolf, and Volcán Sierra Negra (**Figure 10**). Magmas are compositionally monotonous and reside in a 1–3 km-deep sill immediately prior to eruption. The high flux of mantle-derived melts creates a crystal mush that acts as a thermal regulator, yielding a thermochemically buffered system capable of homogenizing most melts passing through it (Stock et al., 2018, 2020). Finally, when a Galápagos volcano is carried downstream from the plume, it reaches the *Dying Phase*. When the melt supply rate decreases, a steady-state magmatic plumbing system can no longer be maintained, and the 1–3 km deep magma reservoir likely freezes. Volcán Alcedo has erupted rhyolites fractionated from such a cooling crystal mush (**Figure 10**; Geist et al., 1995; Geist et al., 2014a).

This evolutionary model, however, only considers the western Galápagos shield volcanoes, and melt systematics of Santa Cruz do not align with any of its proposed phases. While the Platform Series exhibits comparably homogeneous trace element signatures to Fernandina and Volcán Sierra Negra, it lacks the monotonous major element compositions that define the thermochemically buffered Mature Steady-State phase of these younger volcanoes (**Figure 10**; Geist et al., 2014a). Though sampling of Santa Cruz is limited to the uppermost stratigraphic layers, to date no felsic material has been observed on the island, suggesting that it does not emulate Volcán Alcedo's Dying Phase, either (Geist et al., 2014a).

Harpp and Geist (2018) and Cleary et al. (2020) propose an alternative paradigm for the formation of the older, eastern Galápagos volcanoes. They note that the distinct magmatic, compositional, and structural characteristics of the western and central/eastern Galápagos Islands define separate geological provinces. The central and eastern volcanoes, including Santiago, Santa Cruz, Floreana, and San Cristóbal, erupt more primitive, heterogeneous lavas, suggesting that magmas spent shorter times in crustal storage, and their plumbing systems were poorly developed with no thermochemical buffering. The eastern islands lack submarine rift zones, have never hosted summit calderas (Cleary et al., 2020), and are dominated by faults and linear vent systems, characteristics consistent with a magma-starved regime compared to that of the present-day western archipelago. In the eastern Galápagos, regional stresses are the dominant influence on structural and eruptive behavior (Schwartz et al., 2022). This regime contrasts with the western volcanoes, where magmatic pressure is the strongest influence on volcano construction, resulting in large shields with calderas, circumferential and radial faults and fissures, and many submarine rift zones (e.g., Lonsdale, 1989; Chadwick and Howard, 1991; Smith et al., 2002; Bagnardi et al., 2013).

Influence of the Proximal Galápagos Spreading Center on Eastern Volcano Construction

Harpp and Geist (2018) suggest that Santa Cruz and most of the other central and eastern islands are not older, evolved versions of the western shields, but were constructed in a distinct tectonic setting from the younger volcanoes, one strongly influenced by the adjacent GSC. The GSC has been migrating northeast, away from the Galápagos hotspot at 65 km/Ma (Wilson and Hey, 1995; Mittlestaedt et al., 2011). During the past 5 million years, however, the GSC has experienced multiple southward ridge jumps, which occurred at ~4.5 Ma, ~3.5 Ma, between 2.5 and 3.5 Ma, and ~1 Ma, each time resulting in a 20–30 km displacement of a GSC segment toward the archipelago (Mittelstaedt et al., 2012). The last two ridge jumps established the Galápagos Transform Fault (GTF) and a transtensive stress field expressed as oblique faulting near the transform (Taylor et al., 1994).

The regional stress field created by a transform fault along a mid-ocean ridge can have far-reaching effects on the lithosphere (e.g., Gudmundsson, 1995; Ribe, 1996; Ito et al., 2003; Hall and Kincaid, 2004; Georgen, 2014). Mittelstaedt et al. (2012) proposed that the stress field generated by the two most recent GSC jumps may have perturbed the lithosphere within ~150 km sufficiently to promote the formation of the NW/SE-trending seamount chains of the NGVP, between the main archipelago and the GSC (Harpp and Geist, 2002). If the stress field initiated by the

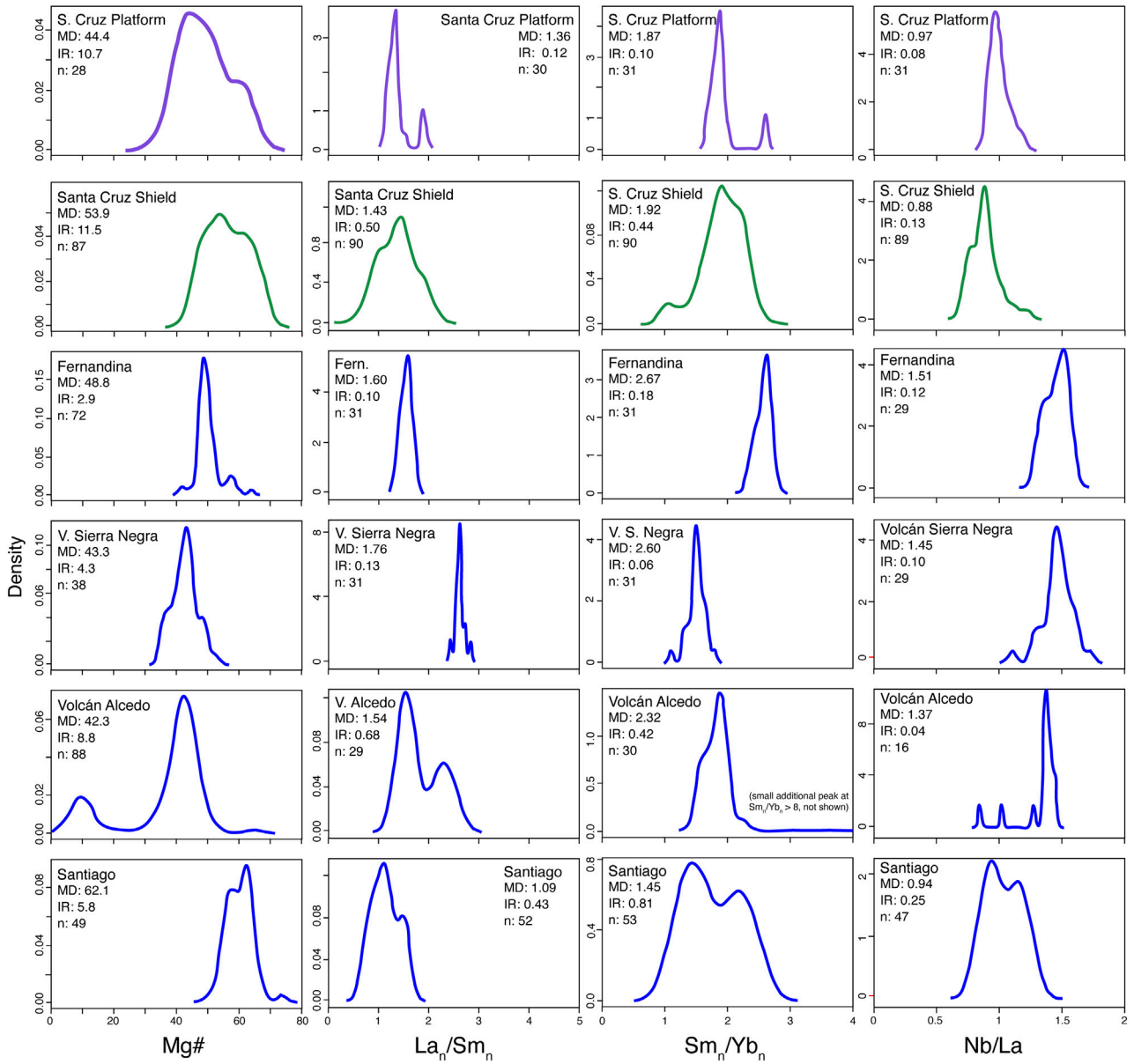

FIGURE 10 | Gaussian kernel distribution statistics for Mg# (proxy for extent of shallow fractionation), La_n/Sm_n (proxy for extent of melting), Sm_n/Yb_n (proxy for depth of melting), and Nb/La (proxy for plume contribution; Kurz and Geist, 1999) for Santa Cruz lavas, shown as Platform and Shield (all sub-groups treated together because they erupted contemporaneously). Also shown for comparison are statistics from Fernandina (White et al., 1993; Kurz and Geist, 1999; Allan and Simkin, 2000), Volcán Sierra Negra (White et al., 1993; Reynolds and Geist, 1995), Volcán Alcedo (Geist et al., 1995), and Santiago (Gibson et al., 2012). MD is the maximum density and IR is the interquartile range, both determined using Wessa (2021). La, Sm, and Yb are normalized to chondrite values (McDonough and Sun, 1995).

GTF is responsible for the Northern Galápagos seamount lineaments, then the present-day central/eastern Galápagos islands forming when the GSC was closer to the plume are likely to have been strongly influenced by the ridge as well. The GTF jumps contemporaneous with Santa Cruz construction, the transtensive kinematics of the GTF (Taylor et al., 1994), and stresses generated by the GSC (e.g., Fujita and Sleep, 1978) may explain the preponderance of linear vent systems and faults across the central and eastern islands, including Santa Cruz. In support of this hypothesis is the fact that Floreana, which would have been the farthest active volcano from the GSC at 1.5 Ma, lacks linear vent structures and faults (Harpp et al., 2014a).

Furthermore, the intensity of the magma flux supplying the central and eastern islands was also likely affected by the proximity of the plume to the GSC. Even though the precise mechanism is debated (e.g., Mittelstaedt et al., 2011; Georgen, 2014; Gibson et al., 2015; Mittal and Richards, 2017; Gleeson and Gibson, 2021), geochemical and morphological behavior clearly

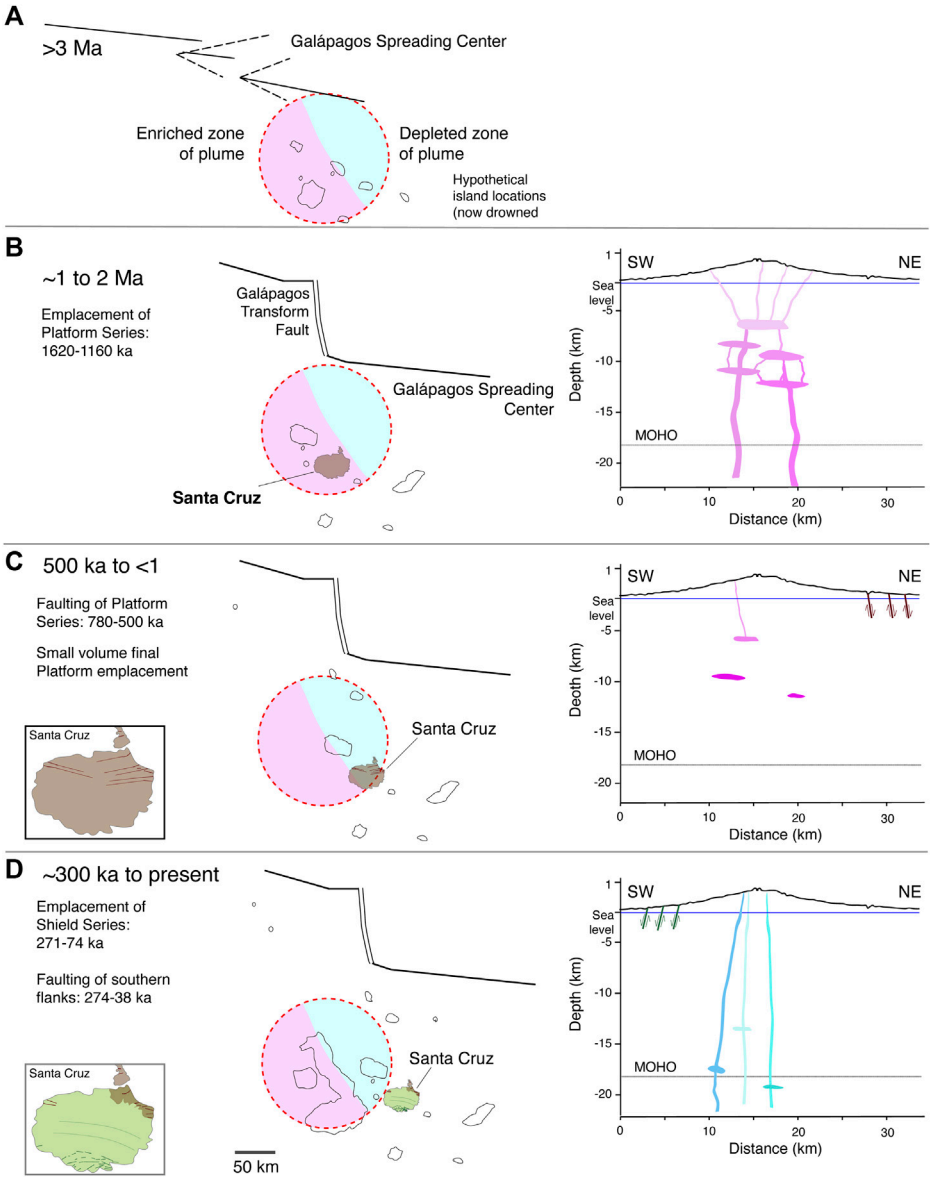

FIGURE 11 | A conceptual timeline of Santa Cruz's volcanic evolution. Left side panels: Map view of archipelago and relationship between plume, islands, and GSC. Right side panels: NE-SW cross-section of Santa Cruz. Note that vertical scales above and below 0 km are different, and that island cross-section has a vertical exaggeration of 4×. Current depth to the MOHO is estimated at ~17 km (Feighner and Richards, 1994). **(A)** LEFT: Prior to ~3 Ma, the GSC was nearly superimposed on the Galápagos plume (Wilson and Hey, 1995). None of the present-day Galápagos Islands date to 3.5 Ma (White et al., 1993), but older islands now submerged downstream to the east existed at the time; their locations are hypothesized here (Christie et al., 1992). The plume's (red dashed circle; limits estimated from Gibson et al., 2012) bilateral compositional asymmetry is indicated with the pink (more enriched, LLSVP-sourced) and blue (more depleted, lower mantle-sourced) zones (Harpp and Weis, 2020). Evolution of the GSC is based on Mittelstaedt et al. (2012). **(B)** LEFT: At ~2 Ma, Santa Cruz begins to form and emerge; between 1629 and 1160 ka, most of the Platform Series lavas sampled in this study are emplaced (brown; Schwartz et al., 2022). The Platform Series is being emplaced as Santa Cruz approaches the compositional boundary of the plume, resulting in geochemical signatures slightly less enriched than present-day Fernandina lavas. According to Mittelstaedt et al. (2012), the Galápagos Transform Fault is formed in the most recent southward jump of the GSC ~1 Ma. RIGHT: The Platform Series lavas constitute the main shield-building phase of Santa Cruz. The proximity of the GSC causes diversion of some plume material toward the ridge, resulting in lower flux to the nascent Santa Cruz volcano than currently supplies Fernandina, sufficient to support formation of a magmatic network capable of partially homogenizing melts prior to eruption, but unable to generate thermochemically buffered conditions. **(C)** LEFT: Between 780 and 500 ka, the Platform Series experiences normal faulting, likely in response to the ~1 Ma southward jump of the GSC. Faults are shown in crimson on the north side of Santa Cruz and Baltra (*see* inset; possible extensions of the faults toward the center of the island are shown as dashes). RIGHT: Normal faulting from Galápagos Transform Fault-related stresses may initiate additional, small volume eruptive activity. **(D) LEFT:** The Shield Series (green) is emplaced between 271 and 74 ka, primarily from aligned vents that cross the volcano's central highlands (green dashed lines). Nearly contemporaneously, normal faulting (dark green lines) occurs along the southern flank of the island (274–38 ka; *see* inset; Schwartz et al., 2022). **RIGHT:** Southern flank of Santa Cruz begins to slump, forming extensional structures. Magma in small, ephemeral, poorly networked reservoirs that are incapable of storing or homogenizing melts is erupted as the Shield Series, with more variable and more primitive compositions compared to the Platform Series. The island has crossed into the plume's eastern compositional zone, causing lavas to have more depleted geochemical signatures (blue colors).

indicates that the GSC currently incorporates material from the Galápagos plume (e.g., Schilling et al., 1982; Ribe, 1996; Canales et al., 1997, 2002; Detrick et al., 2002; Sinton et al., 2003; Behn et al., 2004; Christie et al., 2005; White et al., 2008; Ingle et al., 2010). When the GSC was closer to the plume 1–3 Ma, the ridge probably siphoned even more plume material toward its axis than it does today, diverting it from the nascent volcanoes, and resulting in a constructional regime that was magma-starved compared to today's western Galápagos volcanoes (Harpp and Geist, 2018). At the time of their formation, therefore, Santa Cruz, along with the other central and eastern volcanoes, had a reduced magma supply incapable of establishing thermochemically buffered, crustal-scale mush columns or calderas normally associated with robust magma supplies.

In addition to changes in magma supply related to the migration of the GSC, the constructional and evolutionary trajectories of the eastern volcanoes may also have been controlled by the presence of especially thin lithosphere underlying those structures, owing to their near-ridge location. The lithosphere underlying an ocean island is flexed by the volcanic load, which in turn can have a strong influence on magma ascent pathways during construction (McGovern et al., 2015). On relatively young, thin lithosphere, such as that underlying the western Galápagos (Feighner and Richards, 1994; Gibson and Geist, 2010), the island's load induces compression, which limits and focuses magma ascent, encouraging formation of sill complexes (McGovern et al., 2013; McGovern et al., 2015; LeCorvec and McGovern, 2018). Consistently, the magma reservoirs supporting Fernandina and Volcán Sierra Negra volcanoes are constructed from networks of sills (e.g., Chadwick et al., 2006; Yun et al., 2006; Bagnardi et al., 2013).

The central Galápagos platform has a thinner, weaker lithosphere with an elastic thickness <6 km (Feighner and Richards, 1994; Gibson and Geist, 2010), owing in part to the GTF that displaces the eastern GSC ~100 km closer to the archipelago. When the central volcanoes such as Santa Cruz were forming, from at least 1.6 Ma and up to another million years earlier, the GSC was even closer to the archipelago, and the lithosphere was thinner than it is today. When the lithospheric flexure models of McGovern et al., 2013; Le Corvec and McGovern, 2018; P.J. McGovern, *pers. comm.*, 2021, are extended to near-zero lithospheric thickness, as was probably the case when Santa Cruz was first forming, there is little stress to control the construction process; magma ascent paths are therefore relatively unconstrained, preventing the formation of sill-dominated, centralized magmatic plumbing systems. Instead, magma is free to ascend, resulting in small, dispersed, poorly networked magma storage systems, consistent with the heterogeneous, minimally fractionated lavas erupted across the eastern Galápagos Islands (Harpp and Geist, 2018).

Evolution of Santa Cruz in the Context of the Galápagos Archipelago

To integrate the structural study of Santa Cruz by Schwartz et al. (2022) into our findings for the petrologic evolution of Santa Cruz, we propose the following model (**Figure 11**):

1. Proximity of GSC to plume: Between 3.5 and 2.5 Ma, the GSC experienced a ridge jump of several 10s of kilometers southward toward the plume (Mittelstaedt et al., 2012). Throughout this period, the GSC is considerably closer to the plume than it is currently, diverting plume material toward the ridge (e.g., Ribe, 1996; Ito et al., 2003). Thus, volcanoes forming at the plume center have a reduced magma supply compared to today's western shields (Harpp and Geist, 2018).

2. Emergence of Santa Cruz (1–2 Ma): Geist et al. (2014b) bracket the emergence of Santa Cruz to between 1.1 and 2.3 Ma. Actual emergence must be closer to the old end of this range, because the oldest lavas on Santa Cruz date to ~1.6 Ma (Schwartz et al., 2022).

3. Eruption of the Platform Series: The Platform Series is emplaced primarily between at least ~1620 ± 15 and 1160 ± 35 ka; at the time, the island was ~80 km closer to the plume (51 km/M.y.; Argus et al., 2011). Even though these lavas are the most enriched on Santa Cruz, they are less so than Fernandina (e.g., White et al., 1993; Allan and Simkin, 2000; Harpp and Weis, 2020). Potential explanations for their less-than-pristine enriched plume signatures include either dilution by depleted upper mantle owing to interaction with the then-adjacent GSC or the island's location at the eastern edge of the enriched zone of the plume, where it may have begun transitioning into the more depleted eastern zone (Harpp and Weis, 2020; **Figure 1**). The Platform Series's relatively homogeneous trace element compositions suggest that magma supply was sufficient to homogenize melts to some extent prior to eruption, but inadequate to establish a thermochemically buffered state like Fernandina (Geist et al., 2014a).

4. Platform Series Faulting: According to Schwartz et al. (2022), a series of E/W-trending faults crosscuts the Platform Series <1160 ± 35 ka, possibly between 780 and 500 ka. Given the proximity of the GSC to the archipelago at the time (~65 km closer than the 150–300 km it is today), the Platform Series faulting may reflect regional stresses generated by the most recent southward GSC jump, which displaced the ridge by ~30 km toward the plume and established the regional transtensive stress regime around the now 100 km-long transform fault. The extensional component of the stress field may have generated E-W oriented magmatic intrusions across the near-ridge region (e.g., Mittelstaedt et al., 2012), which may have initiated the Shield Series.

5. Eruption of the Shield Series: The most recent activity on Santa Cruz is the Shield Series, which mostly erupted from 271 ± 17 to 74 ± 38 ka (Bow, 1979; Schwartz, 2014). Regional extension generated by the ~1 Ma GSC ridge jump and Platform Series faulting may have initiated Shield Series activity. The Shield Series lavas are more depleted than the Platform Series, which reflect the island's location farther east, within the less enriched zone of the bilaterally asymmetric plume (Harpp and Weis, 2020). Shield Series melts are highly heterogeneous and more primitive than Platform Series rocks, owing to the ephemeral nature of the small, poorly networked magmatic reservoirs and limited magma supply.

6. Faulting of the Southern Flank's Shield Series: Between 274 ± 18 and 38 ± 8 ka, fault swarms cut Santa Cruz's southern

flanks (**Figure 1**; Schwartz et al. (2022)). Schwartz et al. (2022) propose that these faults are in response to the E/W-oriented intrusions that supplied the Shield Series, although the sequence of events could be reversed (i.e., extensional faulting generates decompression melting; a similar mechanism is modeled for the seamounts and islands in the Northern Galápagos Volcanic Province; *see* Mittelstaedt et al., 2012).

7. Present-day Santa Cruz: Although there has been no documented eruptive activity since 74 ka on Santa Cruz, there has been relatively recent faulting (~38 ka) along the southern flanks. If this phenomenon reflects ongoing structural instability, there is the potential for future tectonic or eruptive events that could pose a risk to the population living along the southern coast of the island in the town of Puerto Ayora.

Mantle Sources at Santa Cruz and Implications for the Galápagos Plume

Harpp and Weis (2020) explained the wide range of geochemical signatures in the Galápagos as the manifestation of a bilaterally asymmetric plume, with the compositional zonation originating at the core-mantle boundary, as originally posited for Hawai'i (Weis et al., 2011). As volcanoes are carried eastward by the Nazca plate, they cross the NW-trending compositional boundary between the western, enriched zone of the plume into the more PREMA-like eastern zone. Consequently, the last material erupted on a Galápagos island will have less enriched signatures than the older material (Harpp et al., 2014b; Harpp and Weis, 2020).

Santa Cruz data are consistent with the bilaterally asymmetric plume model. Harpp and Weis (2020) delineate the boundary between the highly enriched and the less enriched zones immediately west of Santa Cruz. The oldest Platform Series lavas were emplaced when Santa Cruz was located on the eastern edge of the bilateral plume's strongly enriched zone, where the eastern coast of Volcán Alcedo is located today (Harpp and Weis, 2020). The compositions of these 1.6–1.1 Ma lavas, which are not as enriched as material erupted at Fernandina today, may reflect the transition between the western enriched and the eastern, less enriched zone. The more depleted signatures of the younger Shield Series reflect their emplacement location east of the bilateral plume's compositional boundary.

The proximity of the GSC to Santa Cruz >1 Ma when it was first being constructed may also contribute to the Platform Series' being more depleted than Fernandina, *via* two potential mechanisms. In their modeling study of melt transport from plumes to nearby mid-ocean ridges, Gibson and Richards (2018) propose that low-degree, volatile-rich melts formed by initial, deep melting of the plume (>3 GPa; Gleeson and Gibson, 2021) are transported directly to a nearby spreading center *via* channelized flow, reducing contributions from the more enriched, fusible plume to erupted lavas. When the GSC was closer to the Galápagos plume >1 Ma, the intensity of this deep melt transport may have been enhanced, resulting in greater relative depletion of the mantle source responsible for the Platform Series.

A second, well documented mechanism that could explain the depletion of Platform Series lavas relative to Fernandina also reflects the closer proximity of the plume to the GSC >1 Ma. Depleted geochemical signatures at other near-ridge plume systems, including Kerguelen, the Cretaceous Hawaiian plume, and Easter (e.g., Hart et al., 1992; Frey and Weis, 1995; Kingsley and Schilling, 1998; Harrison et al., 2020), have been attributed to dilution of the more enriched plume material by entrainment of depleted upper mantle owing to the proximity of the two magmatic systems. All of the Santa Cruz lavas in this study have MORB-like ΔNb <0 (**Figure 7**; Fitton et al., 1997), suggesting that depleted upper mantle material likely plays an important role in the depleted Santa Cruz lavas (Harpp and Weis, 2020), consistent with their near-ridge origin.

CONCLUSIONS

Like several of its nearest island neighbors and in contrast to the young western Galápagos volcanoes, the geochemistry of Santa Cruz Island is diverse, erupting lavas with variable major and trace element concentrations, in addition to a range of isotopic ratios. The older Platform Series has a more enriched signature than the younger Shield Series, and both are more depleted than younger western Galápagos volcanoes such as Fernandina. Platform Series lavas have relatively invariant trace and isotopic ratios, comparably homogeneous to those at Fernandina, but with heterogeneous, evolved major element compositions. Shield Series lavas are, in turn, significantly more primitive and heterogeneous than those of the Platform Series.

We propose that Santa Cruz has followed a different evolutionary path from the present-day western Galápagos shields, controlled primarily by its proximity to the GSC and its construction in a relatively magma-starved regime (**Figure 11**; Harpp and Geist, 2018). Santa Cruz was formed >1.6 Ma, when the plume was considerably closer to the GSC than it is today. Enhanced plume flow to the ridge may have reduced the magmatic flux available for the construction of Santa Cruz.

Consequently, the Platform Series, the major constructional unit emplaced between ~1620 ± 15 and 1160 ± 35 ka (Schwartz et al., 2022), was established under relatively magma-starved conditions compared to the present-day younger shields. The Platform Series had a sufficiently robust magma supply to develop plumbing systems capable of homogenizing melts to a limited extent, but unable to support development of the caldera-producing, thermochemically buffered systems that exist today in the western archipelago (Geist et al., 2014a; Cleary et al., 2020). The Platform Series is more compositionally depleted than present-day Fernandina lavas because of two factors: *1*) its location at the eastern edge of the plume's enriched zone (Harpp and Weis, 2020); and *2*) dilution of plume material by depleted upper mantle owing to its closer proximity to the GSC at the time of its formation.

The most recent jump of a GSC segment toward the plume ~1 Ma (Mittelstaedt et al., 2012) may have initiated the E-W-trending faults that crosscut the Platform Series <1160 ± 35 ka (Schwartz et al., 2022). After an apparent hiatus in eruptive activity, the Shield Series lavas erupted between 271 ± 17 and 74 ± 38 ka (Schwartz et al., 2022). These lavas are more depleted than the Platform Series, consistent with

migration of the Nazca Plate eastward over the boundary dividing the enriched and depleted zones of the bilaterally asymmetric Galápagos plume (Harpp and Weis, 2020). Owing to their even weaker magma supply farther from the plume center, the more variable, more primitive Shield Series lavas erupted after little to no crustal processing from small, ephemeral, poorly networked reservoirs. Coincident with the emplacement of the Shield Series, the southern flank of Santa Cruz experienced a period of faulting between 274 ± 18 and 38 ± 8 ka (Schwartz et al., 2022). Given that the faulting along the southern flank is extensional, it is possible that tectonic or eruptive activity could occur in the future, putting the population in the town of Puerto Ayora at risk. Much of the distinctive constructional characteristics of Santa Cruz can be attributed to its proximity to the GSC, its limited magma supply owing to diversion of plume material toward the ridge, and the thin, near-zero age lithosphere underlying the volcano.

DATA AVAILABILITY STATEMENT

The original contributions presented in the study are included in the article/**Supplementary Materials**, further inquiries can be directed to the corresponding author.

AUTHOR CONTRIBUTIONS

EW and KH are co-first authors. All authors participated in fieldwork on Santa Cruz Island, primarily EW, DS and RV. All authors participated in trace element analyses of samples. EW performed major element and isotopic ratio analyses, and wrote the original draft of the manuscript as her MSc thesis from the University of Idaho's Department of Geological Sciences.

FUNDING

All research, including analytical fees and the costs of field work, were supported by OCE-0926491 and EAR-1347731 to KH from the National Science Foundation. The University of Idaho provided teaching assistant support for EW during her Master's work. Colgate University provided some of the publication fees.

ACKNOWLEDGMENTS

We are grateful to D. Geist, J. Schleicher, M. Almeida, and Requelme for their assistance in the field. Additional geochemical analyses were performed by J. Mahr, H. Bercovici, and R. Pimentel. We acknowledge the Galápagos National Park Service for granting us permission to collect samples and conduct fieldwork on Santa Cruz Island. N. d'Ozouville and other staff at the Charles Darwin Research Station provided much logistical support, without whom the field seasons could not have been accomplished. Thanks to D. Geist and M. Jackson for constructive reviews during writing of the manuscript, to P.J. McGovern for sharing his expertise and ideas about Galápagos volcanoes and lithospheric thickness, and to M. Gleeson and two additional anonymous reviewers for their insightful comments that helped improve the manuscript. This work was funded by NSF grants EAR-1347731 and OCE-0926491 to KH.

SUPPLEMENTARY MATERIAL

The Supplementary Material for this article can be found online at: https://www.frontiersin.org/articles/10.3389/feart.2022.845544/full#supplementary-material

REFERENCES

Allan, J. F., and Simkin, T. (2000). Fernandina Volcano's Evolved, Well-Mixed Basalts: Mineralogical and Petrological Constraints on the Nature of the Galapagos Plume. *J. Geophys. Res.* 105, 6017–6041. doi:10.1029/1999JB900417

Anderson, M., Wanless, V. D., Schwartz, D. M., McCully, E., Fornari, D. J., Jones, M. R., et al. (2018). Submarine Deep-Water Lava Flows at the Base of the Western Galápagos Platform. *Geochem. Geophys. Geosyst.* 19, 3945–3961. doi:10.1029/2018GC007632

Argus, D. F., Gordon, R. G., and DeMets, C. (2011). Geologically Current Motion of 56 Plates Relative to the No-Net-Rotation Reference Frame. *Geochem. Geophys. Geosyst.* 12, a–n. doi:10.1029/2011GC003751

Bagnardi, M., Amelung, F., and Poland, M. P. (2013). A New Model for the Growth of Basaltic Shields Based on Deformation of Fernandina Volcano, Galápagos Islands. *Earth Planet. Sci. Lett.* 377-378, 358–366. doi:10.1016/j.epsl.2013.07.016

Behn, M. D., Sinton, J. M., and Detrick, R. S. (2004). Effect of the Galápagos Hotspot on Seafloor Volcanism along the Galápagos Spreading Center (90.9-97.6°W). *Earth Planet. Sci. Lett.* 217, 331–347. doi:10.1016/s0012-821x(03)00611-3

Blichert-Toft, J., and White, W. M. (2001). Hf Isotope Geochemistry of the Galápagos Islands. *Geochem. Geophys. Geosyst.* 2, 9. doi:10.1029/2000gc000138

Bow, C. S., and Geist, D. J. (1992). Geology and Petrology of Floreana Island, Galapagos Archipelago, Ecuador. *J. Volcanology Geothermal Res.* 52, 83–105. doi:10.1016/0377-0273(92)90134-y

Bow, C. S. (1979). *The Geology and Petrogenesis of the Lavas of Floreana and Santa Cruz Islands: Galápagos Archipelago. Ph.D. Dissertation*. Eugene, OR: University of Oregon.

Canales, J. P., Dañobeitia, J. J., Detrick, R. S., Hooft, E. E. E., Bartolomé, R., and Naar, D. F. (1997). Variations in Axial Morphology along the Galápagos Spreading center and the Influence of the Galápagos Hotspot. *J. Geophys. Res.* 102, 27341–27354. doi:10.1029/97jb01633

Canales, J. P., Ito, G., Detrick, R. S., and Sinton, J. (2002). Crustal Thickness along the Western Galápagos Spreading Center and the Compensation of the Galápagos Hotspot Swell. *Earth Planet. Sci. Lett.* 203, 311–327. doi:10.1016/s0012-821x(02)00843-9

Chadwick, W. W., and Dieterich, J. H. (1995). Mechanical Modeling of Circumferential and Radial dike Intrusion on Galapagos Volcanoes. *J. Volcanology Geothermal Res.* 66, 37–52. doi:10.1016/0377-0273(94)00060-T

Chadwick, W. W., Geist, D. J., Jónsson, S., Poland, M., Johnson, D. J., and Meertens, C. M. (2006). A Volcano Bursting at the Seams: Inflation, Faulting, and Eruption at Sierra Negra Volcano, Galápagos. *Geol* 34, 1025–1028. doi:10.1130/G22826A.1

Chadwick, W. W., and Howard, K. A. (1991). The Pattern of Circumferential and Radial Eruptive Fissures on the Volcanoes of Fernandina and Isabela Islands, Galapagos. *Bull. Volcanol* 53, 259–275. doi:10.1007/bf00414523

Chen, C. -Y., and Frey, F. A. (1983). Origin of Hawaiian Tholeiite and Alkalic basalt. *Nature* 302, 785–789. doi:10.1038/302785a0

Christie, D. M., Duncan, R. A., McBirney, A. R., Richards, M. A., White, W. M., Harpp, K. S., et al. (1992). Drowned Islands Downstream from the Galapagos Hotspot Imply Extended Speciation Times. *Nature* 355, 246–248. doi:10.1038/355246a0

Christie, D. M., Werner, R., Hauff, F., Hoernle, K., and Hanan, B. B. (2005). Morphological and Geochemical Variations along the Eastern Galápagos Spreading Center. *Geochem. Geophys. Geosyst.* 6, 1. doi:10.1029/2004gc000714

Clague, D. A., and Dalrymple, G. B. (1988). Age and Petrology of Alkalic Postshield and Rejuvenated-Stage Lava from Kauai, Hawaii. *Contr. Mineral. Petrol.* 99, 202–218. doi:10.1007/BF00371461

Clague, D. A., and Dalrymple, G. B. (1987). "The Hawaiian-Emperor Volcanic Chain. Part I. Geologic Evolution," in *Volcanism in Hawaii*. Editors R. W. Decker, T. M. Wright, and P. H. Stauffer (Washington D.C.: US Gov't Printing Office), 5–54.

Cleary, Z., Schwartz, D. M., Mittelstaedt, E., and Harpp, K. (2020). Dynamic Magma Storage at Near-Ridge Hot Spots: Evidence from New Galápagos Gravity Data. *Geochem. Geophys. Geosyst* 21, 3. doi:10.1029/2019gc008722

Colman, A., Sinton, J. M., White, S. M., McClinton, J. T., Bowles, J. A., Rubin, K. H., et al. (2012). Effects of Variable Magma Supply on Mid-ocean ridge Eruptions: Constraints from Mapped Lava Flow fields along the Galápagos Spreading Center. *Geochem. Geophys. Geosyst.* 13, a–n. doi:10.1029/2012GC004163

Detrick, R. S., Sinton, J. M., Ito, G., Canales, J. P., Behn, M., Blacic, T., et al. (2002). Correlated Geophysical, Geochemical, and Volcanological Manifestations of Plume-ridge Interaction along the Galápagos Spreading Center. *Geochem. Geophys. Geosyst.* 3, 10. doi:10.1029/2002gc000350

Eggins, S. M., Woodhead, J. D., Kinsley, L. P. J., Mortimer, G. E., Sylvester, P., McCulloch, M. T., et al. (1997). A Simple Method for the Precise Determination of ≥ 40 Trace Elements in Geological Samples by ICPMS Using Enriched Isotope Internal Standardisation. *Chem. Geology.* 134, 311–326. doi:10.1016/s0009-2541(96)00100-3

Ellam, R. M. (1992). Lithospheric Thickness as a Control on basalt Geochemistry. *Geol* 20, 153–156. doi:10.1130/0091-7613(1992)020<0153:ltaaco>2.3.co;2

Feighner, M. A., and Richards, M. A. (1994). Lithospheric Structure and Compensation Mechanisms of the Galápagos Archipelago. *J. Geophys. Res.* 99, 6711–6729. doi:10.1029/93jb03360

Fitton, J. G., Saunders, A. D., Kempton, P. D., and Hardarson, B. S. (2003). Does Depleted Mantle Form an Intrinsic Part of the Iceland Plume? *Geochem. Geophys. Geosyst.* 4, 3. doi:10.1029/2002gc000424

Fitton, J. G., Saunders, A. D., Norry, M. J., Hardarson, B. S., and Taylor, R. N. (1997). Thermal and Chemical Structure of the Iceland Plume. *Earth Planet. Sci. Lett.* 153, 197–208. doi:10.1016/s0012-821x(97)00170-2

French, S. W., and Romanowicz, B. (2015). Broad Plumes Rooted at the Base of the Earth's Mantle beneath Major Hotspots. *Nature* 525, 95–99. doi:10.1038/nature14876

Frey, F. A., and Weis, D. (1995). Temporal Evolution of the Kerguelen Plume: Geochemical Evidence from 38 to 82 Ma Lavas Forming the Ninetyeast Ridge. *Contrib. Mineral. Petrol.* 121, 12–28. doi:10.1007/s004100050087

Fujita, K., and Sleep, N. H. (1978). Membrane Stresses Near Mid-ocean ridge-transform Intersections. *Tectonophysics* 50, 207–221. doi:10.1016/0040-1951(78)90136-1

Galer, S. J. G., and O'Nions, R. K. (1985). Residence Time of Thorium, Uranium and lead in the Mantle with Implications for Mantle Convection. *Nature* 316, 778–782. doi:10.1038/316778a0

Geist, D., Howard, K. A., and Larson, P. (1995). The Generation of Oceanic Rhyolites by Crystal Fractionation: the Basalt-Rhyolite Association at Volc N Alcedo, Gal Pagos Archipelago. *J. Petrology* 36, 965–982. doi:10.1093/petrology/36.4.965

Geist, D. J., Bergantz, G., and Chadwick, W. W. (2014a). "Galápagos Magma Chambers," in The Galápagos: A Natural Laboratory For the Earth Sciences, *Geophysical Monograph Series V. 204*. Editors K. S. Harpp, E. Mittelstaedt, N. d'Ozouville, and D. W. Graham (Washington, DC: American Geophysical Union), 55–69. doi:10.1002/9781118852538.ch5

Geist, D. J., Fornari, D. J., Kurz, M. D., Harpp, K. S., Adam Soule, S., Perfit, M. R., et al. (2006). Submarine Fernandina: Magmatism at the Leading Edge of the Galápagos Hot Spot. *Geochem. Geophys. Geosyst.* 7, a–n. doi:10.1029/2006GC001290

Geist, D. J., Harpp, K. S., Naumann, T. R., Poland, M., Chadwick, W. W., Hall, M., et al. (2008). The 2005 Eruption of Sierra Negra Volcano, Galápagos, Ecuador. *Bull. Volcanol.* 70, 655–673. doi:10.1007/s00445-007-0160-3

Geist, D. J., McBirney, A. R., and Duncan, R. A. (1986). Geology and Petrogenesis of Lavas from San Cristobal Island, Galapagos Archipelago. *Geol. Soc. America Bull.* 97, 555–566. doi:10.1130/0016-7606(1986)97<555:gapolf>2.0.co;2

Geist, D. J., Naumann, T. R., Standish, J. J., Kurz, M. D., Harpp, K. S., White, W. M., et al. (2005). Wolf Volcano, Galápagos Archipelago: Melting and Magmatic Evolution at the Margins of a Mantle Plume. *J. Petrol.* 46, 2197–2224. doi:10.1093/petrology/egi052

Geist, D. J., Snell, H., Snell, H., Goddard, C., and Kurz, M. D. (2014b). "A Paleogeographic Model of the Galápagos Islands and Biogeographical and Evolutionary Implications," in The Galápagos: A Natural Laboratory For the Earth Sciences, *Geophysical Monograph Series V. 204*. Editors K. S. Harpp, E. Mittelstaedt, N. d'Ozouville, and D. W. Graham (Washington, DC: American Geophysical Union), 145–166. doi:10.1002/9781118852538.ch8

Geist, D. J., White, W. M., and McBirney, A. R. (1988). Plume-asthenosphere Mixing beneath the Galapagos Archipelago. *Nature* 333, 657–660. doi:10.1038/333657a0

Geist, D., Naumann, T., and Larson, P. (1998). Evolution of Galapagos Magmas: Mantle and Crustal Fractionation without Assimilation. *J. Petrology* 39, 953–971. doi:10.1093/petroj/39.5.953

Georgen, J. E. (2014). Interaction of a Mantle Plume and a Segmented Mid-ocean ridge: Results from Numerical Modeling. *Earth Planet. Sci. Lett.* 392, 113–120. doi:10.1016/j.epsl.2014.01.035

Gibson, S. A., Geist, D. G., Day, J. A., and Dale, C. W. (2012). Short Wavelength Heterogeneity in the Galápagos Plume: Evidence from Compositionally Diverse Basalts on Isla Santiago. *Geochem. Geophys. Geosyst.* 13, 9. doi:10.1029/2012GC004244

Gibson, S. A., and Geist, D. (2010). Geochemical and Geophysical Estimates of Lithospheric Thickness Variation beneath Galápagos. *Earth Planet. Sci. Lett.* 300, 275–286. doi:10.1016/j.epsl.2010.10.002

Gibson, S. A., Geist, D. J., and Richards, M. A. (2015). Mantle Plume Capture, Anchoring, and Outflow during Galápagos Plume-ridge Interaction. *Geochem. Geophys. Geosyst.* 16, 5. doi:10.1002/2015gc005723

Gibson, S. A., and Richards, M. A. (2018). Delivery of Deep-Sourced, Volatile-Rich Plume Material to the Global ridge System. *Earth Planet. Sci. Lett.* 499, 205–218. doi:10.1016/j.epsl.2018.07.028

Gleeson, M. L., and Gibson, S. A. (2021). Insights into the Nature of Plume-ridge Interaction and Outflux of H_2O from the Galápagos Spreading Center. *Geochem. Geophys. Geosyst.* 22, 11. doi:10.1029/2020gc009560

Gleeson, M. L. M., Gibson, S. A., and Stock, M. J. (2020). Upper Mantle Mush Zones beneath Low Melt Flux Ocean Island Volcanoes: Insights from Isla Floreana, Galápagos. *J. Petrol.* 61, 1–26. doi:10.1093/petrology/egaa094

Gleeson, M. L., Soderman, C., Matthews, S., Cottaar, S., and Gibson, S. (2021). Geochemical Constraints on the Structure of the Earth's Deep Mantle and the Origin of the LLSVPs. *Geochem. Geophys. Geosyst.* 22, 9. doi:10.1029/2021gc009932

Goss, A. R., Perfit, M. R., Ridley, W. I., Rubin, K. H., Kamenov, G. D., Soule, S. A., et al. (2010). Geochemistry of Lavas from the 2005-2006 Eruption at the East Pacific Rise, 9°46′N-9°56′N: Implications for ridge Crest Plumbing and Decadal Changes in Magma Chamber Compositions. *Geochem. Geophys. Geosyst.* 11, a–n. doi:10.1029/2009GC002977

Graham, D. W., Christie, D. M., Harpp, K. S., and Lupton, J. E. (1993). Mantle Plume Helium in Submarine Basalts from the Galápagos Platform. *Science* 262, 2023–2026. doi:10.1126/science.262.5142.2023

Gudmundsson, A. (1995). Stress fields Associated with Oceanic Transform Faults. *Earth Planet. Sci. Lett.* 136, 603–614. doi:10.1016/0012-821x(95)00164-8

Hall, P. S., and Kincaid, C. (2004). Melting, Dehydration, and the Geochemistry of off-axis Plume-ridge Interaction. *Geochem. Geophys. Geosyst.* 5, 12. doi:10.1029/2003gc000667

Harpp, K., and Geist, D. (2002). Wolf-Darwin Lineament and Plume-ridge Interaction in Northern Galápagos. *Geochem.-Geophys.-Geosyst.* 3, 1–19. doi:10.1029/2002GC000370

Harpp, K. S., Fornari, D. J., Geist, D. J., and Kurz, M. D. (2003). Genovesa Submarine Ridge: A Manifestation of Plume-ridge Interaction in the Northern Galápagos Islands. *Geochem. Geophys. Geosyst.* 4, a–n. doi:10.1029/2003GC000531

Harpp, K. S., Geist, D. J., Koleszar, A. M., Christensen, B., Lyons, J., Sabga, M., et al. (2014a). "The Geology and Geochemistry of Isla Floreana, Galápagos," in The Galápagos: A Natural Laboratory For the Earth Sciences, *Geophysical Monograph Series V. 204.* Editors K. S. Harpp, E. Mittelstaedt, N. d'Ozouville, and D. W. Graham (Washington, DC: American Geophysical Union), 71–117. doi:10.1002/9781118852538.ch6

Harpp, K. S., and Geist, D. J. (2018). The Evolution of Galápagos Volcanoes: An Alternative Perspective. *Front. Earth Sci.* 6, 50. doi:10.3389/feart.2018.00050

Harpp, K. S., Hall, P. S., and Jackson, M. G. (2014b). "Galápagos and Easter," in The Galápagos: A Natural Laboratory For the Earth Sciences, *Geophysical Monograph Series V. 204.* Editors K. S. Harpp, E. Mittelstaedt, N. d'Ozouville, and D. W. Graham (Washington, DC: American Geophysical Union), 27–40. doi:10.1002/9781118852538.ch3

Harpp, K. S., and Weis, D. (2020). Insights into the Origins and Compositions of Mantle Plumes: A Comparison of Galápagos and Hawai'i. *Geochem. Geophys. Geosyst.* 21, 9. doi:10.1029/2019gc008887

Harpp, K. S., and White, W. M. (2001). Tracing a Mantle Plume: Isotopic and Trace Element Variations of Galápagos Seamounts. *Geochem. Geophys. Geosyst.* 2, a–n. doi:10.1029/2000GC000137

Harpp, K. S., Wirth, K. R., and Korich, D. J. (2002). Northern Galápagos Province: Hotspot-Induced, Near-ridge Volcanism at Genovesa Island. *Geol* 30, 399–402. doi:10.1130/0091-7613(2002)030<0399:ngpphi>2.0.co;2

Harpp, K. S., Wirth, K. R., Teasdale, R., Blair, S., Reed, L., Barr, J., et al. (2014c). "Plume-Ridge Interaction in the Galápagos," in The Galápagos: A Natural Laboratory For the Earth Sciences, *Geophysical Monograph Series V. 204.* Editors K. S. Harpp, E. Mittelstaedt, N. d'Ozouville, and D. W. Graham (Washington, DC: American Geophysical Union), 285–334. doi:10.1002/9781118852538.ch15

Harrison, L. N., Weis, D., and Garcia, M. O. (2020). The Multiple Depleted Mantle Components in the Hawaiian-Emperor Chain. *Chem. Geol.* 532. doi:10.1016/j.chemgeo.2019.119324

Hart, S. R., Hauri, E. H., Oschmann, L. A., and Whitehead, J. A. (1992). Mantle Plumes and Entrainment: Isotopic Evidence. *Science* 256, 517–520. doi:10.1126/science.256.5056.517

Herzberg, C., Asimow, P. D., Arndt, N., Niu, Y., Lesher, C. M., Fitton, J. G., et al. (2007). Temperatures in Ambient Mantle and Plumes: Constraints from Basalts, Picrites, and Komatiites. *Geochem. Geophys. Geosyst.* 8, 2. doi:10.1029/2006gc001390

Herzberg, C., and Gazel, E. (2009). Petrological Evidence for Secular Cooling in Mantle Plumes. *Nature* 458, 619–622. doi:10.1038/nature07857

Hirschmann, M. M. (2000). Mantle Solidus: Experimental Constraints and the Effects of Peridotite Composition. *Geochem. Geophys. Geosyst.* 1, 10. doi:10.1029/2000gc000070

Hoernle, K., Werner, R., Phipps Morgan, J., Garbe-Schönberg, D., Bryce, J., and Mrazek, J. (2000). Existence of Complex Spatial Zonation in the Galápagos Plume. *Geology* 28, 435–438. doi:10.1130/0091-7613(2000)028<0435:eocszi>2.3.co;2

Hooft, E. E. E., Toomey, D. R., and Solomon, S. C. (2003). Anomalously Thin Transition Zone beneath the Galápagos Hotspot. *Earth Planet. Sci. Lett.* 216, 55–64. doi:10.1016/S0012-821X(03)00517-X

Ingle, S., Ito, G., Mahoney, J. J., Chazey, W., Sinton, J., Rotella, M., et al. (2010). Mechanisms of Geochemical and Geophysical Variations along the Western Galápagos Spreading Center. *Geochem. Geophys. Geosyst.* 11, a–n. doi:10.1029/2009GC002694

Ito, G., Lin, J., and Gable, C. W. (1997). Interaction of Mantle Plumes and Migrating Mid-ocean Ridges: Implications for the Galápagos Plume-ridge System. *J. Geophys. Res.* 102, 15403–15417. doi:10.1029/97jb01049

Ito, G., Lin, J., and Graham, D. (2003). Observational and Theoretical Studies of the Dynamics of Mantle Plume–Mid-Ocean ridge Interaction. *Rev. Geophys* 41, 4. doi:10.1029/2002rg000117

Ito, G., and Mahoney, J. J. (2005). Flow and Melting of a Heterogeneous Mantle: 1. Method and Importance to the Geochemistry of Ocean Island and Mid-ocean ridge Basalts. *Earth Planet. Sci. Lett.* 230, 29–46. doi:10.1016/j.epsl.2004.10.035

Jackson, M. G., Hart, S. R., Saal, A. E., Shimizu, N., Kurz, M. D., Blusztajn, J. S., et al. (2008). Globally Elevated Titanium, Tantalum, and Niobium (TITAN) in Ocean Island Basalts with high3He/4He. *Geochem. Geophys. Geosyst.* 9, a–n. doi:10.1029/2007GC001876

Johnson, D. M., Hooper, P. R., and Conrey, R. M. (1999). XRF Analysis of Rock and Minerals for Major and Trace Elements on a Single Low Dilution Li-Tetraborate Fused Bead. *Adv. X-ray Anal.* 41, 843–867.

Kingsley, R. H., and Schilling, J.-G. (1998). Plume-ridge Interaction in the Easter-Salas Y Gomez Seamount Chain-Easter Microplate System: Pb Isotope Evidence. *J. Geophys. Res.* 103, 24159–24177. doi:10.1029/98jb01496

Klein, E. M., and Langmuir, C. H. (1987). Global Correlations of Ocean Ridge Basalt Chemistry with Axial Depth and Crustal Thickness. *J. Geophys. Res.* 92, 8089–8115. doi:10.1029/JB092iB08p08089

Kurz, M. D., and Geist, D. (1999). Dynamics of the Galapagos Hotspot from Helium Isotope Geochemistry. *Geochimica et Cosmochimica Acta* 63, 4139–4156. doi:10.1016/s0016-7037(99)00314-2

Kurz, M. D., Rowland, S. K., Curtice, J., Saal, A. E., and Naumann, T. (2014). "Eruption Rates for Fernandina Volcano," in The Galápagos: A Natural Laboratory For the Earth Sciences, *Geophysical Monograph Series V. 204.* Editors K. S. Harpp, E. Mittelstaedt, N. d'Ozouville, and D. W. Graham (Washington, DC: American Geophysical Union), 41–54. doi:10.1002/9781118852538.ch4

Langmuir, C. H., Vocke, R. D., Jr, Hanson, G. N., and Hart, S. R. (1978). A General Mixing Equation with Applications to Icelandic Basalts. *Earth Planet. Sci. Lett.* 37, 380–392. doi:10.1016/0012-821x(78)90053-5

Le Corvec, N., and McGovern, P. J. (2018). The Effect of Ocean Loading on the Growth of Basaltic Ocean Island Volcanoes and Their Magmatic Plumbing System. *Front. Earth Sci.* 6, 119. doi:10.3389/feart.2018.00119

Lonsdale, P. (1989). A Geomorphological Reconnaissance of the Submarine Part of the East Rift Zone of Kilauea Volcano, Hawaii. *Bull. Volcanol.* 51, 123–144. doi:10.1007/bf01081981

Macdonald, G. A., Abbott, A. T., and Peterson, F. L. (1983). *Volcanoes in the Sea: The Geology of Hawaii.* Honolulu, HI: University of Hawaii Press.

MacDonald, G. A., and Katsura, T. (1964). Chemical Composition of Hawaiian Lavas1. *J. Petrology* 5, 82–133. doi:10.1093/petrology/5.1.82

Mahr, J., Harpp, K. S., Kurz, M. D., Geist, D., Bercovici, H., Pimentel, R., et al. (2016). "Rejuvenescent Volcanism on San Cristóbal Island, Galápagos: a Late "Plumer"," in *AGU Fall Meeting Abstracts* (San Francisco, CA).

McDonough, W. F., and Sun, S.-s. (1995). The Composition of the Earth. *Chem. Geology.* 120, 223–253. doi:10.1016/0009-2541(94)00140-4

McGovern, P. J., Grosfils, E. B., Galgana, G. A., Morgan, J. K., Rumpf, M. E., Smith, J. R., et al. (2015). Lithospheric Flexure and Volcano Basal Boundary Conditions: Keys to the Structural Evolution of Large Volcanic Edifices on the Terrestrial Planets. *Geol. Soc. Lond. Spec. Publications* 401, 219–237. doi:10.1144/sp401.7

McGovern, P. J., Rumpf, M. E., and Zimbelman, J. R. (2013). The Influence of Lithospheric Flexure on Magma Ascent at Large Volcanoes on Venus. *J. Geophys. Res. Planets* 118, 2423–2437. doi:10.1002/2013je004455

McKenzie, D., and O'Nions, R. K. (1991). Partial Melt Distributions from Inversion of Rare Earth Element Concentrations. *J. Petrology* 32, 1021–1091. doi:10.1093/petrology/32.5.1021

McLennan, S. M., and Ross Taylor, S. (2012). "Geology, Geochemistry and Natural Abundances," in *Encyclopedia of Inorganic and Bioinorganic Chemistry* (John Wiley & Sons). doi:10.1002/9781119951438.eibc2004

Mittal, T., and Richards, M. A. (2017). Plume-ridge Interaction via Melt Channelization at Galápagos and Other Near-ridge Hotspot Provinces. *Geochem. Geophys. Geosyst.* 18, 4. doi:10.1002/2016gc006454

Mittelstaedt, E., Ito, G., and van Hunen, J. (2011). Repeat ridge Jumps Associated with Plume-ridge Interaction, Melt Transport, and ridge Migration. *J. Geophys. Res.* 116, B01102. doi:10.1029/2010jb007504

Mittelstaedt, E., Soule, S., Harpp, K., Fornari, D., McKee, C., Tivey, M., et al. (2012). Multiple Expressions of Plume-ridge Interaction in the Galápagos: Volcanic Lineaments and ridge Jumps. *Geochem. Geophys. Geosyst.* 13, 5. doi:10.1029/2012gc004093

Morgan, W. J. (1972). Deep Mantle Convection Plumes and Plate Motions. *AAPG Bull.* 56, 203–213. doi:10.1306/819a3e50-16c5-11d7-8645000102c1865d

Naumann, T., Geist, D., and Kurz, M. (2002). Petrology and Geochemistry of Volcan Cerro Azul: Petrologic Diversity Among the Western Galapagos Volcanoes. *J. Petrol.* 43, 859–883. doi:10.1093/petrology/43.5.859

Norrish, K., and Hutton, J. T. (1969). An Accurate X-ray Spectrographic Method for the Analysis of a Wide Range of Geological Samples. *Geochimica et Cosmochimica Acta* 33, 431–453. doi:10.1016/0016-7037(69)90126-4

Reynolds, R. W., and Geist, D. J. (1995). Petrology of Lavas from Sierra Negra Volcano, Isabela Island, Galápagos Archipelago. *J. Geophys. Res.* 100, 24537–24553. doi:10.1029/95JB02809

Ribe, N. M. (1996). The Dynamics of Plume-ridge Interaction: 2. off-ridge Plumes. *J. Geophys. Res.* 101, 16195–16204. doi:10.1029/96jb01187

Saal, A., Kurz, M., Hart, S., Blusztajn, J., Blicherttoft, J., Liang, Y., et al. (2007). The Role of Lithospheric Gabbros on the Composition of Galapagos Lavas. *Earth Planet. Sci. Lett.* 257, 391–406. doi:10.1016/j.epsl.2007.02.040

Schilling, J.-g., Kingsley, R. H., and Devine, J. D. (1982). Galapagos Hot Spot-Spreading Center System: 1. Spatial Petrological and Geochemical Variations (83°W-101°W). *J. Geophys. Res.* 87, 5593–5610. doi:10.1029/jb087ib07p05593

Schwartz, D. M., Harpp, K. S., Kurz, M. D., Wilson, E. L., and VanKirk, R. (2022). Low-Volume Magmatism Linked to Flank Deformation on Isla Santa Cruz, Galápagos Archipelago, using Cosmogenic ^{3}He Exposure and ^{40}Ar/^{39}Ar Dating of Fault Scarps and Lavas. *Bull. Volcanol.* 84, 82. doi:10.1007/s00445-022-01575-3

Schwartz, D. M., Wanless, V. D., Soule, S. A., Schmitz, M. D., and Kurz, M. D. (2020). Monogenetic Near-Island Seamounts in the Galápagos Archipelago. *Geochem. Geophys. Geosyst.* 21. doi:10.1029/2020GC008914

Schwartz, D. (2014). *Volcanic, Structural, and Morphological History of Santa Cruz Island, Galápagos Archipelago*. Moscow, Idaho: University of Idaho. Master's thesis.

Siebert, L., Simkin, T., and Kimberly, P. (2010). *Volcanoes of the World*. Berkeley: University of California Press.

Sinton, C. W., Harpp, K. S., and Christie, D. M. (2014). "A Preliminary Survey of the Northeast Seamounts, Galápagos Platform," in The Galápagos: A Natural Laboratory For the Earth Sciences, *Geophysical Monograph Series V. 204.* Editors K. S. Harpp, E. Mittelstaedt, N. d'Ozouville, and D. W. Graham (Washington, DC: American Geophysical Union), 335–362. doi:10.1002/9781118852538.ch16

Sinton, J., Detrick, R., Canales, J. P., Ito, G., and Behn, M. (2003). Morphology and Segmentation of the Western Galápagos Spreading Center, 90.5-98 W: Plume-ridge Interaction at an Intermediate Spreading ridge. *Geochem. Geophys. Geosyst* 4, 12. doi:10.1029/2003gc000609

Smith, D. K., Kong, L. S. L., Johnson, K. T., and Reynolds, J. R. (2002). "Volcanic Morphology of the Submarine Puna Ridge, Kilauea Volcano," in Hawaiian Volcanoes: Deep Underwater Perspectives, *Geophysical Monograph Series V. 128.* Editors E. Takahashi, P. W. Lipman, M. O. Garcia, J. Naka, and S. Aramaki (Washington, DC: American Geophysical Union), 125–142. doi:10.1029/gm128p0125

Stock, M. J., Geist, D., Neave, D. A., Gleeson, M. L. M., Bernard, B., Howard, K. A., et al. (2020). Cryptic Evolved Melts beneath Monotonous Basaltic Shield Volcanoes in the Galápagos Archipelago. *Nat. Commun.* 11, 3767. doi:10.1038/s41467-020-17590-x

Stock, M. J., Bagnardi, M., Neave, D. A., Maclennan, J., Bernard, B., Buisman, I., et al. (2018). Integrated Petrological and Geophysical Constraints on Magma System Architecture in the Western Galápagos Archipelago: Insights from Wolf Volcano. *Geochem. Geophys. Geosyst.* 19, 12. doi:10.1029/2018gc007936

Taylor, B., Crook, K., and Sinton, J. (1994). Extensional Transform Zones and Oblique Spreading Centers. *J. Geophys. Res.* 99, 19707–19718. doi:10.1029/94jb01662

Villagómez, D. R., Toomey, D. R., Geist, D. J., Hooft, E. E. E., and Solomon, S. C. (2014). Mantle Flow and Multistage Melting beneath the Galápagos Hotspot Revealed by Seismic Imaging. *Nat. Geosci* 7, 151–156. doi:10.1038/ngeo2062

Villagómez, D. R., Toomey, D. R., Hooft, E. E. E., and Solomon, S. C. (2007). Upper Mantle Structure beneath the Galápagos Archipelago from Surface Wave Tomography. *J. Geophys. Res.* 112, B07303. doi:10.1029/2006JB004672

Weis, D., Garcia, M. O., Rhodes, J. M., Jellinek, M., and Scoates, J. S. (2011). Role of the Deep Mantle in Generating the Compositional Asymmetry of the Hawaiian Mantle Plume. *Nat. Geosci* 4, 831–838. doi:10.1038/ngeo1328

Weis, D., Kieffer, B., Maerschalk, C., Barling, J., De Jong, J., Williams, G. A., et al. (2006). High-precision Isotopic Characterization of USGS Reference Materials by TIMS and MC-ICP-MS. *Geochem. Geophys. Geosyst.* 7, 8. doi:10.1029/2006GC001283

Werner, R., Hoernle, K., van den Bogaard, P., Ranero, C., von Huene, R., and Korich, D. (1999). Drowned 14-m.y.-old Galápagos Archipelago off the Coast of Costa Rica: Implications for Tectonic and Evolutionary Models. *Geol* 27, 499–502. doi:10.1130/0091-7613(1999)027<0499:dmyogp>2.3.co;2

Wessa, P. (2021). *Free Statistics Software*. version 1.2.1. Office for Research Development and Education. Available at: https://www.wessa.net.

White, S. M., Meyer, J. D., Haymon, R. M., Macdonald, K. C., Baker, E. T., and Resing, J. A. (2008). High-resolution Surveys along the Hot Spot–Affected Galápagos Spreading Center: 2. Influence of Magma Supply on Volcanic Morphology. *Geochem. Geophys. Geosyst.* 9, 9. doi:10.1029/2008gc002036

White, W. M., and Hofmann, A. W. (1978). Geochemistry of the Galápagos Islands: Implications for Mantle Dynamics and Evolution. *Carnegie Inst. Wash. Yearb.* 77, 596–606.

White, W. M., McBirney, A. R., and Duncan, R. A. (1993). Petrology and Geochemistry of the Galápagos Islands: Portrait of a Pathological Mantle Plume. *J. Geophys. Res.* 98, 19533–19563. doi:10.1029/93jb02018

Wilson, D. S., and Hey, R. N. (1995). History of Rift Propagation and Magnetization Intensity for the Cocos-Nazca Sspreading Center. *J. Geophys. Res.* 100, 10041–10056. doi:10.1029/95jb00762

Wolfe, C. J., Solomon, S. C., Laske, G., Collins, J. A., Detrick, R. S., Orcutt, J. A., et al. (2009). Mantle Shear-Wave Velocity Structure beneath the Hawaiian Hot Spot. *Science* 326, 1388–1390. doi:10.1126/science.1180165

Workman, R. K., and Hart, S. R. (2005). Major and Trace Element Composition of the Depleted MORB Mantle (DMM). *Earth Planet. Sci. Lett.* 231, 53–72. doi:10.1016/j.epsl.2004.12.005

Yun, S., Segall, P., and Zebker, H. (2006). Constraints on Magma Chamber Geometry at Sierra Negra Volcano, Galápagos Islands, Based on InSAR Observations. *J. Volcanology Geothermal Res.* 150, 232–243. doi:10.1016/j.jvolgeores.2005.07.009

Conflict of Interest: The authors declare that the research was conducted in the absence of any commercial or financial relationships that could be construed as a potential conflict of interest.

Publisher's Note: All claims expressed in this article are solely those of the authors and do not necessarily represent those of their affiliated organizations, or those of the publisher, the editors and the reviewers. Any product that may be evaluated in this article, or claim that may be made by its manufacturer, is not guaranteed or endorsed by the publisher.